

UCLA

UCLA Electronic Theses and Dissertations

Title

Tuning Separation Processes Using Electroactive Membranes for Oil Fouling Prevention and Salt Rejection Optimization

Permalink

<https://escholarship.org/uc/item/1507r3fs>

Author

Zhu, Xiaobo

Publication Date

2019

Peer reviewed|Thesis/dissertation

UNIVERSITY OF CALIFORNIA

Los Angeles

Tuning Separation Processes Using Electroactive Membranes for Oil Fouling Prevention and
Salt Rejection Optimization

A dissertation submitted in partial satisfaction of the
requirements for the degree of Doctor of Philosophy
in Civil Engineering

by

Xiaobo Zhu

2019

© Copyright by

Xiaobo Zhu

2019

ABSTRACT OF THE DISSERTATION

Tuning Separation Processes Using Electroactive Membranes for Oil Fouling Prevention
and Salt Rejection Optimization

by

Xiaobo Zhu

Doctor of Philosophy in Civil Engineering

University of California, Los Angeles, 2019

Professor David Jassby, Chair

Membrane technology is an advanced water treatment process that well addresses water scarcity. It provides versatile treatment processes to expand freshwater resources, including seawater and brackish water desalination, wastewater and contaminated groundwater recycling. However, membranes are prone to fouling. In addition, they suffer from low water recovery, as well as a trade-off between water permeability and salt selectivity in desalination processes. Here, we incorporated carbon nanotubes (CNT) based electro-conducting thin film into commercial membranes, and evaluated their viability as an effective approach to minimize membrane fouling along with adjusting the membrane's selectivity toward different salt ions.

We first studied the fouling of model oil (hexadecane) emulsions stabilized by anionic, cationic and nonionic surfactants in a crossflow filtration system using ultrafiltration (UF) and nanofiltration (NF) membranes. In the UF filtration experiments, emulsions stabilized with the cationic surfactant quickly fouled the negatively charged UF membranes. Anionic and non-ionic surfactants stabilized emulsions, on the other hand, experienced less fouling. NF membranes exhibited exponential fouling with all types of surfactant stabilized emulsions. When 10 mM NaCl was used as the electrolyte, the differences between the surfactants were quenched. We demonstrated that the electrostatic interaction between the membrane surface and emulsion droplets was of key importance in membrane fouling. Therefore, we utilized electro-conducting CNT membranes to treat emulsion droplets at ionic strengths as high as 100 mM. Membrane fouling was reduced dramatically when electrical potentials were applied to the membrane surface. We concluded that the reduced fouling was due to less oil coalescence, which was caused by a re-distribution of charged surfactant molecules at the oil/water interface in response to the electric field. Finally, we fabricated electro-conducting NF membrane by incorporating multi-walled CNT (MWCNT) and single/double-walled CNT (S/DWCNT) network into the polyamide (PA) film. By tuning the electrical potentials applied to the membrane surfaces, the membrane's ion selectivity was dramatically changed. In particular, the application of negative potentials assisted MWCNT-PA membrane to better reject NaCl, but allowed more NaCl to pass through S/DWCNT-PA membranes. We concluded that the phenomena resulted from different membrane film structures.

The Dissertation of Xiaobo Zhu is approved.

Jennifer Ayla Jay

Sanjay K. Mohanty

Michael K. Stenstrom

David Jassby, Committee Chair

University of California, Los Angeles

2019

TABLE OF CONTENTS

Chapter 1. Introduction.....	1
1.1 Water Scarcity	2
1.2 Membrane Technology	3
1.2.1 Membrane classification and transport mechanisms	3
1.2.2 Concentration polarization and membrane fouling.....	6
1.3 Membrane Separations for Treating Oily Wastewater.....	8
1.3.1 Membrane oil fouling overview.....	8
1.3.2 Fouling mechanisms	9
1.3.3 Recent development of oil repellent membranes.....	11
1.4 NF Membranes for Water Treatment.....	13
1.4.1 NF overview.....	13
1.4.2 NF separation mechanisms	13
1.4.3 Challenges.....	16
1.4.4 Recent advances in NF membranes	17
1.5 Electroactive Membranes for Water Treatment.....	18

1.5.1	EMs for desalination	19
1.5.2	Low-pressure EMs for water reuse	26
1.5.3	Economic Analysis of EM Processes	31
1.6	Research Objectives	32
Chapter 2. Surfactant-Stabilized Oil Separation from Water using Ultrafiltration and Nanofiltration 35		
2.1	Introduction	38
2.2	Materials and Methods	40
2.2.1	Chemicals.....	40
2.2.2	Emulsion preparation	41
2.2.3	Emulsion characterization.....	41
2.2.4	Contact angle and interfacial tension measurement.....	41
2.2.5	Membranes and filtration process.....	42
2.3	Results and Discussion.....	45
2.3.1	Zeta potential and emulsion sizes	45
2.3.2	Contact angle and interfacial tension measurements	46
2.3.3	UF filtration results	48
2.3.4	UF flux step fouling tests.....	48
2.3.5	UF hydraulic cleaning.....	51

2.3.6	NF filtration results	54
2.3.7	NF flux step fouling tests	55
2.3.8	NF hydraulic cleaning	56
2.3.9	Membrane permeate analysis	58
2.3.10	Emulsion breakthrough during the UF process	60
2.3.11	Oil surface wetting of UF and NF membranes	63
2.4	Conclusions	69
2.5	Acknowledgements	71
2.6	Supporting information	72
Chapter 3. Field-Induced Redistribution of Surfactants at the Oil/Water Interface Reduces Membrane Fouling on Electrically Conducting Carbon Nanotube UF Membranes		
78		
3.1	Introduction	80
3.2	Materials and Methods	83
3.2.1	Membranes and chemicals	83
3.2.2	Membrane fabrication and characterization	83
3.2.3	Emulsion preparation and characterization	84
3.2.4	Contact angle and interfacial tension measurement	84
3.2.5	Membrane filtration process	84

3.2.6	Permeate water quality analysis.....	85
3.3	Results and Discussions	86
3.3.1	Contact angle and interfacial tension.....	86
3.3.2	Membrane and emulsion characterization	86
3.3.3	Membrane filtration results.....	89
3.3.4	Membrane permeate quality	93
3.3.5	Force analysis for droplets near membrane surface.....	94
3.4	Additional Information.....	102
3.5	Acknowledgements	102
3.6	Supporting information	103
Chapter 4.	Tuning salt selectivity of nanofiltration membranes using Carbon Nanotubes embedded Polyamide membranes	122
4.1	Introduction	124
4.2	Materials and Methods.....	127
4.2.1	Chemicals.....	127
4.2.2	Membrane fabrication.....	127
4.2.3	Membrane filtration process	128
4.2.4	Membrane characterization.....	129
4.3	Results and Discussions	131

4.3.1	Membrane characterization.....	131
4.3.2	Membrane morphology	135
4.3.3	Selective ion separation under electrical potentials	136
4.4	Conclusions	142
4.5	Acknowledgements	143
4.6	Supporting information	143
Chapter 5.	Conclusion	144
References.....		150

LIST OF FIGURES

Figure 1.1: Concentration polarization and membrane fouling in a crossflow filtration process.....	5
Figure 1.2: Concentration polarization and membrane fouling in a crossflow filtration process.....	7
Figure 1.3: Electrochemical mineral scaling prevention and cleaning on EM for desalination.	23
Figure 1.4: Fluorescent microscope images of bacterial deposition (top row) and detachment (bottom row) on an EM surface under different applied potentials;	24
Figure 1.5: Electron pathways in direct heating EM MD materials.	25
Figure 1.6: SEM images of hollow fiber EMs after electrochemical cleaning in MBR process.....	28
Figure 1.7: EMs for organic fouling inhibition through electrostatic repulsion (a), and electrochemical transformation of micropollutants (b).....	30
Figure 2.1: Membrane filtration diagram.....	44
Figure 2.2: Zeta potentials and average droplet size of emulsified oil drops stabilized with different surfactants in DI water and in the presence of 10 mM NaCl.	45
Figure 2.3: Interfacial tension and contact angles with membrane surfaces of hexadecane in water in the presence and absence of surfactants	47
Figure 2.4: UF membrane fouling during the filtration of different surfactant-stabilized oil emulsions.	48

Figure 2.5: NF membrane fouling during the filtration of different surfactant-stabilized oil emulsions.	54
Figure 2.6: TOC analysis of the membrane permeate.	58
Figure 2.7: Critical pressure required for emulsions to penetrate through the UF membranes	61
Figure 2.8: Difference between compressive force ($F_{\Delta p}$) and the force resisting membrane wetting (F_{wr}) as a function of droplet size and pressure drop across cake layer on a UF membrane surface;	66
Figure 2.9: Difference between compressive force ($F_{\Delta p}$) and the force resisting membrane wetting (F_{wr}) as a function of droplet size and pressure drop across cake layer on a NF membrane surface	67
Figure 3.1: Membrane and droplet characterization: Membrane surface morphology and surface roughness.....	89
Figure 3.2: Membrane filtration process under different ionic strengths.	90
Figure 3.3: Proposed surfactant redistribution at (a) 5 V _{dc} with membrane as cathode, (b) 0 V, and (c) 5 V _{dc} with membrane as anode;	97
Figure 3.4: (a) Illustration of mechanistic pathways of membrane surface wetting under anodic and cathodic membrane potentials.	101
Figure 4.1: Membrane surface properties study using a) CV scans to determine possible chemical reactions; b) XPS analysis to quantify the surface chemical compositions; c) ATR-FTIR analysis to distinguish surface functional groups.	133

Figure 4.2: The comparison of membrane surface morphologies between MWCNT and S/DWCNT based membranes.....	134
Figure 4.3: AFM topography images of a) MWCNT-PA membrane and b) S/DWCNT-PA membrane.....	135
Figure 4.4: Membrane flux and rejection evaluation under electrical potentials.	138
Figure 4.5: Mixed salt rejection towards specific ions including Na ⁺ (black square), Mg ²⁺ (red circle), SO ₄ ²⁻ (blue triangle), Cl ⁻ (inversed triangle) of a) MWCNT-PA and b) S/DWCNT-PA membranes.....	140
Figure 4.6: Membrane flux and rejection evaluation under different pHs..	Error!
Bookmark not defined.	

LIST OF TABLES

Table 1.1: Classical membrane fouling models.....	11
Table 1.2: Theoretical models for emulsion coalescence.	11
Table 4.1: CNT membrane electrical properties.....	132
Table 4.2: Ion separation performance of mixed salt at different electrical potentials	Error! Bookmark not defined.

ACKNOWLEDGEMENTS

I would like to thank my advisor, Dr. David Jassby, for his mentorship and extensive guidance. David admitted me into the lab when I was an exchange student from China at the senior year. Since then, David has guided me to explore a wide range of researches on electro-conducting membranes. In addition, I greatly appreciate that David was willing to bring me from UCR to UCLA at my 4th year, and also helped my future career by recommending me to other great professors. I will never forget about all these invaluable research lessons and life lessons that I received from David. I would also like to thank my committee member: Dr. Jenny Jay, Dr. Michael Stenstrom, and Dr. Sanjay Mohanty for their time and help.

I would also want to acknowledge all my lab-mates who have helped me along the way. Our research lab provides not only a good research platform but also a sense of family, warm and encouraging. In particular, I would like to thank Wenyan Duan and Alexander Vladimirovi Dudchenko for providing training and help, it wouldn't be easy for me to transit from an undergraduate student to graduate school. I would like to thank undergraduate students including Bradley Evans, Bi Chen, Xiaotian Gu, Xin He, Douglas Chang, and Lew Xuan Yu for spending their time to help on the research projects.

VITA

2014 Bachelor's degree in Chemical Engineering
Zhejiang University of Technology
Hangzhou, Zhejiang, China

JOURNAL PUBLICATIONS

Zhu, X., Jassby, D. "Electroactive Membranes for Water Treatment: Enhanced Treatment Functionalities, Energy Considerations, and Future Challenges." *Acc. Chem. Res.* 2019, 52, 5, 1177-1186

Zhu, X., Dudchenko, V. A., Khor, C. M., Xin, H., Guy, Z. R., Jassby, D., "Field-Induced Redistribution of Surfactants at the Oil/Water Interface Reduces Membrane Fouling on Electrically Conducting UF Membranes" *Environ. Sci. Technol.*, 2018, 52, 11591-11600

Zhu, X., Dudchenko, A., Gu, X., Jassby, D., "Surfactant-stabilized oil separation from water using ultrafiltration and nanofiltration." *J. Membr. Sci.*, 2017, 529, 159-169

Kim, Y. C., **Zhu, X.**, Herzberg, M., Walker, S., Jassby, D., "Impact of Physical and Chemical Cleaning Agents on Specific Biofilm Components and the Implications for Membrane Biofouling Management." *Ind. Eng. Chem. Res.*, 2018, 57, 3359-3370

Tang, L., Iddya A., **Zhu, X.**, Dudchenko, A., Duan, W., Turchi, C., Vanneste, J., Cath, Y. T., Jassby, D., "Enhanced Flux and Electrochemical Cleaning of Silicate Scaling on Carbon Nanotube-Coated Membrane Distillation Membranes Treating Geothermal Brines." *ACS Appl. Mater. Interfaces*, 2017, 9, 38594-38605

Duan, W., Dudchenko, A., Mende, E., Flyer, C., **Zhu, X.**, Jassby D., "Electrochemical mineral scale prevention and removal on electrically conducting carbon nanotube - polyamide reverse osmosis membranes." *Environ. Sci.: Processes Impacts*, 2014, 16, 1300-1308

CONFERENCE PRESENTATIONS

Zhu, X., Dudchenko, A., Gu, X., Jassby, D., "Surfactant-stabilized Oil Separation from Water Using Ultrafiltration and Nanofiltration" ACS, San Francisco, CA, 2017

Zhu, X., Dudchenko, A., Khor, C. M., Xin H., Guy, Z. R., Jassby, D., "Field-Induced Redistribution of Surfactants at the Oil/Water Interface Reduces Membrane Fouling on Electrically Conducting UF Membranes" North American Membrane Society, Lexington, KY, 201

Chapter 1.

Introduction

1.1 Water Scarcity

Without access to fresh water, it would not be possible for humans and other animals on Earth to survive. However, only 0.8% of Earth's water is direct fresh water,¹ that is readily available for human usage. Further, due to population growth and climate change, there is a growing demand for fresh water for agricultural irrigation, industrial production, and domestic use.² In addition, water pollution caused by human activity, such as the use of products that contain micropollutants, has threatened the availability of fresh water even further.³ Water management strategies such as dam construction and water transfer have implemented to address this water shortage; however, they have proven ineffective, expensive and even detrimental to the local ecosystem.⁴ Therefore, there is a need for technology that addresses water scarcity in a manner that is both effective and environmentally benign.

The main strategies to address water scarcity include water reuse (wastewater or contaminated groundwater recycling), and desalination (remove salt ions from seawater and brackish water).³ Membrane technology is an available tool for both strategies. It provides a solution for producing unlimited fresh water from sea water or brackish water, and at the same time allows for the recycling of fresh water from contaminated water resources. It has been branded as the benchmark technology for desalination due to its low energy demand for water recovery, and also its effective production of high-quality water.⁵ However, membrane technology is not flawless. It suffers from severe membrane fouling that deteriorates membrane performance, thus multiple pretreatment steps must be used to reduce membrane fouling,^{6,7} and additional energy or chemicals are required to recover the

membrane.⁸ In some cases, membranes are ineffective at rejecting small and neutral charged species such as phenol, acetone, and boron.⁹ Moreover, it is necessary to develop advanced post-treatment processes to deal with the high salinity retentate being produced.¹⁰

The remaining challenges in membrane technology are persuading researchers to develop the next generation of membrane materials to resist fouling, effectively remove uncharged molecules, and allow higher water recovery with lower energy consumption.

1.2 Membrane Technology

Membrane technology uses a physical barrier to separate substances. It has been well demonstrated as a promising separation technology for a wide range of chemical species including water, organic solvents, and gas species. For example, membranes for water treatment allow water to pass through and exclude pollutants such as bacteria, organics and salt ions. Gas separation membranes are less effective at separating gas mixtures; they can only enrich certain gas species that diffuse faster than the others. Therefore, an ideal separation of gas mixtures may require multi-stage membrane processes. In the following sections, membrane classification, transport mechanisms, and fundamental aspects of filtration processes will be discussed.

1.2.1 Membrane classification and transport mechanisms

Membranes are most commonly used in pressure-driven processes, which can be classified as microfiltration (MF), ultrafiltration (UF), nanofiltration (NF), pervaporation, and gas separation.¹¹ These processes rely on pressure differences to transport products across the membranes and are classified based on their membrane pore size (Figure 1.1). MF uses micron-sized porous membranes to separate large pollutants including oil

emulsions, bacteria, and particles. UF uses membranes with a smaller pore size that is in the range of 1 to 100 nm, which is effective at removing natural organic matters (NOMs). NF uses membranes with a pore size around 1 nm, which is able to remove multivalent ions and surfactants. RO is effective at removing monovalent ions, which makes it as a state-of-art seawater and brackish water desalination technology. Pervaporation membranes separate liquid mixtures such as organic-organic mixture and organic-water mixture. Gas separation uses membranes to selectively separate gas species. The transport of molecules across both MF and UF membranes are best described by the pore flow model, where membrane pores are relatively large and stable during separation. RO, pervaporation, and gas separation follow the solution diffusion model, which needs nonporous membranes to initially dissolve or adsorb molecules in the voids (free-volume elements) between polymer chains, then these molecules diffuse through the thermal motion of polymer chains. During the process, the voids between polymer chains are changing dynamically.¹²

The transport of permeate in the pore flow model and the solution diffusion model are described by Darcy's law (Equation 1) and Fick's law (Equation 2). Where J_i is the membrane permeate flux of the specie i , k and μ are the permeability and viscosity of the fluid transport through a porous media. D_i is the diffusion coefficient that describes the rate of specie i , passing through a nonporous media. The pressure and concentration gradients $\frac{dp}{dx}$ and $\frac{dc_i}{dx}$, are the driving force for the permeate flow.

$$J_i = \frac{k}{\mu} \frac{dp}{dx} \quad (1)$$

$$J_i = -D_i \frac{dc_i}{dx} \quad (2)$$

Membranes are not only evaluated based on their permeability, which represents the transport rate of product across the membrane, but also their selectivity, which describes the effectiveness of separation. In water treatment processes, membrane selectivity is normally described as a rejection R , as shown in Equation 3:

$$R = \left(1 - \frac{c_p}{c_f}\right) \times 100\% \quad (3)$$

Where c_p and c_f represent the solute concentration in the permeate and the feed solutions.

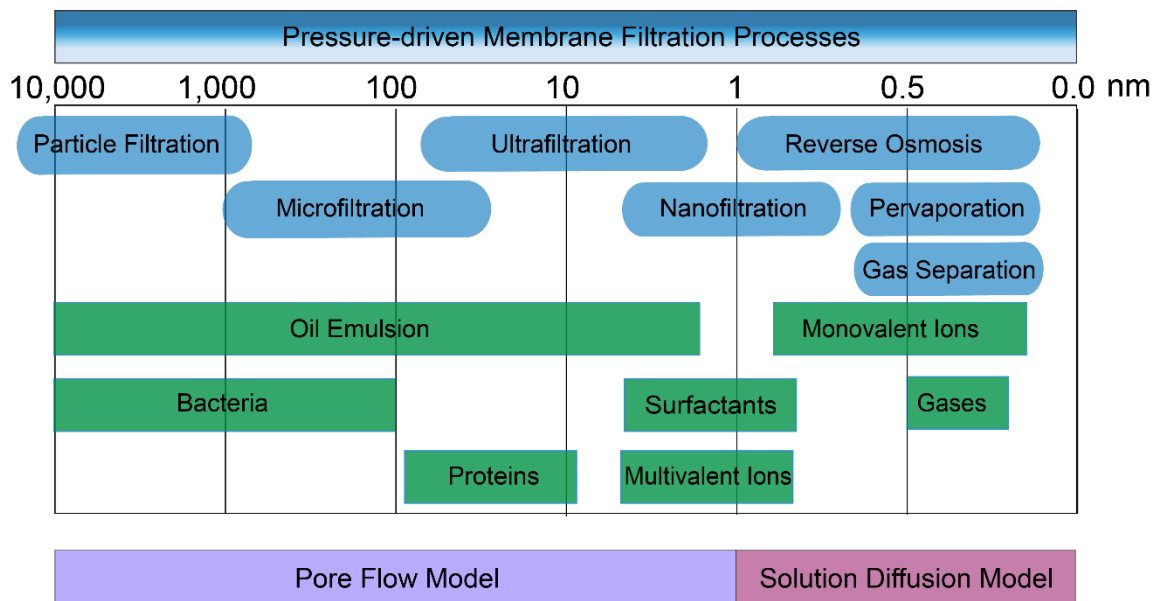


Figure 1.1: Concentration polarization and membrane fouling in a crossflow filtration process.

In general, in constructing membranes, researchers must make a trade-off between permeability and selectivity. For instance, a membrane with a smaller pore size would achieve higher selectivity with reduced permeability. Therefore, an appropriate selection

of membranes for target goals such as required rejection and permeability are crucial to achieving optimal conditions.

1.2.2 Concentration polarization and membrane fouling

One of the most important fundamental aspects of the membrane filtration process is concentration polarization and its resulted in membrane fouling. Membranes for water treatment allow a fast transport rate of water through the membrane, while large substances are excluded and accumulated on the membrane surface. The concentration difference of unwanted species between the bulk solution and the membrane surface is called concentration polarization (Figure 1.2). The accumulation of such species including salt ions, colloids, and gas molecules deteriorates membrane performance in the form of a reduced effective driving force and severe fouling phenomena. In RO and NF processes, membranes are effective at rejecting salt ions, which lead to the concentration build-up of salt ions at the water-membrane interface (Figure 1.2). Thus, higher pressure is needed to overcome the extra osmotic pressure ($C_p - C_{bulk}$) generated by concentration polarization in order to maintain the same permeability. Operational efforts have been made to reduce the concentration polarization by inducing a better mixing of the solution near the membrane surface. For example, introducing a continuous and fast crossflow of the feed solution on the membrane surface is shown to be effective. In UF and MF processes, membranes are more porous and usually operate at much higher fluxes compared to RO and NF. Pollutants are rejected due to their size, which is larger than membrane pores (pore flow mechanism). The permeate drag acting on these pollutants including particles, organics, and bacteria causes their concentration build-up (concentration polarization, Figure 1.2) on the

membrane surface, and subsequently forms a dense gel layer or cake layer that fouls the membrane surface and results in a dramatic drop of membrane performance.

Simplified mathematical models were used to characterize the concentration polarization in RO processes (Equation 4),¹¹ and membrane fouling in UF/MF processes (Equation 5-6),¹³ where A is the water permeability coefficient, Δp and $\Delta\pi$ are the hydraulic pressure difference and osmotic pressure difference across the membrane, μ is the dynamic viscosity of the permeate, R_t , R_m , R_p , R_{ef} , and R_{if} represent the total resistance, intrinsic membrane resistance, polarization layer resistance, cake layer resistance, and internal fouling resistance, respectively.

$$J_i = A(\Delta p - \Delta\pi) \quad (4)$$

$$J_i = \frac{\Delta p}{\mu R_t} \quad (5)$$

$$R_t = R_m + R_p + R_{ef} + R_{if} \quad (6)$$

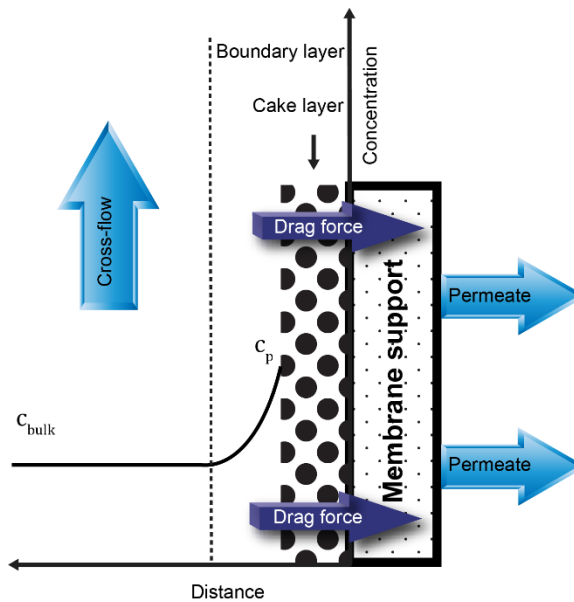


Figure 1.2: Concentration polarization and membrane fouling in a crossflow filtration process.

1.3 Membrane Separations for Treating Oily Wastewater

1.3.1 Membrane oil fouling overview

Oily wastewater is largely produced in industrial unit processes and thus raises huge environmental concerns. For example, oil and gas industries produce 60 million barrels of produced water daily within the United States.¹⁴ Among pollutants found in these oily waste streams, oil emulsions are a problematic class of concerns. While free oil or unstable emulsion droplets that are larger than 10 μm can be removed using gravity-based separations, emulsified droplets with less than 10 μm are best removed using membranes.¹⁵ However, oil is capable of wetting the membrane surface, which can destroy membrane performance.¹⁶ In particular, the compression and coalescence of oil emulsions complicate the membrane oil fouling phenomenon.

Emulsion oil droplets are stabilized by amphiphilic molecules comprised of hydrocarbon-based hydrophobic tails and hydrophilic heads (known as surfactants). A stable emulsion is formed when the hydrophobic tails partition into the oil phase and the hydrophilic heads remain in the water phase at the oil-water interface. Therefore, the properties of emulsion droplets including charge, size, and interfacial tension are highly dependent on the surfactants' hydrophilic heads, which are of fundamental importance in the fouling phenomena. Unlike traditional fouling caused by colloidal particles, which is mainly due to the concentration polarization and subsequent cake layer formation, membrane oil fouling is more complicated due to the dynamic changes of foulant layer such as emulsion deformation and coalescence, which further leads to membrane surface wetting.

1.3.2 Fouling mechanisms

1.3.2.1 Traditional fouling models

The flux decline in UF and MF membrane filtration processes were extensively studied using 4 classical fouling models that are summarized in Table 1.1:¹⁷⁻¹⁹ 1) Completely pore blocking assumes the membrane pores were fully covered after the deposition of single layer foulants. Thus, the permeate flux was only allowed to go through the uncovered membrane pores. 2) Intermediate pore blocking assumes the possible deposition of new foulants on top of the initial fouling layer; 3) Cake filtration assumes the formation of a cake layer on top of the membrane surface. This cake layer is porous to permeate flow but provides additional resistance; 4) Standard blocking assumes foulants can enter pores, and accumulate on the pore wall, which decreased membrane porosity. Mathematical equations that describe each model were also reported in Table 1. Symbols of V , t , J_0 , a , K_b , K_i , K_c , and K_s represent cumulative permeate volume, filtration time, initial permeate flux, membrane surface area, and coefficients for completely pore blocking, intermediate pore blocking, cake filtration, and standard blocking, respectively. These models provide a straightforward method to correlate the complicated filtration results from different types of fouling studies to simple coefficients. However, such models are only applicable for ideal unstirred dead-end filtration processes that are less commonly found in industrialized filtration processes.²⁰ These models also failed to capture the emulsion coalescence event happened in membrane oil fouling process.

1.3.2.2 Emulsion coalescence event

Several approaches have been developed to study the emulsion coalescence event (Table 1.2).²¹ Film drainage is one of the most popular models that describes two bubbles or droplets are prevented from coalescing by a layer of film. For example, a water layer is the film that is trapped between two interfaces of oil droplets. In this model, droplets coalescence can be divided into three events^{22,23}: 1) a thin film was formed when two droplets collided, 2) attractive forces between two interfaces gradually drained the film until it reached a critical thickness, 3) the film ruptured and droplets coalesced. The overall coalescence is controlled by the droplets contact time and the film drainage time. Collision models were proposed to characterize the coalescence based on the collision frequency between contacting droplets, which are highly dependent on droplet size and approaching velocities.²² Moreover, an more explicit energy model was proposed to link the coalescence efficiency to droplets generalized properties of droplets including kinetic collision energy and interfacial energy.²⁴ Most recently, Rekiav et. al. used a coarse-grained dissipative particle dynamics approach to investigate the interaction between oil/water/surfactant interfaces and film rupture event at the molecular scale.²⁵ Instead of using theoretical models, Tummons et. al. set up a customized crossflow MF system to visualize the oil fouling phenomena in real-time and concluded that the fouling is controlled by the emulsion coalescence and the crossflow induced shear.¹⁵ However, it is still challenging to link the droplets coalesce to the subsequent membrane fouling due to the complexity of the process.

Table 1.1: Classical membrane fouling models.

Model	Completely pore blocking	Intermediate pore blocking	Cake filtration	Standard blocking
Governing equation	$\frac{dV}{dt} = J_0 a - K_b V$	$\frac{dt}{dV} = \frac{1}{J_0 a} + K_i t$	$\frac{t}{V} = \frac{1}{J_0 a} + \frac{K_c V}{2}$	$\frac{t}{V} = \frac{1}{J_0 a} + \frac{K_s t}{2}$

Table 1.2: Theoretical models for emulsion coalescence.

Model	Film drainage model	Collison model	Energy model	Molecular simulation
Equations or comments	$\lambda = \exp\left(-\frac{t_{drainage}}{t_{contact}}\right)$	$h \sim d, v$	$\lambda = \exp\left(-\frac{E_\sigma}{E_{kin}}\right)$	Dissipative particle dynamics

$\lambda, h, d, v, t_{drainage}, t_{contact}, E_\sigma, E_{kin}$ are emulsion coalescence efficiency, collision frequency, particle diameter, particle velocity, drainage time, contact time, interfacial energy, kinetic collision energy.

1.3.3 Recent development of oil repellent membranes

A significant effort has been spent on the development of anti-fouling membrane materials for oil/water separations, with the goal of creating oil-repellent materials that resist wetting.²⁶ In general, poly(vinylidene fluoride) (PVDF) is commonly used as a base material to fabricate anti-fouling membranes due to its extraordinary chemical resistance to acids, hydrocarbons, and organic solvents; and stable performance under a wide range of temperatures.²⁷ However, a neat PVDF membrane suffers from severe membrane fouling which results in the reduced permeate flux and lower oil rejection. Recent

researches mainly focused on two approaches to improve the performance of PVDF membranes: 1) Cast membranes using the mixture of PVDF solution and hydrophilic polymers, especially amphiphilic polymers, or nanofillers such as titanium oxide and aluminum oxide nanoparticles. This process is normally known as blending.^{28,29} Blending hydrophilic polymers such as noncharged poly(methyl methacrylate) and charged sulfonated polycarbonate or sulfonated polyether ether ketone were shown to be effective at reducing the membrane surface energy, thus increasing membrane surface hydrophilicity.^{28,30,31} However, membranes may collapse due to the incompatibility between two polymers.²⁸ More recently, amphiphilic copolymers were used instead to resolve the compatibility issues with PVDF and still improve membrane surface hydrophilicity. A series of amphiphilic copolymers with different structures including co-block and tri-block were used to increase the membrane's anti-oil fouling resistance.^{32,33} 2) Modify the surface of PVDF membrane through physical grafting or chemical binding a hydrophilic layer. It is essential to create enough reactive sites on the membrane surface through plasma treatment, ultraviolet, and electron beam radiation. Thereafter, polymer brushes can form by covalently bond to the membrane surface.³⁴⁻³⁷ Both methods provide PVDF membranes more resistance to oil fouling. However, modified membranes are unable to recover once the fouling event happens. In addition to these traditional PVDF based membranes, inspired by biological nature, superhydrophilic membranes surfaces are fabricated via a combination of biomimetic materials and unique surface patterns.^{38,39} The superior surface properties make them promising materials for oil/water separations.

1.4 NF Membranes for Water Treatment

1.4.1 NF overview

NF membranes are drawing great attentions due to its nanometer ranged pore size allowing a higher water permeability and a more diverse separation of substances including salt ions and small organic molecules.⁴⁰ These excellent properties lead to a wide application of NF membranes for water softening (removing Mg^{2+} , Ca^{2+}), wastewater treatment (NOM and disinfection by-product precursors removal), food processing (concentration of valuable organic molecules such as sugars and proteins), and even for separation of organic solvents.⁴⁰⁻⁴³ Several commercially available NF membranes were previously characterized and reported with pore diameters of 0.8 to 2.0 nm,⁴⁴⁻⁴⁸ and MWCO were reported from 150 to 2000 Da.⁴² Such membrane variations result in a dramatic difference in salt rejection performance: $MgSO_4$ is still well rejected above 90% by all membranes. However, the rejection toward NaCl is extremely different which differs from 10% to 92%. These differences are particularly attractive for nanometer ranged separation processes. For example, the use of loose NF membranes in the food processing industry provides excellent rejection of pectin and easy passage of phenol and monovalent salt ions.⁴⁹ Therefore, NF offers an effective separation process for producing liquid products with a better quality.

1.4.2 NF separation mechanisms

The versatile separation performance of NF membranes is caused by a combination of complicated transport mechanisms. The widely accepted transport phenomena that govern the NF membrane rejection is size and charge based separation mechanisms,

namely Donnan exclusion.⁵⁰ The semipermeable NF membranes create steric hinderance that prevent the passage of large molecules, and their intrinsic electrical charges along the membrane surface and pore further pose electrostatic repulsions toward molecules with similar size and same charges. To maintain the electron neutrality condition on two sides of the membranes, smaller oppositely charged molecules are retained. Thus, polyamine-based NF membranes, governed by Donnan exclusion mechanism, achieved an ideal rejection of multivalent salts such as MgSO_4 and Na_2SO_4 . More recently, dielectric exclusion was proposed to account for the charge polarization caused repulsions. When hydrated ions diffuse through polymer films, ions induced same charges of the membrane pore wall due to the dielectric difference between the water layer (hydration layer) and polymer film (pore wall), thus an enhanced separation was achieved.⁵¹ These dominant mechanisms are successful at explaining the salt rejections toward salt solutions. Luo et al. summarized the pH effects on salt rejections: the abundance of carboxylic groups on the polyamide (PA) NF membrane gives a nearly neutral charge of the membrane surface around pH 6. The adjustment of pH to the lower end and the higher end increased membrane surface charge and further resulted in a more significant Donnan exclusion mechanism. Thus, membranes demonstrate V-shape rejection curves for symmetric electrolytes (NaCl , KCl) and S-shape rejection curves for asymmetric salts (Na_2SO_4 , MgCl_2) under pH ranges from 3-10.^{52,53} However, Donnan exclusion is limited in explaining the rejection difference between different monovalent ions. More recently, hydration/dehydration phenomena were further investigated for this regard. Richard et al. measured the rejections of fluoride, chloride, nitrate and nitrite ions through commercial

NF membranes, and found that fluoride was best rejected, which is abnormal because fluoride has both the smallest hydrated and dehydrated sizes. They further measured the solute fluxes at different temperatures to quantify the energy barriers of fluoride, chloride, nitrate and nitrite ions transporting through commercial NF membranes (Arrhenius equation), and linked energy barriers to ion hydration/dehydration free energy.⁵⁴ Epsztein et al. further examined the ionic charge densities of anions including fluoride, chloride, bromide, and nitrate. The observed rejections at a wide range of pHs suggested that these ions with higher ionic charge densities (higher hydration strength) are more affected by the Donnan exclusion mechanism.⁵⁵ In addition to anions, Levi et al. investigated the cation transport in carbon nanopores, and correlated the dehydration process, namely, the bulk solution hydration number, to the ion transport through NF membranes using electrochemical quartz crystal microbalance.⁵⁶ Yang et al. simulated the cation transport and reported a selectivity in the order of potassium, caesium, and sodium, and concluded that ion hydration and pore hydration change (equilibrium free energy of partitioning) were mainly responsible for the observed trend.⁵⁷ Another mechanism, pore swelling, caused by the accumulation of salt ions in the pores and high pH, was proposed to explain the reduced salt rejection.^{58,59} At high salt ion concentrations and high pHs, the membrane pore surface charge was increased, thus leading to a higher packing density of salt ions in the pores. The higher concentration of counterions, in turn, create stronger electrostatic repulsion between ions in the pores, which further cause pore swelling and subsequent rejection drop.^{58,60,61} Researchers reported the decrease of hydration layer at the membrane pore walls broadened the pore size and caused reduced rejections.^{62,63} Moreover, the membrane pore distribution

is also thought to be crucial for such a decreased rejection, because the flux of solute through small pores is limited at a higher extent than large pores at high pHs, and the membrane rejection is more affected by the solute transport through large pores.⁵⁸ However, these mechanisms are still requiring further investigations.

1.4.3 Challenges

As an emerging and promising membrane unit process, NF still faces operational challenges and some theoretical knowledge are missing.^{64,65} Membrane fouling is one of the most important challenges that hinder the membrane's performance and shorten its lifespan. Unlike porous UF and MF membranes, commercial NF membranes have a thin and dense active layer, which are more prone to fouling, in particular in the case of mineral scaling and biofouling.^{66,67} It is also more difficult to clean fouled membranes due to the membrane structure prohibited the use of physical cleaning method. Therefore, pretreatment processes are often required before the NF process. Furthermore, NF's diverse separation toward different ionic species sometimes are not favorable due to its insufficient separations that are unable to meet the discharge requirements. More recently, researchers summarized 7 knowledge gaps of mass transport in single-digit nanopores:⁶⁴ 1) the flux enhancement through slip flow, which indicates the flux at the solution membrane interface is nonzero (flux at the boundary layer is nonzero);⁶⁸ 2) the temperature and pressure distortion of the fluid confined in these pores (the property change of the fluid restricted in nanopores);⁶⁹ 3) the impact on phase separation of the fluid from one-phase to multi-component phases;⁷⁰ 4) the large size defects resulted separation changes;⁷¹ 5) Solvation or desolvation of solutes effect (such as hydration/dehydration phenomena);⁷² 6) the

confinement impact on ion solvation and desolvation process;⁷³ 7) the separation performance for different monovalent ions.⁷⁴ All these experimental and theoretical challenges are awaiting more research efforts to overcome.

1.4.4 Recent advances in NF membranes

Most recently, plenty of researches were utilizing advanced nanomaterials to fabricate NF membranes. Incorporating engineered nanomaterials into thin film nanocomposite (TFN) membranes were effective at modifying the active layer structure and the surface chemistry, thus improving membrane performance including permeability, selectivity, and antifouling properties. For example, Lee et al. immobilized silver nanoparticles on PA films to prevent the biofouling, the membranes exhibited strong anti-bacterial growth properties and didn't loss membrane permeability and salt rejection.⁷⁵ Rajaeian et al. fabricated TiO₂ based TFN membranes to alter the permeate flux and rejection.⁷⁶ By increasing the concentration of nanoparticles small amount (0.05wt%), membranes were tuned to better reject salt ions without and the permeate remained high. At higher concentrations, membranes were turned to be more porous and achieved a higher flux and small loss of salt rejections. Moreover, carbon-based nanomaterials such as graphene oxide (GO) and carbon nanotubes (CNT) are drawing attention due to their great mechanical stability, antifouling properties, and specific molecular structure, which in turn contribute to superior permeability and selectivity.⁷⁷⁻⁷⁹ CNT intercalated GO membranes were shown to be effective at separating salt ions under low ionic strengths.⁸⁰ In particular, the excellent electrical conductivities of carbon materials made it possible for electrically adjusting the membrane surface charges. Hu et al. synthesized electrically conductive

reduced RO-CNT membranes and tested their desalination performance under 50 mM feed concentration. The application of both ± 1 V cell potentials dramatically improved rejection of NaCl (25% to 65%), Na₂SO₄ (30% to 65%), and CaCl₂ (55% to 70%), comparing to no addition of electrical potentials. However, the membranes were limited to the low permeate fluxes (0.2-0.3 Lm⁻²h⁻¹bar⁻¹, LMH/bar).⁸¹ Zhang et al. constructed conductive polyaniline-polystyrenesulfonate CNT membranes, which achieved high permeate fluxes of ~ 15 LMH/bar when treating 5 mM NaCl and Na₂SO₄ solutions. Rejections were also enhanced at negative 2.5V cell potentials (82% to 93% for Na₂SO₄; 54% to 82% for NaCl). Therefore, all these findings suggested that incorporating engineered nanomaterials into NF membranes could greatly enhance membrane's overall performance.

1.5 Electroactive Membranes for Water Treatment⁸²

(Adapted with permission from ref 82. Copyright 2019 American Chemical Society)

Electrically-driven physical and chemical phenomena, such as electrophoresis, electrostatic repulsion, dielectrophoresis, and electricity-driven redox reactions, have long been coupled to membrane-based separation processes, in a process known as electrofiltration. However, it is only in recent years that appropriate membrane materials (i.e., electrically conducting membranes (EMs)) have been developed that enable the efficient use of these electro-driven processes. Specifically, the development of EM materials (both polymeric and inorganic) have reduced the energy consumption of electrofiltration by using the membrane as an electrode in an electrochemical circuit. In essence, a membrane-electrode allows for the concentrated delivery of electrical energy directly to the membrane/water interface where the actual separation process takes place.

In the past, metal electrodes were placed on either side of the membrane, which resulted in large potentials needed to drive electrochemical/electrokinetic phenomena. The use of a membrane-electrode dramatically reduces the required potentials, which reduces energy consumption and can also eliminate electrocorrosion and the formation of undesirable byproducts.

In the following section, we review recent developments in the field of electrofiltration, with a focus on two water treatment applications: desalination and water reuse (wastewater or contaminated groundwater recycling). Specifically, we discuss how EMs can be used to minimize multiple forms of fouling (biofouling, mineral scaling, organic fouling); how electrochemical reactions at the membrane/water interface are used to destroy toxic contaminants, clean a membrane surface, and transform the local pH environment, which enhances the rejection of certain contaminants; how electric fields and electrostatic forces can be used to re-orient molecules at the membrane/water interface; and how electrical energy can be transformed into thermal energy to drive separation processes. A special emphasis is placed on explicitly defining the additional energy consumption associated with the electrochemical phenomena, as well as the additional cost associated with fabricating EM materials.

1.5.1 EMs for desalination

An attractive solution to freshwater scarcity is the desalination of seawater and brackish groundwater. In addition, there is a growing interest in the desalination of high-salinity brines (>70 g/L) generated from various industrial activities (such as oil-and-gas production); because of their high osmotic pressure, these brines require thermal

desalination.^{82,83} The state-of-the-art seawater desalination technology, based on thin-film composite RO membranes, is a highly efficient process that operates very near the thermodynamic limit.³ However, RO membranes are still limited by fouling (inorganic scaling, biofouling), are susceptible to chlorine attack, and have low rejection of small and neutral molecules, such as boron.^{5, 10,84} To overcome these limitations, significant pretreatment and/or multi-pass systems are needed, both of which increase process complexity and cost.

Two classes of EM desalination membranes have been developed: pressure-driven, dense membranes (NF and RO), and thermally-driven, porous and hydrophobic MD materials.^{67,85-87} These membranes are constructed by depositing a thin layer of carbon nanotubes (CNTs) on a porous support, followed by cross-linking the CNTs with a range of polymers.^{87,88} The choice of support and cross-linking polymer determine the porosity and surface properties of the composite material.⁸⁹ Importantly, these membranes are made of non-aligned CNTs, which form a percolating (and conducting) non-woven mat. It is doubtful that a significant volume of water (liquid or vapor) passes through the inner core of CNTs arranged in such mats. For pressure-driven membranes, CNTs are deposited on a relatively hydrophilic support (such as polysulfone) and cross-linked with PA, together forming a dense composite suitable for salt rejection. For thermal desalination, the CNTs are deposited on a hydrophobic support (such as polytetrafluoroethylene (PTFE)), and cross-linked with small amounts of either a hydrophilic (e.g., polyvinyl alcohol) or hydrophobic (e.g., polydimethylsiloxane) material, creating a porous composite material.^{86,87} These composite membrane materials achieve high electrical conductivity, in

the range of 1,000 - 2,000 S/m (metals $>10^5$ S/m, insulators $<10^{-6}$ S/m); these conductivity values are achieved using multi-walled CNTs (MWCNTs) of mixed chirality. While thin-films of purely metallic single-walled CNTs achieve far higher conductivities, their extreme cost prohibits their use in any water-related real-world applications.⁹⁰ RO and NF EMs created using this approach achieve similar salt rejection and flux to commercially-available products.^{85,91} However, the incorporation of CNTs in MD EMs leads to an increase in water flux, although the mechanism responsible for this remains unclear.⁹²

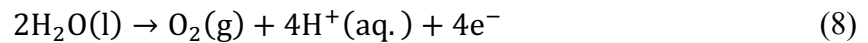
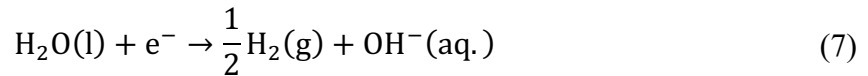
1.5.1.1 Electrochemical management of scaling using EMs

Mineral scaling is a phenomenon caused by crystal nucleation and growth on the surface of desalinating membranes, which can reduce membrane permeability and rejection.^{66,93} Scaling is particularly problematic in brackish groundwater desalination due to elevated Ca^{2+} , Mg^{2+} , CO_3^{2-} , SO_4^{2-} , and silicate concentrations.⁹⁴ Scaling occurs as the concentrations of these ions increase at the membrane/water interface, eventually exceeding the solubility of minerals such as CaCO_3 and CaSO_4 .^{95,96} To control scaling, careful adjustment of temperature, pH and antiscalant addition are used.^{95,97}

Applying 1.5 V_{DC} total cell potential (membrane as anode) to the surface of an RO EM dramatically reduced CaSO_4 fouling.⁸⁵ The mechanism responsible for the reduced scale formation was determined to be an electrokinetic reorganization of the electrical double layer, which led to an imbalance in the ratio between anions and cations along the membrane surface that reduced the nucleation rate. Furthermore, crystals that did form were larger and formed a porous layer on the membrane surface, which was not as resistant to the flow of water (Figure 1.3a, b). Because of the low potential (and poor catalytic

properties of the EMs), current consumption was only 186 mA/m², which translates into an additional energy consumption of 0.014 kWh/m³ when the membrane operates at 20 liters/m² hr (LMH). This value represents 1.86% of the energy typically associated with groundwater RO desalination (0.75 kWh/m³).⁹⁸

A different approach to scaling management involves the electrochemical modification of the local pH along the membrane surface. Water electrolysis along the membrane surface can result in either proton or hydroxide ion production, when the membrane is used as an anode or cathode, respectively (Equations 1 and 2).^{85,92} An EM RO membrane scaled by CaCO₃ was effectively cleaned *in-situ* by applying 2.5 V_{DC} cell potential to the membrane/counter electrode (membrane as anode), which decreased the pH along the membrane surface and dissolved the deposits (Figure 1.3c, d). An opposite approach was used to manage silica scaling on MD EMs treating geothermal brines.⁹² Here, the MD EMs were used as cathodes, which increased the local pH and led to the depolymerization of silicate deposits that completely recovered performance (Figure 1.3e, f). Because these cleaning steps are only applied when performance declines to an unacceptable level, energy consumption is minimal (0.002 kWh/m³ and 0.294 kWh/m³ for the RO and MD membranes, respectively).



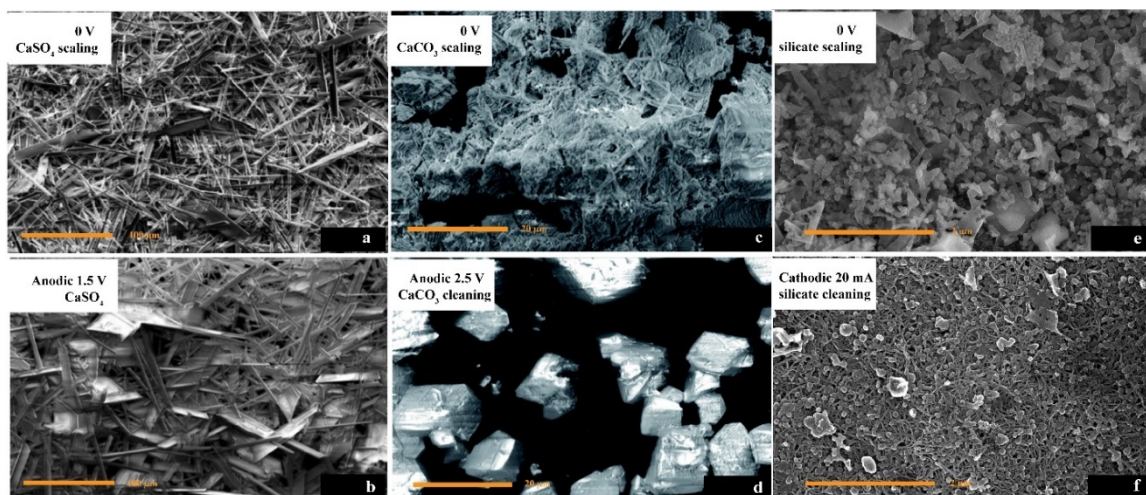


Figure 1.3: Electrochemical mineral scaling prevention and cleaning on EM for desalination. (a, b) CaSO₄, (c, d) CaCO₃ on RO, (e, f) silicate on MD. Reproduced with permissions from (a-d) ref 86. Copyright 2014 Royal Society of the Chemistry. (e-f) ref 93. Copyright 2017 American Chemical Society.

1.5.1.2 Biofilm management on EMs

The formation of a sticky biofilm composed of micro-organisms and extra-polymeric substances on the membrane surface contributes to mass transfer resistance, which reduces membrane performance.^{99–101} All membrane processes, including porous UF/MF membranes and dense NF/RO membranes suffer from biofouling. In general, biofouling control involves pretreatment combined with physical and chemical cleaning.^{99,102} A highly effective method to prevent biofouling involves the application of low potentials to the membrane surface.^{67,103–105} Both anodic and cathodic potentials have been demonstrated to be effective, with potentials as low as 1 V_{DC} cell potential shown to prevent attachment to the surface of EMs (Figure 1.4).^{67,104,105} Under cathodic conditions, it is hypothesized that electrochemical reduction of O₂ to H₂O₂ (490 mV vs. Ag/AgCl) creates unfavorable conditions for bacteria, which prevents them from attaching to the charged surface.¹⁰⁴ Anodic conditions are hypothesized to prevent biofouling through

direct oxidation of bacterial membrane proteins.^{105,106} At potentials below thresholds for hydrogen evolution or above oxygen evolution, microbubble generation and locally extreme pH have been implicated in contributing to the observed anti-biofouling.^{67,105} The bursting of microbubbles generate shock waves that lead to bacteria and biofilm detachment.¹⁰⁷ Since only low potentials are needed to induce the anti-biofouling effect, energy consumption is modest, with values as low as 4.31×10^{-4} kWh/m³ reportedly effective (at a flux of 22 LMH).⁶⁷

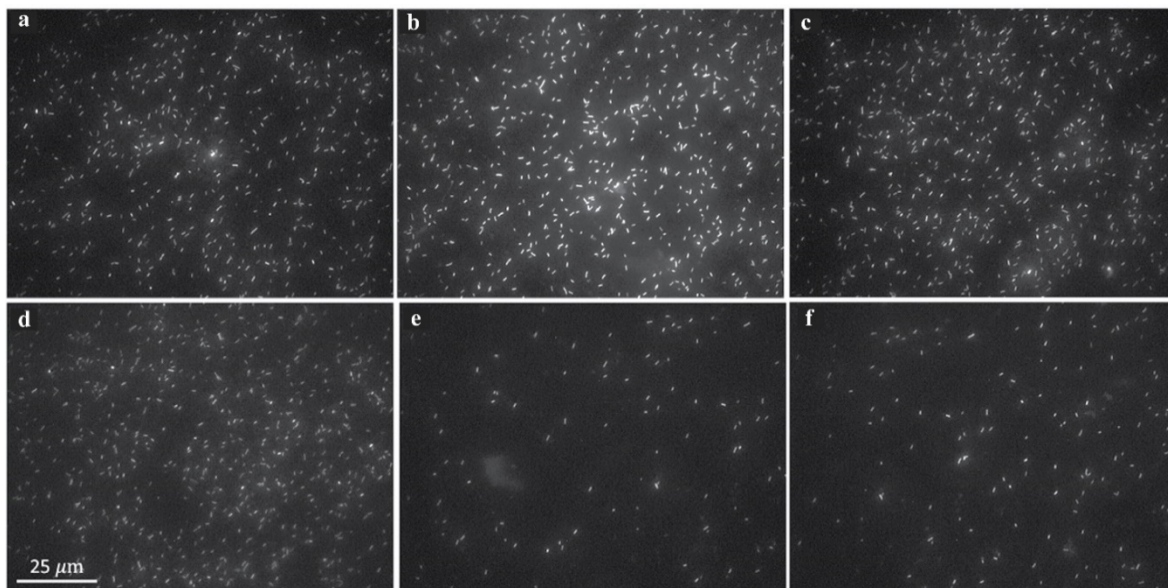


Figure 1.4: Fluorescent microscope images of bacterial deposition (top row) and detachment (bottom row) on an EM surface under different applied potentials; (a, d) 0 V, (b, e) 1.5 Vanodic, (c, f) 1.5 Vcathodic. Far fewer bacteria remain attached when potentials are applied to EM surface. Adapted with permission from ref 105. Copyright 2015 American Chemical Society.

1.5.1.3 Direct heating of MD EMs

MD is a thermally-driven membrane desalination technology suited for the small-scale treatment of high salinity brines or when low-cost, low-grade heat is available.¹⁰⁸ One of the main drawbacks of standard MD is the need for elaborate heat management schemes (using heat exchangers), necessary to maintain the thermal driving force and thermal

efficiency.¹⁰⁸ It has been demonstrated that supplying thermal energy (MD's driving force) by directly heating the membrane surface (optically, electrochemically) can dramatically increase the performance of MD.^{109,110} An alternative heat management approach involves the use of Joule heating EM MD materials. Dudchenko *et al.*⁸⁷ reported on such an EM MD material composed of a 15 μm -thick CNT-polyvinyl alcohol (PVA) film on a hydrophobic PTFE support; using this material eliminates the need for all but a condenser, which dramatically reduced the capital costs of the system. A major obstacle to using EM to heat water was electrooxidation of the CNTs, which was overcome by applying an alternating current at sufficiently high frequencies (Figure 1.5).⁸⁷ This rapid potential switching minimized electrooxidation reactions, which prevented the oxidation of the CNTs. In theory, nearly 100% of water can be recovered using this method, with the only limiting factor being the membrane length and fouling. The heating of a membrane's surface has other potentially useful applications, including the prevention of biofilm formation, as well as changing diffusion rates of molecules through conducting dense films.

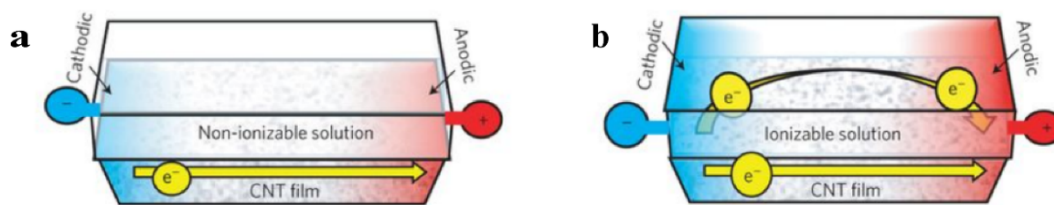


Figure 1.5: Electron pathways in direct heating EM MD materials. (a) In non-ionizable media, electrons can only travel through the conducting materials; (b) in ionizable media, electrons can participate in redox reactions (e.g., electrooxidation), which destroy the CNTs, unless a sufficiently high AC frequency is used. Adapted with permission from ref 88. Copyright 2017 Springer Nature.

1.5.2 Low-pressure EMs for water reuse

An alternative solution to provide accessible clean water is through water reuse. Porous UF and MF membranes do not typically reject ions, but are effective at removing large contaminants such as organic matter, bacteria, and emulsions; these membranes are often used as pre-treatment before the desalination step.⁴⁰ These low pressure membranes operate at higher fluxes and are less energy intensive compared to dense RO and NF membranes.¹¹¹ However, severe fouling from organic, colloidal, biological, and oil fouling are often encountered, which result in membrane pore blocking and cake layer build-up. Therefore, these processes are frequently disrupted by periodic physical and chemical cleaning.¹¹²

Porous EMs have been successfully made using both inorganic (metals and metal oxides) and organic polymeric materials. Ceramic EMs are fabricated through high temperature reduction of metal oxides to their Magnéli phase (e.g., TiO_2 , to Ti_4O_7).¹¹³ In some cases, these membranes are doped with transition metal catalysts to improve electrochemical degradation processes.¹¹⁴ Several approaches have been used to fabricate low-pressure polymeric EM materials, including applying thin-film coatings of CNTs, using conducting polymers (e.g., polypyrrole, polyaniline), embedding carbon fabric into polymers, and using graphene.^{89,115–117} The conductivity of these materials varies, with values ranging between 1,000 – 9,000 S/m, 700-6,000 S/m, and $>10^5$ S/m for CNT, ceramic, and metallic EMs, respectively. The surface and transport properties of CNT-based membranes is highly dependent on the polymers used to cross-link the CNTs, with hydrophilic polymers (e.g., PVA) transforming the normally hydrophobic CNT layer into

a hydrophilic one. Furthermore, the amount of cross-linking polymer can change the pore sizes through the CNT layer, with higher polymer loadings reducing the pore size from MF to UF.⁸⁸ In contrast, ceramic and metallic membranes are typically fabricated from sintered nanoparticles, with pore sizes available in both the MF and UF range.¹¹³

1.5.2.1 *Organic contaminant and biofouling management using low-pressure EMs*

Due to the high concentrations of organic contaminants in wastewater, UF and MF membranes used during the water reuse process are subjected to severe fouling.³ NOMs is one of the major contaminants that can lead to cake layer formation and pore blocking.¹¹⁸ The application of an electrical potential to EMs leads to capacitive charging of the membrane's surface, which promotes hydrophilicity and forms a powerful electrostatic repulsive force that prevents the deposition of like-charged foulants (Figure 1.7a).^{115,116} Modeling the repulsive electrostatic forces using the modified Poisson-Boltzmann equation showed that higher applied potentials allowed organic foulants to “levitate” over the membrane surface. However, this electrostatic repulsive force is sensitive to the solution ionic strength, losing effectiveness in higher salinity environments.¹¹⁵ Furthermore, EMs coupled with electrochemical impedance spectroscopy have been shown to be effective in investigating membrane fouling.^{119,120} The anti-fouling properties of EM are of particular interest in the high-fouling environment of a membrane bioreactor (MBR). Numerous studies have demonstrated that the application of cathodic potentials to an EM results in significantly less fouling in MBRs (Figure 1.6).^{91,121,122} The mechanisms responsible for the observed anti-fouling are electrostatic repulsion, pH modification (electrochemically-generated high pH can degrade deposited organic molecules), and

electrochemical generation of oxidative species (H_2O_2 and Cl_2).¹²¹ The observed anti-fouling has two important implications to MBR processes: 1) less hydraulic and chemical cleaning is needed to maintain membrane performance, which reduces the volumes of waste and chemical storage requirements; and, 2) anaerobic MBRs, which are highly susceptible to fouling because air-scouring of the membranes is not possible, become a viable treatment process. Excellent anti-fouling performance in an anaerobic MBR application was achieved with a power density of 10 W/m^2 , which translated to an additional energy demand of 0.4 kWh/m^3 , when the system was operated at 26 LMH .⁹¹

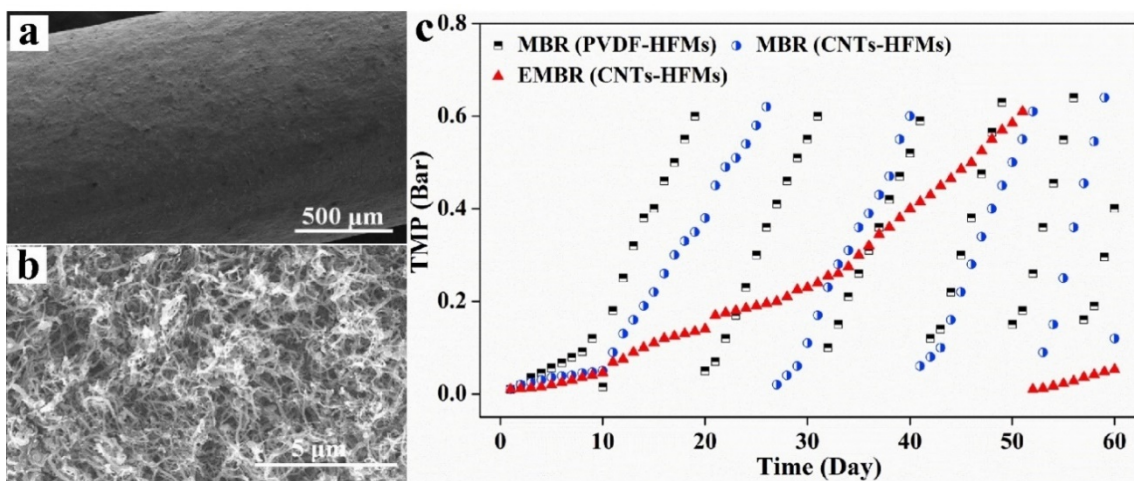


Figure 1.6: SEM images of hollow fiber EMs after electrochemical cleaning in MBR process (a) and (b). System performance of EM and traditional membranes in MBR process (c). Adapted with permission from ref 123. Copyright 2018 Elsevier.

1.5.2.2 Electrochemical reaction-assisted separation

When water (and contaminants) are forced through the pores of EMs (i.e., the membrane acts as a flow-through electrode), the diffusion pathway between said contaminants and the electroactive surface shrinks (to the pore radius).¹¹⁴ This increases mass transfer rates and enhances electrochemical reactions, such as direct electrooxidation/reduction and indirect electrooxidation (e.g., by $\text{OH}\bullet$) (Figure 1.7b).¹²²

Using this method, EMs have been demonstrated to transform a wide range of contaminants, such as trace metals, antibiotics, and pesticides.^{124,125} Thus, low pressure EMs can target contaminants that traditionally demand high-pressure membranes for effective removal. However, a careful examination of electrochemical degradation of contaminants using EMs is needed, as an insufficient treatment can lead to more toxic byproducts. For example, the electrochemical formation of chlorine from NaCl in the source water can lead to toxic disinfection byproducts from reactions with NOMs.

Vecitis *et al.*¹²⁵ used a CNT EM with an average pore size of 115.2 ± 46.7 nm and a thickness of 41.1 ± 7.6 μm to remove two common dyes, methylene blue, and methylene orange. The degradation of these dyes was achieved through a combination of adsorption and electrochemical oxidation rather than size exclusion. An anodic potential of 3 V (cell potential) transformed 90% of the dyes with a 2 s membrane retention time. Similar membranes, made by B- and N-doped CNTs, were used to degrade phenol, which is poorly rejected by standard RO membranes. Here, 8 mg C/L removal was achieved with a 1 s retention time when a 3 V_{anodic} cell potential was applied.¹⁰³ Zaky *et al.*¹²⁴ reported on a Ti₄O₇ ceramic membrane that generates hydroxyl radicals at potentials >2.0 V (versus the standard hydrogen electrode), which were responsible for the degradation of *p*-methoxyphenol. A further study demonstrates that adding Pd-Cu and Pd-In catalysts into this membrane ensures relatively high NO₃⁻ removal through electrochemical reduction.¹¹⁴ Hexavalent chromium (Cr(VI)) contamination in drinking water was electrochemically reduced to the non-soluble (and non-toxic) trivalent form on CNT-based UF EMs.¹²⁴ An exceptionally high ammonia recovery rate from wastewater was achieved using a nickel-

coated CNT gas-stripping membrane, achieved by increasing the pH along the membrane surface, which transformed ammonium to volatile ammonia that was removed through the membrane.¹²⁶ A significant advantage of these processes is that they transform pollutants, rather than just separating them as in standard membrane systems, which eliminates complicated waste disposal. The energy consumption of these processes is higher than previously summarized EM processes, because removal requires a higher potential to affect electrochemical transformation. The additional energy needed to remove 1 ppm of Cr(VI) (>99%) from tap water was determined to be 1.48 kWh/m³, which is less costly than alternatives (e.g., ion exchange and reduction/coagulation processes) and does not generate a hazardous waste.¹²⁴

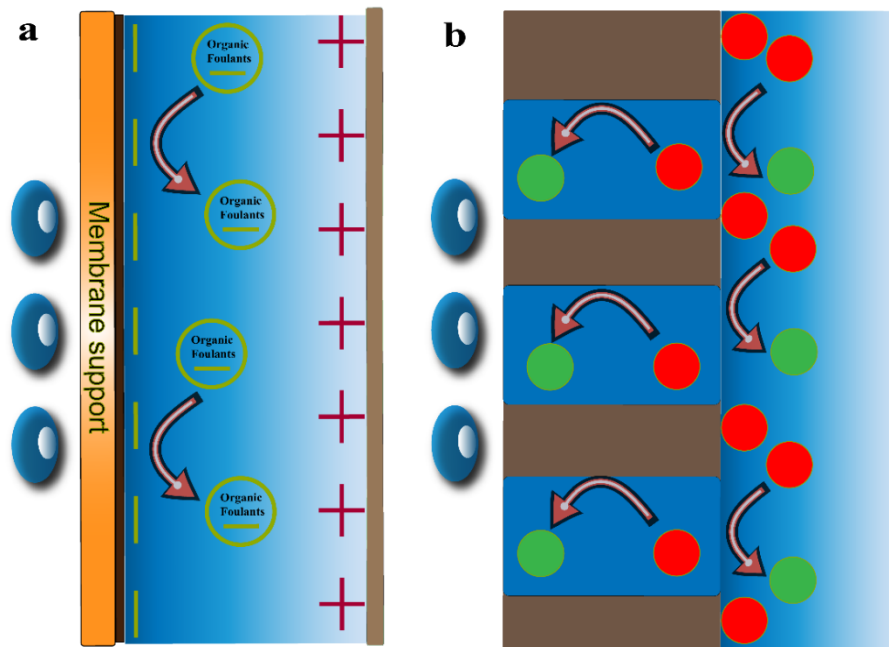


Figure 1.7: EMs for organic fouling inhibition through electrostatic repulsion (a), and electrochemical transformation of micropollutants (b).

1.5.3 Economic Analysis of EM Processes

The fabrication of CNT-based EMs involves the additional cost of adding a CNT layer on top of a porous support. Approximately 0.66 g of functionalized multi-walled CNTs are needed to form a 1 μm thick CNT layer on a 1 m^2 area, which translated into an additional material cost of \$1.83/ m^2 . This accounts for 7% of the cost of a commercial UF membrane. The deposition of CNTs over large areas can be achieved using standard manufacturing techniques such as spray coating, which are not anticipated to dramatically increase the cost of fabrication. A standard RO membrane module (8040) contains approximately 36 m^2 of membrane, which would require approximately 23.8 g of CNTs; CNTs are readily available for purchase at the kg level, and thus, the availability of CNTs is unlikely to be an impediment to the manufacturing of EMs.

Beyond the costs of the raw materials, EM processes consume additional electrical energy. The prevention of mineral scale and biofouling on EM membranes consumes an additional 0.002-0.014 and 4.31×10^{-4} kWh/ m^3 , which represents 0.27-1.87% and 0.06% increase over the energy demands of standard groundwater RO processes.⁹⁸ If the EM process is expected to operate at high potentials (e.g., to modify local pH), corrosion-resistant counter electrodes will likely be necessary. These materials are significantly more expensive (e.g., platinum-coated titanium), so there is a strong incentive to minimize the area of these electrodes, although the impact of dimensional differences between the membrane and counter electrodes has not been explored.

Ultimately, EMs enable higher water recovery and reduced pretreatment and chemical use to prevent fouling. For small capacity RO plants in Egypt, pretreatment units

and chemicals contribute between \$0.59-1.16/m³ to the cost of RO-treated seawater, accounting for approximately 52% of the total cost.¹²⁷ The energy consumption of the pretreatment step ranges between 0.2-0.4 kWh/m³ (8-12% of total energy demand of seawater RO process).¹²⁸ EMs for electrochemical degradation of pollutants have also been demonstrated to be a low energy consumption process.^{114,122} Therefore, EMs offer outstanding potential in terms of minimizing membrane pretreatment costs, particularly in smaller installations.

1.6 Research Objectives

The overall research objective of the dissertation was to explore the application of CNT based electroactive membranes for enhanced water treatment processes. In particular, utilizing these membranes to improve the membrane's oil fouling resistance and to control membrane's rejection toward salt ions in response to different electrical potentials.

Chapter 2 reported UF and NF membrane oil fouling by different emulsion droplets were investigated. Oil droplets were stabilized by surfactants with different charges including anionic, cationic, and nonionic surfactant. Membrane surface fouling was investigated at constant flux mode. The intrinsic properties of emulsion droplets and membrane surfaces such as interfacial tension, droplet size, contact angle, zeta potential and corresponding pressure change in the filtration process were characterized and analyzed, which were linked into a theoretical calculation of membrane surface wetting event. Our results revealed that membrane surface oil fouling is highly dependent on emulsion's surface charges.

Chapter 3 explored membrane oil fouling reduction using CNT-based electroactive membranes at an extreme high ionic strength. A dramatic change in the shape of oil droplets at the membrane/water interface was observed when electric potentials were applied. We proposed that this change was due to the re-distribution of surfactant molecules at the membrane/water interface, which in turn reduced interfacial tension of oil droplets. Thus, the oil coalescence event and subsequent fouling were significantly reduced.

Chapter 4 presented the fabrication of electroactive NF membranes. Electrically conductive NF membranes were fabricated by polymerizing the PA film on top of MWCNT, and single/double walled CNT (S/DWCNT) films, where were named as MWCNT-PA and S/DWCNT-PA membranes. These membrane's rejections were easily tuned by applying different electrical potentials when treating different solution solutions including single salt NaCl, MgCl₂, Na₂SO₄, and MgSO₄, as well as NaCl and MgSO₄ mixed solution. The application of cathodic potentials were shown effective to enhance membrane's rejection toward NaCl and to reduce rejection for MgCl₂ for MWCNT-PA membranes, while no significant change of Na₂SO₄, and MgSO₄ rejections were observed. In contrast to MWCNT-PA membranes, cathodic potentials decreased S/DWCNT membrane's rejection toward NaCl and MgCl₂ solutions, and enhanced the rejection for Na₂SO₄ and MgSO₄ solutions.

Chapter 5 concluded the main results of the dissertation and discussed the application of electroactive membranes for oil fouling mitigation and selective separation of salt solutions. We further discussed the limitation that hindered the application of

electroactive membranes and provided some future research needs to address these challenges.

Chapter 2. **Surfactant-Stabilized Oil Separation from Water using
Ultrafiltration and Nanofiltration**

Adapted with permission from Ref. 16 Copyright Elsevier 2017

Abstract:

The treatment of oily wastewater containing well-stabilized oil emulsions remains a challenge. As gravity-based separation methods cannot effectively remove emulsified oil droplets with sizes below 10 μm , water polishing steps need to be applied to reduce the organic load of the treated effluent. Membrane-based separation processes ensure high permeate quality, but are prone to fouling when treating oily wastes. Surfactants play an important role in producing well-stabilized oil emulsions, but there has been limited work on the effect of surfactants on membrane fouling. To fundamentally understand the surfactant effect on fouling, we studied the fouling of model oil (hexadecane) emulsions stabilized by anionic, cationic and nonionic surfactants in a crossflow filtration system using either ultrafiltration (UF) or nanofiltration (NF) membranes. For this, we investigated the impact of membrane surface and emulsion properties on the different fouling mechanisms observed in our experiments. UF filtration experiments revealed that emulsions stabilized with cationic surfactant quickly fouled negatively charged UF membranes due to electrostatic attraction, while anionic and non-ionic surfactants stabilized emulsions experienced less fouling. In NF filtration tests, membranes exhibited exponential fouling when filtrating all types of surfactant stabilized emulsions. Permeate quality confirms that the NF process achieves better permeate quality than the UF process because of its ability to reject surfactants. However, cationic surfactants are able to pass through NF membranes because of their positive charge. When salt is added to the water, electrostatic forces collapse, and the differences between the surfactants are quenched. Our experimental results combined with theoretical calculations reveal that initial membrane

fouling by emulsified oil drops is dominated by a cake layer formation. However, once a critical pressure drop across the cake layer is achieved, membrane wetting occurs, which results in irreversible membrane fouling in both UF and NF.

KEYWORDS: Oil-water separation, surfactant, ultrafiltration, nanofiltration, membrane surface wetting.

2.1 Introduction

Oily wastewater is produced during oil refining and oil and gas extraction processes [1,2], food processing steps ¹³⁰, metal working and finishing activities ¹³¹, and machinery cleaning activities ¹³². This wastewater is a cause of environmental concern due to the large volumes generated and the challenging treatment steps needed to remove the oily contaminants ^{130,134,135}. Therefore, numerous methods have been developed to treat oily wastewater, including coagulation and dissolved air flotation ¹³⁵, oxidation ¹³⁶, bioslurries ¹³⁸, hydrophobic materials with high oil absorbing capacities ^{139,140}, and membrane separation ^{15, 131,140–144}. Three forms of oil are known to exist in oily wastewater: free floating oil, unstable emulsified oil droplets, and well stabilized oil emulsions ^{134,145}. Free oil is easily separated by gravity, while unstable emulsions require relatively gentle physical or chemical treatment to reduce their stability, which leads to coalescence that allows for gravity separation methods to be effective. However, separating well-stabilized emulsified oil droplets from solution is extremely difficult due to their small size ($< 10 \mu\text{m}$) and high stability ¹³⁴. Emulsified oil droplets are commonly found in metal working and metal finishing industries that produce large amounts of emulsions composed of water soluble coolants, surfactants and lubricant oil from mechanical operations ¹⁴⁶, bilge water that mainly consisting of lubricant oil and detergents from a ship's engine room ¹⁴⁷, and in oil spill clean-up wastewater where dispersants, such as corexit ¹⁴⁸, are frequently applied.

Membrane separation is one of the best options when treating well-suspended emulsified oil droplets because of its high quality permeate and simple operation ^{134,149}.

Microfiltration (MF), ultrafiltration (UF), nanofiltration (NF) and reverse osmosis (RO) have been studied for oil/water separation^{15, 130, 143,150}. MF and UF are able to remove micron and nano-sized particulates like emulsified oil/grease^{151–153}. NF membranes, which have higher rejection due to their dense nature can minimize the passage of large organic molecules (such as surfactants), as well as multivalent ions. RO has the capability of removing monovalent ions such as Na⁺ and Cl⁻. Hence, NF and RO produce a higher quality effluent, and have been used to treat saline oily wastes such as produced water^{141, 144,155–157}.

During the treatment of oily wastewater, emulsified oil droplets accumulate on the membrane surface, which can lead to cake layer formation, pore blocking, oil coalescence, and membrane wetting; these processes all lead to membrane fouling and flux decline^{15, 130,157,158}. Traditional membrane filtration models such as the film model, the blocking model, and the cake filtration model have been extensively applied to describe emulsion fouling^{158–166}. For example, Matsumoto *et al.*, (1999) described nonionic surfactant-stabilized mineral oil emulsions filtrated by a ceramic microfiltration membrane in a dead end process using a cake resistance model. The model demonstrated that the cake layer was highly compressible and had a much higher specific resistance compared to polymethyl methacrylate solid particles¹⁶³. To investigate if oil droplets penetrate into membrane pores under hydraulic pressure, Nazzal (1996) *et al.*, calculated the critical pressure needed for spherical droplets entering membrane pores^{152,167}. More recently, Lu *et al.*, (2015) used a combination of blocking and cake filtration models to analyze different surfactant-stabilized crude oil and diesel emulsion fouling of a dead-end ceramic UF membrane, and

correlated the impact of the emulsions' electrostatic charge on membrane fouling ¹⁹. To visualize the oil coalescence event, Tummons *et al.*, (2016) used track-etch microfiltration membranes in a crossflow filtration system, and direct visualization and force analysis on oil droplets were used to study surfactant emulsified hexadecane emulsion fouling. The results demonstrated that membrane fouling is increased by oil droplet coalescence and reduced by crossflow induced shearing ¹⁵.

In this paper, we study the fouling of anionic, cationic and nonionic surfactant-stabilized emulsions filtrated by UF and NF polymeric membranes in a crossflow filtration system. Emulsions are characterized in terms of size, zeta potential, interfacial tension, and their contact angle with the UF and NF materials. In the filtration experiments, we evaluate the fouling events by using flux step experiments to observe and evaluate membrane fouling inside the system. We explore physical cleaning methods (backflushing and cross-flushing) in an attempt to recover membrane performance, and use these results to help explain our fouling experiments. In addition, the permeate quality is analyzed as a function of the membrane process and surfactant properties, and a theoretical framework is proposed to help explain our experimental findings.

2.2 Materials and Methods

2.2.1 Chemicals

Non-charged surfactant (Triton X-100) (laboratory grade, TX-100) and negatively charged surfactant (sodium dodecylbenzenesulfonate (technical grade, DDBS)) were purchased from Sigma Aldrich and used as received. Sodium chloride (99+%, NaCl),

isopropanol (99.9%+), and a positively charged surfactant (cetyltrimethylammonium bromide (99+%, CTAB)) and hexadecane (99.8%) were purchased from Fisher Scientific and used as received. All surfactants molecular weights, critical micelle concentrations, and molecular structures are reported in Table S1.

2.2.2 Emulsion preparation

The three types of surfactants were used to create feed solutions for the membrane filtration experiments. Feed solutions were prepared by mixing hexadecane (1000 ppm) with a surfactant (100 ppm) in deionized (DI) water using an IKA T-50 homogenizer (Cole-Parmer, IL) at 4000 rpm for 2 minutes. Emulsions were continuously stirred during the filtration process to maintain a homogeneous mixture. In certain experiments, 10 mM NaCl was added to the emulsion solution.

2.2.3 Emulsion characterization

Zeta potentials of the emulsion droplets were characterized by using a ZetaPALS zeta potential meter (Brookhaven Instruments Corporation, NY); prior to their measurement, emulsions were diluted to 5 ppm. Emulsion size distributions were determined by using optical microscopy and image analysis software (ImageJ), as well as using dynamic light scattering (DLS) (Brookhaven Instruments Corporation, NY).

2.2.4 Contact angle and interfacial tension measurement

The contact angle of hexadecane droplets and emulsified hexadecane droplets in contact with UF and NF membranes, as well as the interfacial tension of hexadecane in different solutions was measured using a contact angle goniometer (rame-hart, model 250,

NJ). UF membranes were pre-wetted by isopropanol to remove trapped air within the membrane pores followed by an extended rinse with DI water. Interfacial tension was determined by using the pendant drop method ¹⁶⁸. All measurements were done in triplicate.

2.2.5 Membranes and filtration process

Two commercially available membranes: PS-35 Polysulfone UF membranes (Nanostone Water, CA), and NF-8 polyamide NF membranes (Nanostone Water, CA) were used to treat the oily water and study the fouling mechanisms. Pore sizes of the pristine membranes was characterized by scanning electron microscopy (SEM), with the average pore size of the membranes calculated based on measuring 50 pores ^{169,170}.

The filtration system and control hardware and software are described in Figure 2.1 and elsewhere ^{115,171,172}. The flat sheet membrane module has an open channel with the dimensions of 100 mm x 40 mm x 3.80 mm. The membrane system was operated in constant flux mode, with a proportional-integral-derivative control valve used to adjust the hydraulic pressure to maintain the constant flux of the system. The feed tank for the system was constantly stirred, and the liquid level was kept constant with a liquid level control to maintain constant concentration. A buffer tank stores the excess amount of the permeate which is then used to back flush the UF membrane, as well as to restore the feed solution (Figure 2.1). During the filtration process, feed flowrate was maintained at 1 l/min (crossflow velocity of 11 cm/s) using a diaphragm pump (Hydra-Cell, MN). Prior to the filtration tests, membranes were compressed at 100 psi with deionized (DI) water to

stabilize the membrane permeate flux; the pristine and compressed UF flux ranged between 280-320 $l\ m^{-2}\ hr^{-1}$ (LMH), and the NF flux ranged between 100-110 LMH.

Membranes were operated in the flux step mode^{171,173}. In this mode, the UF membrane was operated at a constant flux for 6 hours, with the flux increasing from 25 – 100 LMH in 25 LMH increments (6 hours in each flux). Between each flux step, the membrane was back-flushed for 5 minutes with the membrane permeate followed with 5 minutes of cross-flushing with the feed solution (at no pressure). For the NF experiments, the fluxes were set to 20, 30 or 40 LMH, and membranes were only cleaned by cross-flushing for 5 minutes between each flux step. To further study whether the flushing process could recover oil-fouled membranes, UF constant flux mode was used to test DDBS and TX-100 stabilized emulsions running at 75 and 100 LMH, and CTAB stabilized emulsions were treated at 25 and 50 LMH separately. For the NF tests, constant fluxes with DDBS stabilized emulsions were filtrated at 30 and 40 LMH, while CTAB and TX-100 stabilized emulsions were tested at 20 LMH. In both UF and NF constant flux modes, fouling was allowed to progress for 2 hours followed by a five minutes hydraulic cleaning step (backflushing or cross-flushing), with this sequence repeated five times. All membrane filtration processes were ended when the required pressure to maintain the constant flux reached 100 psi. All filtration experiments were conducted in triplicate. Membrane rejection was determined by analyzing the permeate using total organic carbon (TOC) analysis (O.I. Analytical, TX).

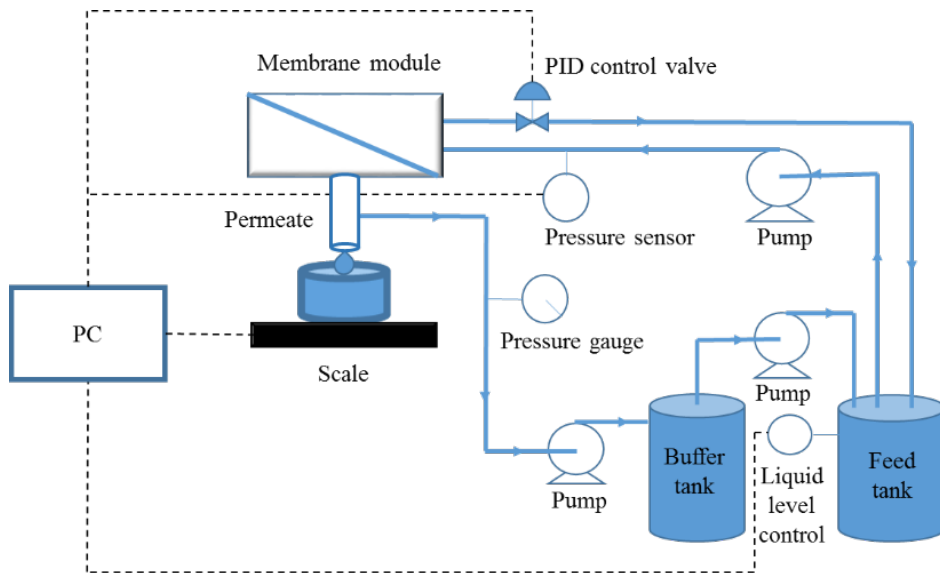


Figure 2.1: Membrane filtration diagram. Blue solid lines represent fluid flow, and black dashed lines represent data and power connections.

2.3 Results and Discussion

2.3.1 Zeta potential and emulsion sizes

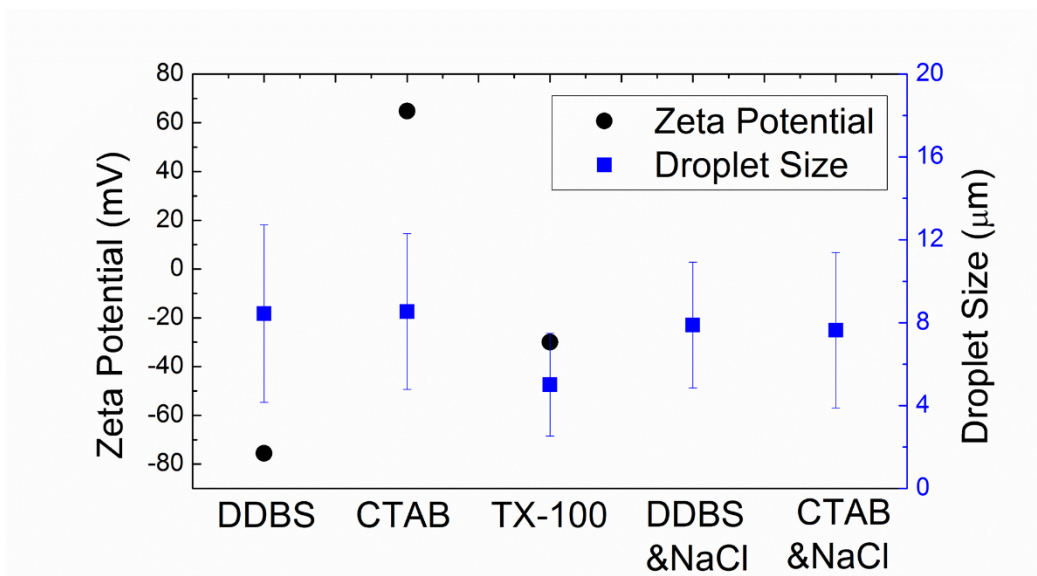


Figure 2.2: Zeta potentials and average droplet size of emulsified oil drops stabilized with different surfactants in DI water and in the presence of 10 mM NaCl. Droplet sizes determined through optical microscopy image analysis.

Properties (diameter, and zeta potential) of the different surfactant-stabilized oil drops can be seen in Figure 2.2. The zeta potentials of prepared emulsions are highly dependent on the charge and polarity of the surfactant. DDBS and CTAB stabilized emulsions have a zeta potential of -75.5 ± 11.0 mV and 64.7 ± 2.4 mV, respectively, due to their charged hydrophilic heads (Figure 2). The zeta potential of TX-100 was found to be -29.9 ± 1.4 mV. The negative zeta potential for TX-100 stabilized surfactant is the result of hydroxide ions (from the surrounding water) that are associated with the hydrophilic head of the surfactant molecule^{156,174,175}. DDBS, CTAB, and TX-100 stabilized emulsions were found

to have an average diameter of $8.4 \pm 4.3 \mu\text{m}$, $8.5 \pm 3.7 \mu\text{m}$, and $5.0 \pm 2.5 \mu\text{m}$, respectively. With the addition of 10 mM NaCl, the size of the DDBS and CTAB stabilized emulsions did not change dramatically, with average sizes of $7.9 \pm 3.4 \mu\text{m}$ and $7.6 \pm 3.7 \mu\text{m}$, respectively. Because the nominally neutral TX-100 emulsions exhibited a negative zeta potential in water (much like the DDBS stabilized emulsions), investigating the impact of NaCl on emulsion properties and membrane fouling was restricted to DDBS and CTAB stabilized emulsions. Membrane pores is characterized by SEM and reported in Figure S1. UF membranes have an average pore size of $19.7 \pm 5.6 \text{ nm}$, while NF membranes have the MWCO from 200 – 300 Da (reported from the manufacture, seen as nonporous in SEM).

2.3.2 Contact angle and interfacial tension measurements

The contact angle of the emulsified oil drops with the two membrane materials and the interfacial tension of different types of emulsions in water can be found in Figure 3 (interfacial tension and contact angle images can be seen in the Supporting Information (Figure S2)). The contact angle of pure hexadecane in DI water with the UF membrane material (polysulfone) was found to be $102 \pm 2^\circ$. The addition of surfactants increases the contact angle to $115 \pm 2^\circ$, $133 \pm 2^\circ$, and $121 \pm 3^\circ$ for the DDBS, CTAB, and TX-100 stabilized oil, respectively (Figure 3). This increase is due to the adsorption of surfactants on the membrane surface and at the oil/water interface, which adds electrostatic and steric forces between the droplets and the surface, which reduces their interaction¹⁷⁶. For NF membranes, the contact angle between the oil and the membrane surface is $154 \pm 2^\circ$, $151 \pm 3^\circ$, $146 \pm 2^\circ$ and $156 \pm 3^\circ$, for the bare, DDBS, CTAB, and TX-100 stabilized oil,

respectively (Figure 3). Upon the addition of NaCl to the emulsion, the contact angle of the DDBS and CTAB stabilized oil with the UF membrane was determined to be $126 \pm 4^\circ$ and $131 \pm 2^\circ$, respectively (Figure 3), indicating that electrostatic forces do not significantly affect the wetting properties of emulsions. The addition of 10 mM of NaCl to the DDBS and CTAB emulsions changed the contact angle with the NF membrane to $154 \pm 4^\circ$ and $157 \pm 4^\circ$, respectively.

Interfacial tension measurements determined that DDBS, CTAB and TX-100 stabilized emulsions in DI water have surface tensions of 27.6 ± 0.3 , 11.2 ± 0.3 , and 10.5 ± 0.2 mN/m, respectively (Figure 3). In the presence of NaCl, the interfacial tensions of DDBS and CTAB stabilized emulsions decreased to 10.7 ± 0.6 and 5.2 ± 0.2 mN/m. This drop is due to the compression of the electrical double layer (EDL), which leads to decreased electrostatic repulsion between the charged heads of the surfactant molecules¹⁷⁷.

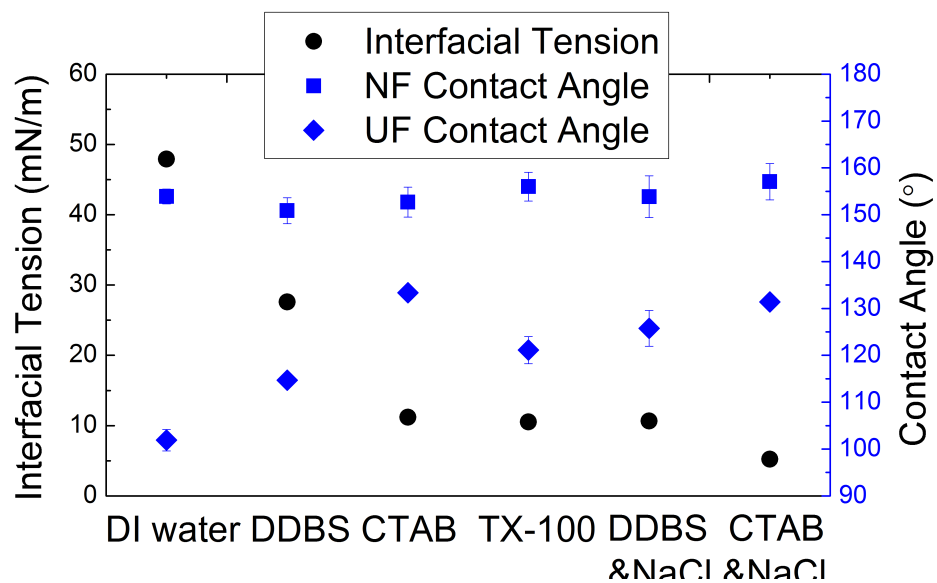


Figure 2.3: Interfacial tension and contact angles with membrane surfaces of hexadecane in water in the presence and absence of surfactants

2.3.3 UF filtration results

2.3.4 UF flux step fouling tests

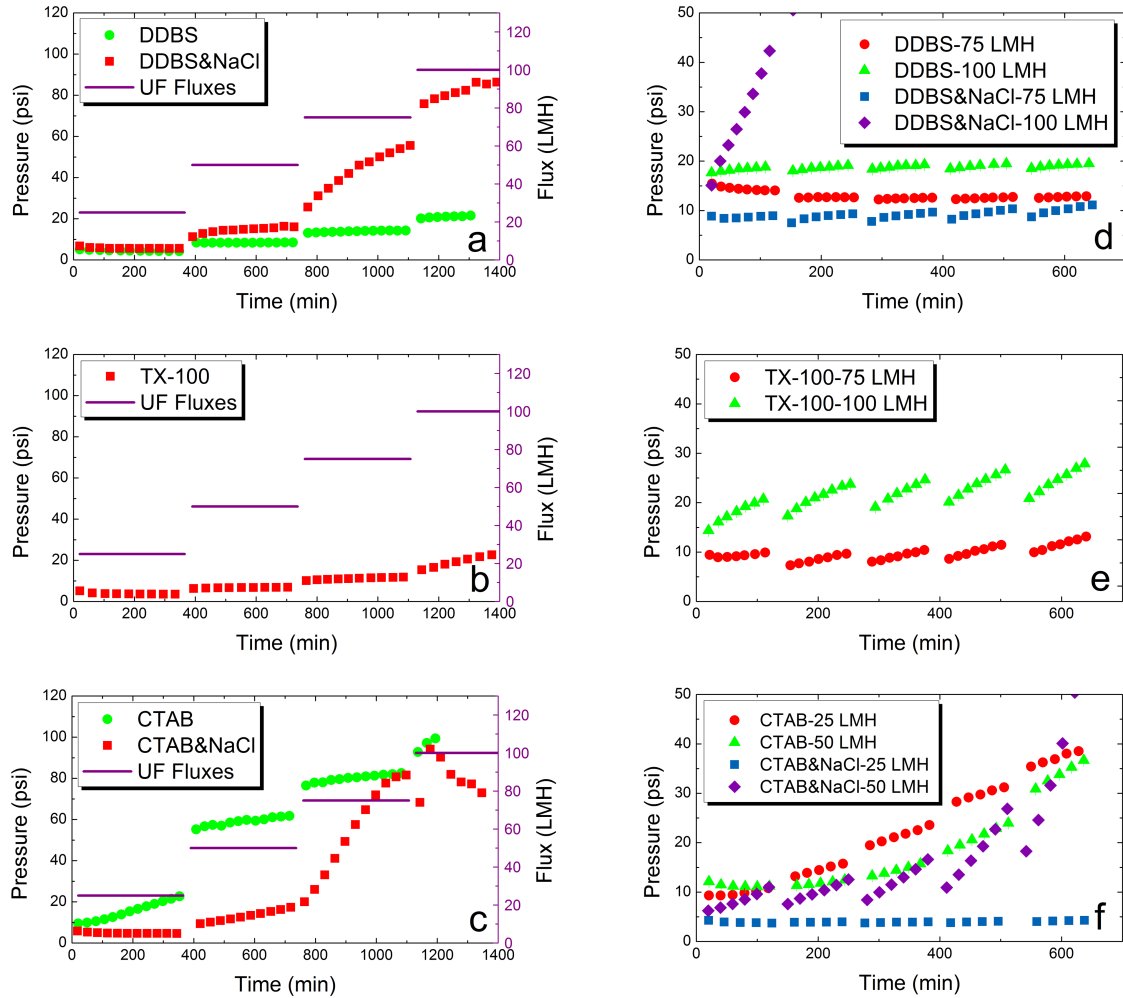


Figure 2.4: UF membrane fouling during the filtration of different surfactant-stabilized oil emulsions. Solid purple lines represent the fluxes set to 25, 50, 75 and 100 LMH in a-c; backflushing events are denoted by the breaks in the pressure data-lines in d-f. a) UF flux step tests for DDDBS stabilized hexadecane in DI water and 10 mM NaCl solution. b) UF flux step results of TX-100 stabilized oil in DI water. c) UF flux step test for CTAB stabilized hexadecane in DI water, and 10 mM NaCl solution. d) UF hydraulic cleaning tests in the presence of DDDBS in DI water DDDBS with 10 mM NaCl filtered at different fluxes. e) Hydraulic cleaning of TX-100 stabilized emulsions in DI water. f) UF hydraulic cleaning tests of CTAB stabilized oil in DI water and 10 mM NaCl under different fluxes.

The results of the flux step UF experiments using the DDBS, CTAB and TX-100 stabilized emulsions are illustrated in Figure 4. As the flux was maintained constant in each step, an increase in pressure corresponds to membrane fouling¹⁷³. In the absence of the background electrolyte, membrane fouling was negligible when filtering DDBS and TX-100 stabilized emulsions, in comparison to the CTAB stabilized emulsions, where significant fouling occurred (Figure 4a-c). When the TX-100 stabilized emulsions were treated at 100 LMH, some fouling was observed, with a linear increase in pressure from 17 to 24 psi over time (Figure 4b). When CTAB stabilized emulsions were treated by the UF membrane, fouling quickly occurred at 25 LMH, as evident by the rapid increase in pressure (from 10 to 23 psi, Figure 2.4c). As the flux was increased in the following steps, the membrane continued to foul, although at a slightly slower rate. We speculate that the fouling observed at 25 LMH is unrelated to the low flux, but rather to the surfactant properties (cationic surfactant). The UF membrane tested in this experiment is made of polysulfone and is negatively charged under the experimental conditions¹⁷⁸. Therefore, the positively charged CTAB emulsions are electrostatically adsorbed to the surface and inside the pores of the membrane, which leads to the observed fouling behavior. To explore the impact of electrostatic interactions between surfactant-stabilized oil and the membrane surface, 10 mM of NaCl were added to the DDBS and CTAB emulsions. The addition of electrolytes to the solution is expected to compress the EDL and reduce the impact of electrostatic interactions between the membrane surface and the surfactant-stabilized oil, as well as between neighboring surfactant-stabilized oil drops¹⁷⁹. As TX-100 stabilized emulsions only have a small negative charge in DI water (Figure 2.2), we did not test the impact of

additional electrolyte on their filtration behavior, as we expect it to be similar to the DDBS stabilized emulsions. Flux step filtration data of DDBS and CTAB stabilized emulsions in 10 mM NaCl are described in Figure 2.4a and 4c. The addition of NaCl to the DDBS stabilized oil emulsions did not have a dramatic impact on membrane fouling at low fluxes (25 and 50 LMH) (Figure 2.4a). However, at higher fluxes (75 and 100 LMH) the membrane rapidly fouled (Figure 2.4a). This is likely due to the elimination of electrostatic repulsive forces between neighboring drops accumulated in the cake layer, which were forced closer due to the stronger drag forces generated at elevated fluxes, leading to oil fouling¹⁸⁰. When NaCl was added to the CTAB suspension, the initial rapid fouling observed at low flux in the absence of NaCl disappeared (Figure 2.4c). This indicates that electrostatic attraction between the positively charged CTAB stabilized oil and the negatively charged membrane surface was responsible for the initial rapid fouling observed at 25 LMH when no NaCl was present; once added, the electrolyte compressed the EDL, which eliminated electrostatic attraction, reducing membrane fouling. At higher fluxes (75 LMH), rapid fouling was observed (similar to the DDBS case), and could be attributed to membrane surface wetting. At the highest flux (100 LMH), the pressure declined (Figure 2.4c). However, under these conditions we observed a sharp increase in TOC concentrations in the permeate, indicating that oil drops deformed and penetrated the membrane (see Sections 3.5 and 3.6 for detailed discussion).

DDBS and CTAB solutions were filtered by UF membranes and their fouling behaviors were reported in Figure 2.S5 (a,b). Pure DDBS solution fouled the membrane at 75 and 100 LMH which may be contributed by the excess amount of surfactant when comparing

to its stabilized emulsions (Figure 2.4a, green circles). For CTAB solution, it caused much less fouling than CTAB stabilized emulsions (Figure 2.4b). In 10 mM NaCl solution, ionic strength started to minimize the charge on the hydrophilic head, thus transforming the surfactants into oil-like molecules (hydrocarbons). DDBS solution experienced less fouling on the UF membrane than its stabilized oil; When filtering the CTAB solution, the membrane was completely fouled at 50 LMH. However, if large amount oil was added, it gives active sites for surfactant adsorption, and fouling could be dominated by the surfactant stabilized emulsions, which can be proved by two similar fouling trends (Figure 2.4a red squares and Figure 2.4c red squares). Therefore, we conclude that membrane fouling happened in UF processes are dominated by surfactant stabilized emulsions.

2.3.5 UF hydraulic cleaning

To investigate the effectiveness of hydraulic cleaning (back and cross-flushing) in recovering fouled UF membranes, constant flux fouling experiments were performed (Figure 2.4d-f). 75 and 100 LMH were tested for DDBS and TX-100 stabilized emulsions because these surfactant-stabilized oil drops did not foul the UF membrane at lower fluxes (Figure 2.4a, 4b). Interestingly, during the first few minutes of operation, the pressure dropped; we speculate that this is due to free surfactant molecules in the solution coating the membrane surface and pores, making them more hydrophilic, which would increase membrane permeability^{181,182}. Backflushing is shown to be effective at recovering DDBS-fouled membranes, as the pressure continuously returned to ~12 psi at 75 LMH and 18 – 20 psi at 100 LMH (Figure 2.4d). TX-100 stabilized emulsions exhibit more significant and irreversible fouling, evident by the steeper pressure increase and the fact that

backwashing was not successful in completely recovering the membrane (evident by the steadily increasing pressure needed to maintain the flux) (Figure 2.4e). In the presence of 10 mM NaCl, hydraulic cleaning of DDBS stabilized oil becomes inefficient (Figure 2.4d). Here, the initial pressure (after backwashing) increases from 7 to 12 psi at 75 LMH, and the membrane rapidly, and irreversibly fouls at 100 LMH. The elimination of electrostatic forces between the oil drops and the membrane upon the introduction of NaCl is likely responsible to the decreased effectiveness of hydraulic cleaning. Once deposited on the membrane, van der Waals forces can hold the drops at the surface, resisting sheer forces exerted during the cleaning process. At 100 LMH, when oil coalescence and wetting of the membrane surface is more likely to occur, hydraulic cleaning is completely ineffective at removing the oil film. Cleaning of membranes treating CTAB stabilized oil at 25 and 50 LMH is described in Figure 2.4f. Under both fluxes, membrane fouling followed a similar pattern, characterized by rapid fouling followed by a more gradual increase in pressure (Figure 2.4f). Hydraulic cleaning was not capable of recovering membrane performance, as evident by the continual increase in pressure over the lifetime of the experiment. When 10 mM of NaCl was added, no significant fouling was observed at 25 LMH. However, at 50 LMH, hydraulic cleaning was unable to restore membrane performance.

The fouling mechanism responsible for the observed UF membrane fouling can be explained by a three step process ¹⁵: 1) oil droplets accumulate on the membrane surface (cake layer formation), 2) droplets deform in response to the pressure drop across the cake layer, and 3) the droplets can coalesce and/or spread along the membrane surface (membrane wetting). Our findings suggest that CTAB stabilized emulsion fouling in the

UF membrane process is mainly driven by the electrostatic attraction between positively charged emulsions and negatively charged membranes. This suggests that positively charged emulsions would lead to more severe fouling than negatively charged emulsions during the UF processes (if the membranes are negatively charged). However, when electrostatic forces are eliminated (i.e. in the presence of sufficient electrolyte concentrations) other emulsion properties such as interfacial tension and emulsion size also have a significant impact on membrane fouling behavior. The ineffectiveness of back-washing for TX-100 stabilized emulsions and DDBS and CTAB in NaCl solution at high fluxes is probably attributed to the combination of oil coalescence and membrane surface wetting (and/or pore wetting), which we further explore in Sections 3.6 and 3.7.

2.3.6 NF filtration results

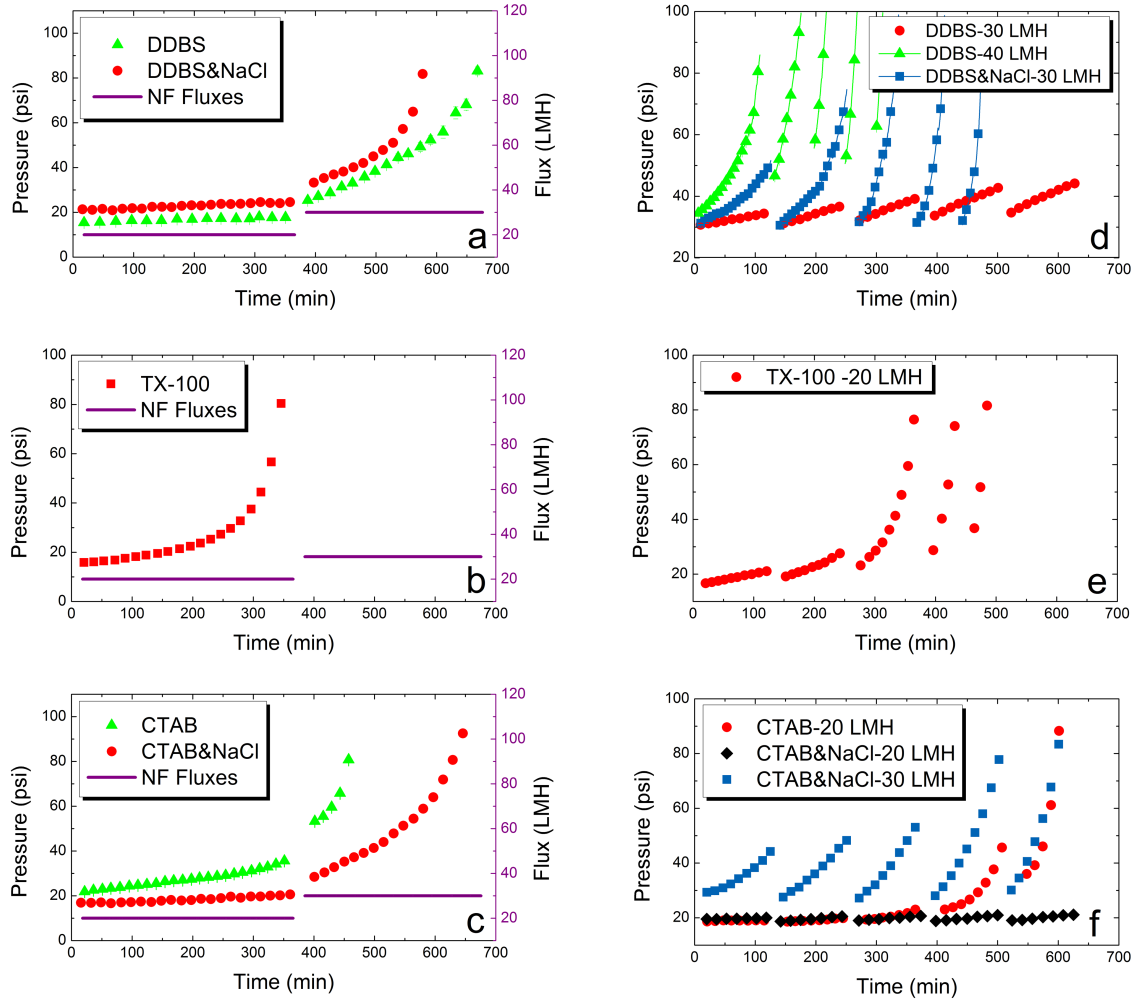


Figure 2.5: NF membrane fouling during the filtration of different surfactant-stabilized oil emulsions. Purple lines correspond to the operating flux of the system were set to 20 and 30 LMH in a-c; hydraulic cleaning (crossflushing) events are denoted by the breaks in the pressure data lines in d-f. a) NF membranes step flux tests of DDBS stabilized oil in DI water and 10 mM NaCl. b) NF filtration test of TX-100 stabilized emulsions in DI water. c) NF membranes step flux tests for CTAB stabilized emulsions in DI water and 10 mM NaCl. d) NF hydraulic cleaning tests of DDBS stabilized emulsions in DI water and 10 mM NaCl. e) NF hydraulic cleaning test of TX-100 stabilized emulsions in DI water. f) NF hydraulic cleaning test of CTAB stabilized emulsions in DI water and 10 mM NaCl.

2.3.7 NF flux step fouling tests

DDBS, CTAB and TX-100 stabilized oil emulsions were treated using NF membranes (Figure 2.5a-c). DDBS stabilized emulsions could resist fouling when the flux was maintained at 20 LMH. However, when the flux reached 30 LMH, rapid fouling occurred; the fouling behavior could be separated into a linear fouling region (375 – 600 min) and an exponential fouling region (600 – 680 min, Figure 2.5a green triangles). For TX-100 stabilized emulsions, the membrane rapidly fouled at 20 LMH (Figure 2.5b); the fouling could be separated into a linear fouling region extended (0–250 min.), and an exponential region (250 – 360 min). For CTAB stabilized emulsions, the membrane was fouled at 20 LMH, with a linear increase in pressure from 22 psi to 37 psi. At 30 LMH, the membrane rapidly fouled (Figure 2.5c). In the presence of 10 mM NaCl, membrane fouling with DDBS stabilized emulsions occurred earlier than in the absence of the electrolyte (Figure 2.5a). In contrast, CTAB stabilized emulsions are more resistant to fouling in the presence of 10 mM NaCl (Figure 2.5c red squares). In both cases, no significant fouling was observed at 20 LMH. However, at 30 LMH, both the DDBS and CTAB stabilized emulsions behaved similarly, with linear fouling between 380 - 500 min. followed by exponential fouling.

DDBS and CTAB solutions were filtered by NF membranes and reported in Figure 2.S4 (c,d). No significant fouling was observed at 30 LMH. Therefore, we conclude that the membrane fouling was mainly caused by emulsions.

2.3.8 NF hydraulic cleaning

NF hydraulic cleaning tests are described in Figure 2.5d-f. No significant fouling occurred when DDBS stabilized emulsions were treated at 20 LMH (Figure 2.5a). Therefore, hydraulic cleaning experiments were conducted at 30 and 40 LMH (Figure 2.5d). No exponential fouling was observed at 30 LMH when periodic cross flushing was applied, although membrane fouling was observed, evident by the gradually increasing pressure, which increased from 31 to 44 psi. Exponential fouling was observed at 40 LMH, indicating that cross flushing is not effective at cleaning oil-fouled membranes. With the addition of 10 mM NaCl to the DDBS stabilized emulsions, exponential fouling was observed at 30 LMH, and membrane performance was not recoverable (Fig 5d). For TX-100 stabilized emulsions, irreversible membrane fouling was observed at the lowest flux tested (20 LMH) (Figure 2.5e). In the CTAB stabilized emulsion cleaning tests, the addition of NaCl eliminated the irreversible fouling observed when no NaCl was present (Figure 2.5f, 20 LMH). At 30 LMH, the membrane is still irreversibly fouled in the presence of 10 Mm NaCl (Figure 2.5f, blue squares).

We hypothesize that the two fouling regimes (linear and exponential) are associated with two fouling mechanisms. In the linear (early) region, a cake layer composed of the rejected emulsified oil drops accumulates on the membrane surface. The narrow paths through the cake layer result in a pressure drop across the layer¹⁶². To maintain a constant flux, the system pressure must increase to compensate for this pressure drop. Based on the Carmen-Kozeny equation (used to describe cake layer fouling), a linear increase of

pressure over time is associated with a non-compressible cake layer ¹⁶³. Thus, in our experiments, conditions during the linear fouling period are not extreme enough to induce oil deformation, which leads to an exponential pressure increase ¹⁶³. In the second, exponential fouling region, two likely events are occurring simultaneously – oil drop deformation and membrane wetting. Certainly, if the membrane becomes wetted by the oil, hydraulic cleaning would only have a limited effect on flux restoration. Also, as the oil drops on the bottom-most layer of the cake layer deform, their contact area with the membrane surface increases, which increases their ability to wet the membrane (see Section 3.7 for detailed discussion). As the cake layer builds in thickness, the bottom-most layer of oil drops must support the forces pushing down on the entire cake layer ⁶. Once a critical cake layer thickness is exceeded (corresponding to a critical pressure drop), the emulsified oil drops will deform, which can lead to the surfactant molecules becoming displaced and the oil coming into contact directly with the membrane surface ¹⁷¹. This wetting of the membrane by the oil will reduce the active membrane surface area and result in drastic pressure increase and membrane failure. This mechanism is further discussed in Section 3.7.

2.3.9 Membrane permeate analysis

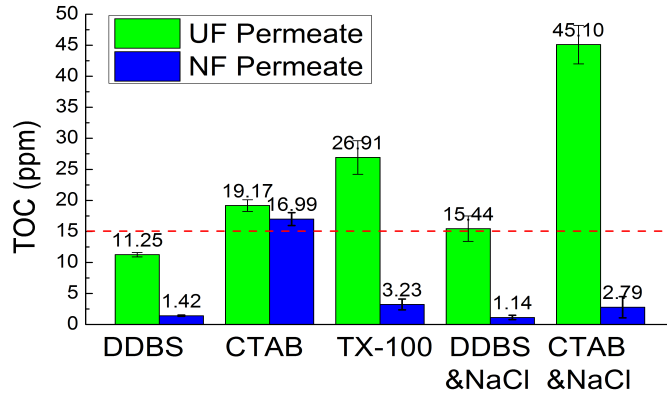


Figure 2.6: TOC analysis of the membrane permeate.

The permeate quality (expressed as TOC) from the UF and NF filtration tests are presented in Figure 2.6. TOC concentrations in the UF permeate were determined to be 11.25 ± 0.25 ppm, 19.17 ± 0.94 ppm and 26.91 ± 2.71 ppm for DDBS, CTAB and TX-100 stabilized emulsions, respectively; these TOC values were obtained after operating the UF system at 100 LMH. Based on these values, the UF membranes achieved a removal of 98.8 ± 0.1 , 97.9 ± 0.1 , and $97.0 \pm 0.3\%$ for the DDBS, CTAB and TX-100 stabilized emulsions, respectively. Unfortunately, under these conditions, the UF membrane was not successful in reducing TOC concentrations in the permeate to below EPA's regulatory limit (15 ppm) when treating CTAB and TX-100-stabilized oil^{132,153}. As expected, NF permeate was superior in terms of oil rejection; TOC concentrations in the NF permeate were consistently below EPA's regulatory limit for discharge of oily wastewater from ships (15 ppm), except for the CTAB-stabilized oil which was slightly above the limit (16.99 ± 1.04 ppm)^{132,153}. The addition of NaCl to the system had a dramatic impact on DDBS and CTAB stabilized

oil rejection by the membranes, with permeate TOC concentrations increasing to 15.44 ± 2.05 and 45.10 ± 3.10 ppm, respectively in the UF permeate. The addition of NaCl reduces the interfacial tension of the emulsified oil drops, with the interfacial tension decreasing from 27.5 ± 0.3 and 11.2 ± 0.3 mN/m, to 10.6 ± 0.6 and 5.2 ± 0.2 mN/m for the DDBS and CTAB stabilized emulsions, respectively (Figure 2.3). The lower surface tension allows for easier droplet deformation, which can lead to the penetration of oil drops into the membrane and their subsequent passing into the permeate. This phenomenon is readily visible in the UF permeate, which appeared milky when the membrane was used to treat a CTAB stabilized emulsion (with 10 mM NaCl). A detailed exploration of oil drop deformation and penetration into the membrane is presented in Section 3.6. The addition of NaCl also had an impact on NF permeate quality, with TOC concentrations decreasing to 1.14 ± 0.35 and 2.79 ± 1.72 ppm in the NF permeate, for the DDBS and CTAB stabilized oil, respectively (Figure 2.6). The small pore size of the NF membrane's active layer (made of polyamide) allows it to effectively remove emulsified oil drops from water. However, specific interactions between the charged groups of the polyamide (negative) and surfactants also impact rejection performance. The positively charged CTAB molecules can interact with the negatively charged carboxyl groups present in the polyamide matrix^{183,184}, which allows the CTAB molecules to effectively enter the polyamide material, as evident by the poor rejection of CTAB stabilized oil. Because of these specific interactions, in our experiments (in the absence of NaCl) the rejection of CTAB stabilized oil was nearly identical for the UF and NF membranes. However, once NaCl was added to the suspension,

these specific interactions were eliminated, which decreased the NF permeate TOC concentrations to 2.79 ± 1.72 ppm (Figure 2.6).

TOC permeate of surfactant solutions were also analyzed and reported in Figure 2.S5. Almost all permeate from UF filtration of surfactant stabilized emulsions had higher TOC values than that of surfactant solutions, which implies that oil passing through the membrane. Except DDBS stabilized emulsions that had similar TOC values comparing to the corresponding DDBS solution (12.46 ± 1.95 ppm). Permeate from NF filtration of surfactant solutions and its stabilized emulsions had TOC values below 4 ppm, only except that CTAB stabilized emulsions had much higher TOC value (15.44 ± 2.05 ppm) than that of CTAB solution (2.30 ± 0.14 ppm). We suspect this is due to the CTAB micelle formation, which has relatively large size that can prevent pure CTAB molecules passing through the membrane ¹⁸⁵.

2.3.10 Emulsion breakthrough during the UF process

Oil emulsion breakthrough during the UF process was observed in the case of CTAB emulsions under 10 mM NaCl ionic strength. A relatively simple expression, based on the Young-Laplace equation, can be used to calculate the pressure needed to deform an oil drop and push it through a membrane's pore (Eq. 1) ¹⁵²:

$$P_{critical} = 2\gamma \frac{\cos(180 - \theta)}{r_{pore}} \times \left\{ 1 - \left[\frac{2 + 3 \cos(180 - \theta) - \cos^3(180 - \theta)}{4 \left(\frac{r_{drop}}{r_{pore}} \right)^3 \cos^3(180 - \theta) - (2 - 3 \sin(180 - \theta) + \sin^3(180 - \theta))} \right] \right\}^{1/3} \quad (1)$$

where $P_{critical}$ is the minimum hydraulic pressure required to force an emulsion droplet to enter a membrane pore, γ is the interfacial tension of the emulsion, r_{pore} is the membrane's pore radius, r_{drop} is the oil droplet radius, and θ is the contact angle between the membrane surface (the region wetted by the oil) and the oil drop.

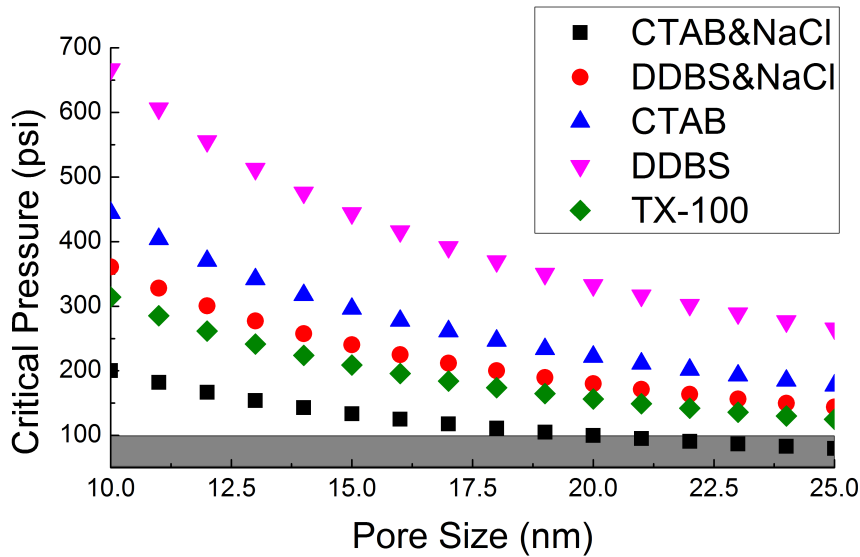


Figure 2.7: Critical pressure required for emulsions to penetrate through the UF membranes based on Eq. 1 as a function of the membrane pore size. The gray region represents the pressure range tested in our experiments.

A plot describing the relationship between $P_{critical}$ and membrane pore size was developed using Eq. 1 (Figure 2.7). In this model, we assume cylindrical pores, and a uniform oil drop size, which is based on the average diameter of the oil droplets measured (Figure 2.2). As expected, because CTAB stabilized oil emulsions in the presence of 10

mM NaCl have the lowest interfacial tension (Figure 2.3), these drops require the least pressure to enter membrane pores. For these emulsions, when the membrane pore size is 20 nm, $P_{critical}$ drops to 100 psi (Figure 2.7). In our study, we found the CTAB stabilized oil in the presence of 10 mM NaCl broke through the UF membrane when the trans-membrane pressure approached 100 psi (Figure 2.4c). These finding correspond well with the UF membrane's average pore sizes (19.7 ± 5.6 nm) as determined by SEM image analysis (Figure 2.S1). At these pores sizes, the model predicts that oil drops under the explored experimental conditions will deform and penetrate the membrane, which could lead to oil in the permeate; this was indeed observed, as evident by the TOC data presented in Figure 2.6. While the model is successful at describing effluent TOC concentrations in the CTAB/NaCl system, it fails to explain elevated TOC concentrations under other conditions (e.g. TX-100, CTAB with no NaCl, and DDBS). Based on the model (using average droplet diameters and interfacial tensions as indicated in Figure 2.2 and 3), the maximum pressures applied in the UF tests never exceed $P_{critical}$ for these conditions, although effluent TOC concentrations are non-negligible (Figure 2.6). It is possible that in all cases, free surfactant molecules passed through the membrane, which would lead to the increased TOC measured in the effluent. This hypothesis is strengthened by the fact that when treated by NF, which can reject surfactant molecules, effluent TOC concentrations are negligible. Another possibility is that small oil drops, which have a smaller $P_{critical}$ value, are passing through the membrane (since $P_{critical}$ is a function of $(r_{drop} / r_{pore})^3$). However, based on the model, DDBS and TX-100 oil drops would have to be on the order of 10's of nm to penetrate the membrane at the pressures used in our experiments. While it is possible

that a fraction of the oil drops is indeed at this size range, we were unable to detect them in the feed and permeate using DLS.

2.3.11 Oil surface wetting of UF and NF membranes

We speculate that membrane surface wetting is occurring during both the UF and NF process, and is responsible for a significant part of the observed pressure increase. In particular, the exponential increase in pressure during the NF process coupled to the failure of hydraulic cleaning to restore membrane flux, indicates that the NF membrane is wetted by oil droplets. The dense active layer of polyamide-based NF membranes renders them practically nonporous (Figure 2.S1)^{187,188}, which makes oil deformation and penetration into the membrane itself unlikely^{155,188}. This essentially rules out the possibility of pore blocking during NF, making surface wetting the likely culprit for the observed exponential fouling. The adhesion energy between emulsion drops and a planar surface can be expressed as^{171,189}:

$$f_w = \pi r_{dc}^2 \gamma \left[\left(\frac{2A}{\sin(\theta)} \right)^{\frac{2}{3}} - A \right] \quad (2)$$

$$A = \frac{2}{1 + \cos(\theta)} - \cos(\theta) \quad (3)$$

$$r_{dc} = \sin(\theta) \left(\frac{3V_d}{\pi((1 - \cos(\theta))^2(2 + \cos(\theta)))} \right)^{\frac{1}{3}} \quad (4)$$

Where f_w is the free energy of adhesion, r_{dc} is the basal radius (the radius of the oil/membrane contact region), A is the contact area of the oil with the membrane, θ is the contact angle between the drop and surface, and V_d is the volume of an emulsion drop. The force required to wet the membrane surface (F_{wr}), defined here as the point where the oil/membrane contact angle reaches 90 degrees (i.e. the point where the membrane surface is fully wetted), can be determined using ¹⁷¹:

$$F_{wr} = \frac{df_w(90^\circ)}{dr_{dc}} - \frac{df_w(\theta)}{dr_{dc}} \quad (5)$$

The force (F_{wr}) required for DDBS, CTAB and TX-100 stabilized emulsions to fully wet the membrane surface (i.e. achieve a contact angle of 90°) as a function of oil drop radius was calculated based on Eq. 2-5. Of the multiple forces that exist between two adjacent emulsion drops in the cake layer that develops on the membrane surface, the dominant (largest) force is a compressive force ($F_{\Delta p}$) caused by the pressure drop across the cake layer (i.e. the sum of drag forces acting on each drop in the cake), acting on the bottom-most emulsion drop; this force can be described as ^{6,160}:

$$F_{\Delta p} = \Delta p S \quad (6)$$

where Δp is the pressure drop across the cake layer (determined from the pressure increase within the linear region of the flux step experiments (Figure 2.5a-c)), and S is the surface area of contact between the oil and the membrane. Thus, if $F_{\Delta p} > F_{wr}$, the membrane will be wetted by the emulsified oil drops, resulting in rapid (i.e. exponential) fouling and failure. During the NF process, as we noted, if the NF membrane undergoes “exponential” fouling, it is impossible to recover using hydraulic cleaning alone (Figure 2.5d-f).

To compare this compressive force ($F_{\Delta p}$) with the force that resists wetting (F_{wr}), we plotted the difference between these two forces ($F_{\Delta p} - F_{wr}$) as a function of the droplet size and pressure drop across the cake layer during UF (Figure 2.8a-e) and NF (Figure 2.9a-e). In these figures, a positive difference (membrane wetting conditions) is denoted by a green color, while a negative difference (non-wetting conditions) is denoted by a red color. In both the UF and NF processes, increasing the emulsion drop size leads to the membrane becoming wetted at lower pressure drops (Figure 2.8, 9). Thus, larger-sized emulsion drops are more likely to wet and irreversibly foul the membrane. This fact is compounded by oil coalescence. The likelihood of oil coalescence is enhanced when oil drops are brought into very close proximity^{190,191}. When emulsified oil drops are densely packed along the membrane surface (within the cake layer), conditions are optimal for coalescence of neighboring oil drops^{190,192}. Thus, oil drops along the membrane surface grow larger over time, making membrane wetting more likely to occur. Membrane fouling during the UF process is defined by a linear increase in pressure (Figure 2.4). This is significantly different than the observed fouling behavior during the NF process, which exhibited linear fouling followed by exponential fouling (Figure 2.5). As stated earlier, we hypothesize that the exponential fouling observed during NF can be ascribed to membrane wetting. However, it is unclear why no exponential fouling is observed during the wetting of UF membranes. One possible reason is the porous structure of the UF membrane that could allow oil that wet the membrane to spread along inner pore walls, which will not necessarily block the entire pore, but would lead to irreversible fouling.

The difference between $F_{\Delta p}$ and F_{wr} during the UF process is presented in Figure 2.8. Based on the membrane and oil characteristics, the model predicts that for the DDBS stabilized oil (with or without NaCl), a pressure drop of approximately 1 psi is required to wet the membrane surface (assuming an average drop size of 8 μm , as reported in Figure 2.2) (Figure 2.8a, e). This prediction fits well with the observed fouling and cleaning data gathered while treating DDBS stabilized oil in 10 mM NaCl; in these experiments, flux is not recovered effectively at 75 LMH (indicated by the increasing initial pressure after each backwashing) because the measured pressure drop is approximately 2 psi; at higher fluxes (100 LMH), the membrane rapidly and irreversibly fouls (Figure 2.4d). When no electrolyte is present, no pressure increase is measured at 75 LMH, and no irreversible fouling is observed (Figure 2.4d). For TX-100 stabilized emulsions, the model predicts that

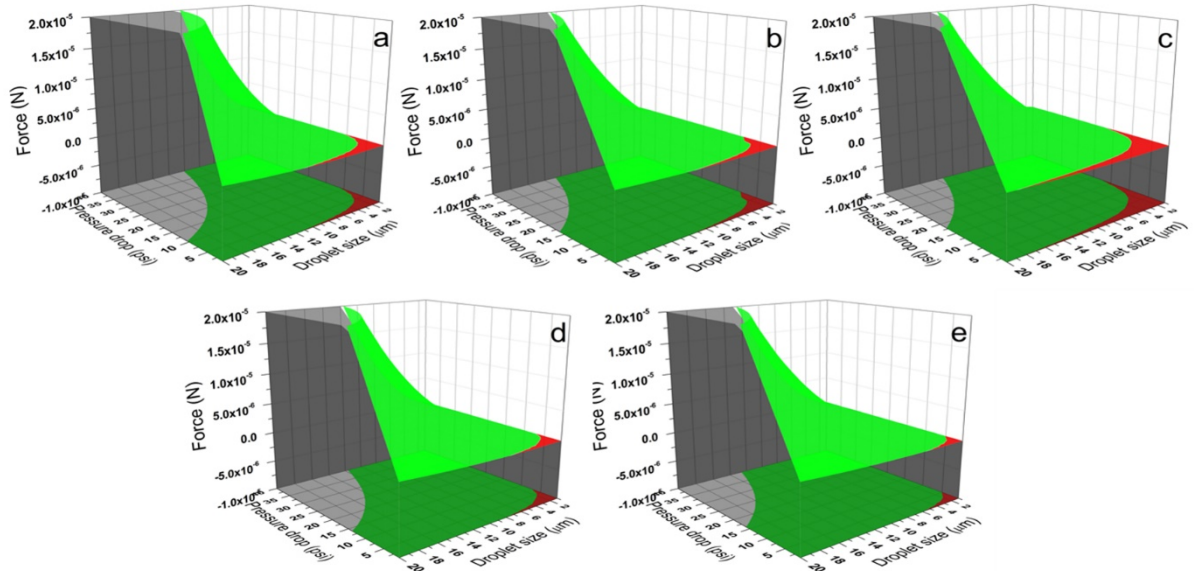


Figure 2.8: Difference between compressive force ($F_{\Delta p}$) and the force resisting membrane wetting (F_{wr}) as a function of droplet size and pressure drop across cake layer on a UF membrane surface; green regions represent a positive differences (wetting) and red regions represent negative differences (non-wetting) conditions, for: a) DDBS in DI water, b) TX-100 in DI water, c) CTAB in DI water, d) DDBS with 10 mM NaCl, and e) CTAB with 10 mM NaCl.

at the average drop size (5 μm), the pressure drop that will lead to oil wetting is 2 psi (Figure 2.8b). Again, this explains the irreversible fouling observed during the UF process, where at 75 LMH the modest pressure increase measured during each filtration period led to irreversible fouling (Figure 2.4e). The conditions during the filtration of CTAB stabilized oil are not captured well in DI water, as the model fails to account for electrostatic interactions between the membrane and surfactant. However, when NaCl is added, the model does do a better job of capturing the interaction between the CTAB stabilized oil and the membrane; based on the model, the membrane will wet at any pressure (Figure 2.8e). Indeed, irreversible fouling is observed at a flux of 50 LMH, and

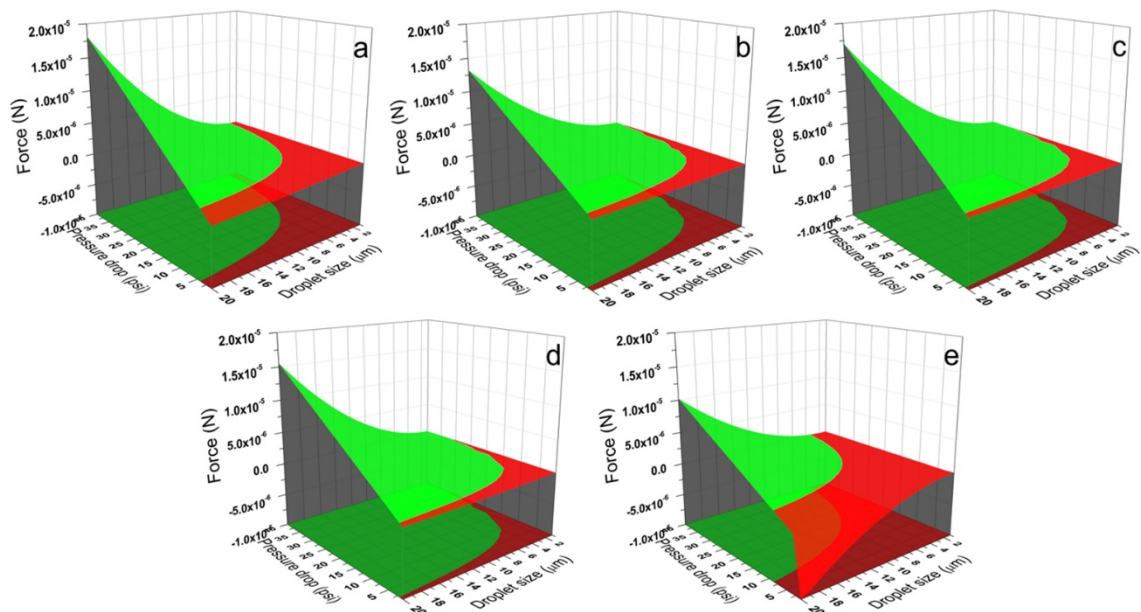


Figure 2.9: Difference between compressive force (F_{Ap}) and the force resisting membrane wetting (F_{wr}) as a function of droplet size and pressure drop across cake layer on a NF membrane surface; green regions represent a positive differences (wetting) and red regions represent negative differences (non-wetting) conditions, for: a) DDBS in DI water, b) TX-100 in DI water, c) CTAB in DI water, d) DDBS with 10 mM NaCl, and e) CTAB with 10 mM NaCl.

no irreversible fouling is observed at 25 LMH where the pressure increase during each filtration period is negligible (Figure 2.4f).

The difference between F_{Ap} and F_{wr} during the NF process is presented in Figure 2.9. The NF fouling process can be described by two regions – a linear and exponential fouling regime. In the NF process, the linear increase in pressure is followed by exponential fouling of the membranes, which we attribute to surface wetting by the oil and/or oil deformation inside the cake layer, although it is impossible to rule out some degree of membrane wetting during the linear fouling region. In DI water, DDBS stabilized emulsions experience a 32 psi increase in pressure (at 30 LMH) in the linear region, which is significantly higher than the linear pressure increase measured during TX-100 (20 LMH) and CTAB (20 LMH) stabilized emulsions (14 psi and 12 psi, respectively) (Figure 2.5a-c). Based on the model (Figure 2.9a-c), assuming average emulsion drop sizes listed in Figure 2.2, the pressure increase required to fully wet the membrane for DDBS, TX-100 and CTAB stabilized emulsions is 10 psi, 7 psi and 5 psi, respectively. This qualitatively matches the linear pressure increase observed in the experiments, where DDBS stabilized emulsions require more pressure increase to fully wet the membrane. When considering the efficacy of hydraulic cleaning (cross-flushing the NF membrane), the cleaning of DDBS-fouled membranes (in DIW) is shown to be not effective under the conditions tested, likely because of the inability to remove oil that wetted the membrane surface; similar results can be seen during the cleaning of TX-100 and CTAB stabilized emulsions (Figure 2.d-f). With the addition of 10 mM NaCl, the pressure increase in the linear region for DDBS stabilized emulsions decreases to 15 psi (Figure 2.5a), which is supported by the lower pressure

increase (5 psi) required to completely wet the membrane (Figure 2.9a, d). For CTAB stabilized emulsions, the addition of NaCl increases the linear region pressure from 12 psi to 30 psi at 30 LMH (Figure 2.5c). A similar change is also predicted by the model, which predicts that a pressure increase of 17 psi is needed to wet the membrane (compared to 5 psi in DI water) (Figure 2.9c). These results support the membrane cleaning results, which demonstrate that hydraulic cleaning is not effective at restoring flux, except when CTAB at 20 LMH is tested (Figure 2.5f). In this case, the linear pressure increase (3 psi) is far smaller than the pressure needed to wet the membrane (17 psi), and the membrane does not wet.

2.4 Conclusions

In this paper, we investigated the fouling of UF and NF membranes by surfactant-stabilized oil emulsions in water. We tested three different surfactants, DDDBS, CTAB, and TX-100, which have a negative, positive, and neutral hydrophilic head, respectively. The emulsions and membranes were characterized using a range of analytical methods. Fouling experiments were conducted using the flux step method. To investigate the impact of electrostatic interactions on membrane fouling, fouling tests were done in DI water or in the presence of 10 mM NaCl. To restore membrane flux, we conducted hydraulic cleaning experiments with the goal of recovering membrane flux. In these experiments, UF membranes were backwashed and NF membranes were cross-flushed every two hours while operating at a constant flux. The permeate from the UF and NF experiments was characterized using TOC analysis to determine the effectiveness of the filtration process to achieve specific water quality goals. In addition to experimental work, we used two

modeling approaches to describe the penetration of oil drops through UF membrane pores and the wetting of the membrane surface by the emulsified oil drops.

Electrostatic interactions between the membrane and the emulsified oil drops were determined to be important for membrane fouling and rejection. The positively charged CTAB emulsions, which are electrostatically attracted to the negatively charged membranes, fouled the membranes rapidly. In addition, these emulsions were able to easily penetrate the UF membranes, which resulted in poor permeate quality. However, upon the addition of NaCl and the subsequent compression of the EDL, no significant difference was observed between CTAB and DDBS stabilized emulsions. In addition, electrostatic forces impact the surface tension of the oil drops. Upon the elimination of these forces, the surface tension declines, which makes oil drop deformation significantly easier. This, in turn, leads to easier drop penetration through UF membranes and increased wetting of both UF and NF surfaces.

We conclude that in both the UF and NF processes, cake layer formation is responsible for the observed linear increase in pressure during the fouling experiments. However, once the pressure drop across the cake layer reaches a critical value, which is dependent on emulsion and membrane properties, including droplet size, contact angle, and droplet interfacial tension, oil drops in the bottom-most layer of the cake layer can wet the membrane surface, which leads to exponential fouling in the NF process. The onset of membrane wetting is characterized by irreversible membrane fouling. When operating below the point where the pressure drop across the cake layer reaches a critical point, membrane flux can be recovered using hydraulic cleaning (i.e. backwashing or cross-

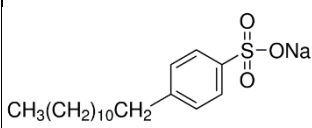
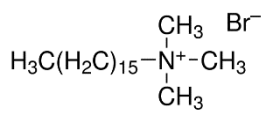
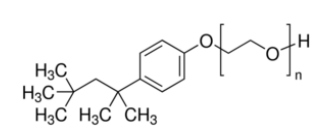
flushing the UF and NF membranes, respectively). However, once the membranes become wetted by the oil, hydraulic cleaning is not effective at restoring flux, and other cleaning methods, such as chemical cleaning, must be employed.

2.5 Acknowledgements

This work was supported by the Office of Naval Research (N00014-14-1-0809).

2.6 Supporting information

Table S1: Characteristics of surfactants used in the system.

Surfactant	DDBS	CTAB	TX-100
MW	348	364	625
*CMC (mM)	1.6 ¹	0.8 ²	0.2-0.9 (20-25°C)
Molecular Structure			

*CMC: critical micelle concentration; Values are based on ¹⁹³ (1.6¹), ¹⁹⁴ (0.8²) and Sigma Aldrich (0.2-0.9 Mm (20-25°C)).

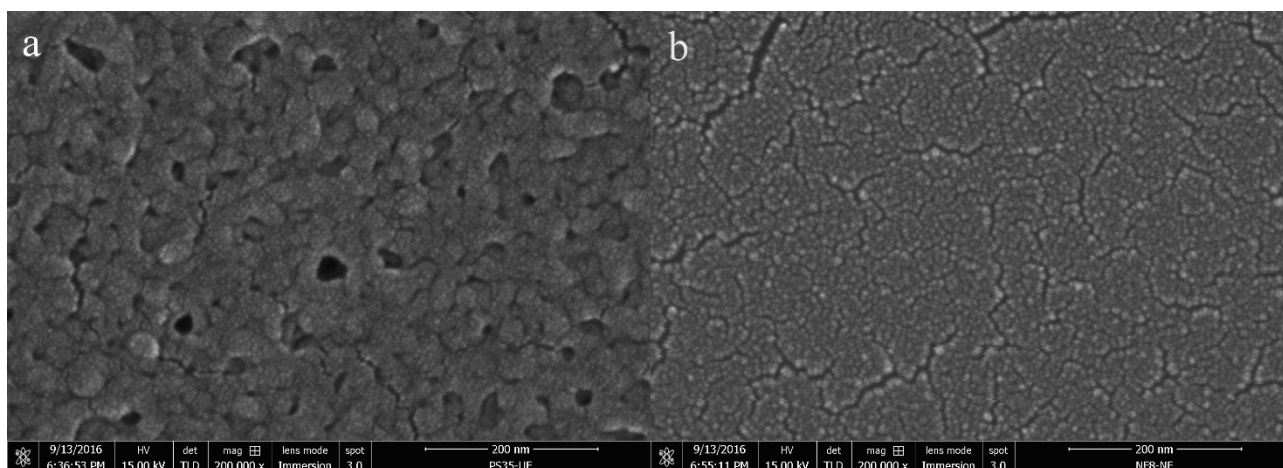


Figure 2.S1: SEM images of UF (a) and NF (b) membrane surface. UF membranes have a relatively large pore size with an average pore size of 19.7 ± 5.6 nm, while the NF membrane is nonporous.

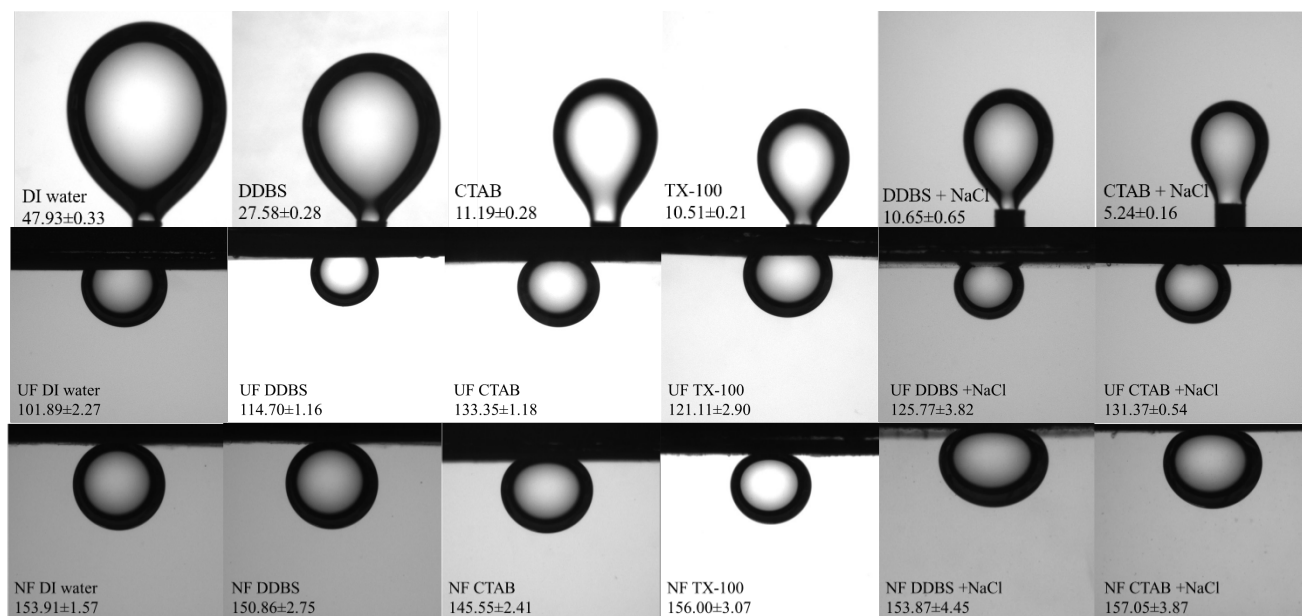


Figure 2.S2: Interfacial tensions (top rows) and contact angles (middle and bottom rows) with membrane surfaces of hexadecane in water in the presence and absence of surfactants. Interfacial tension images and the values are listed in the first line in mN/m. UF and NF membrane contact angle images and values are described in the second and third lines. Oil droplet sizes are 10 μ L in the middle and bottom rows.

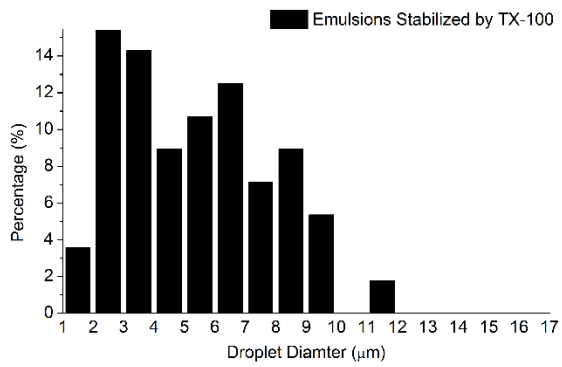
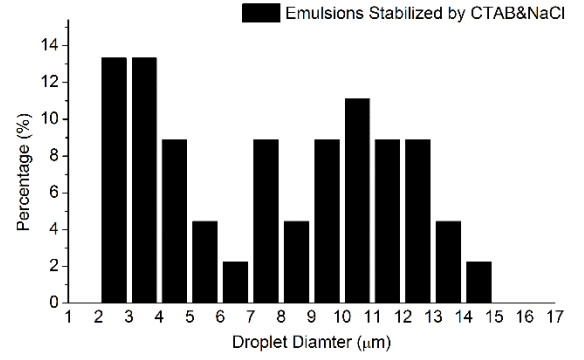
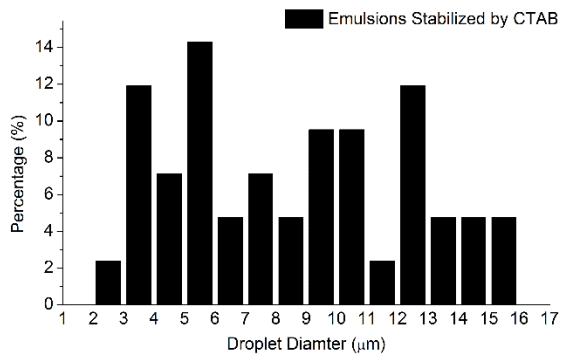
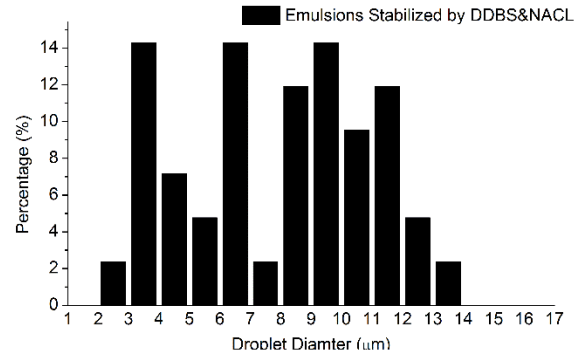
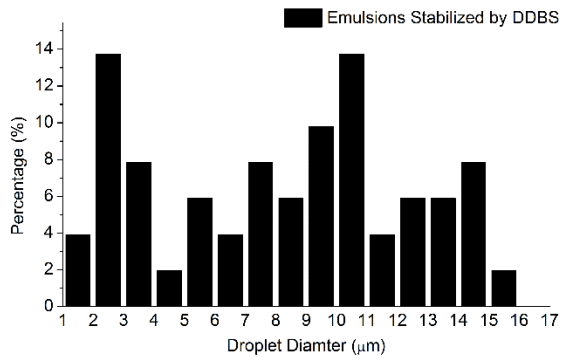


Figure 2.S3: Emulsion droplet size distributions.

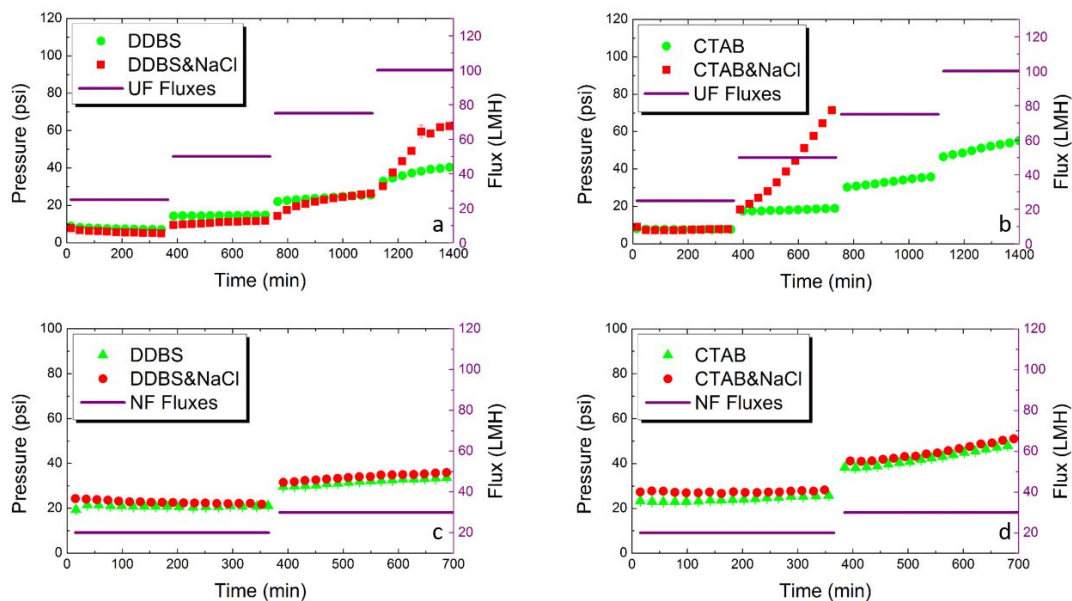


Figure 2.S4: Surfactant solution filtration tests: Solid purple lines represent the fluxes set to 25, 50, 75 and 100 LMH in UF tests (a, b), and 20 and 30 LMH in NF tests (c, d). Flushing events are denoted by the breaks in the pressure data-lines in a-d. a) UF flux step tests for DDBS in DI water and 10 mM NaCl solution. b) UF flux step results of CTAB in DI water and 10 Mm NaCl. c) NF flux step test for DDBS in DI water and 10 mM NaCl solution. d) NF flux step results of CTAB in DI water and 10 Mm NaCl.

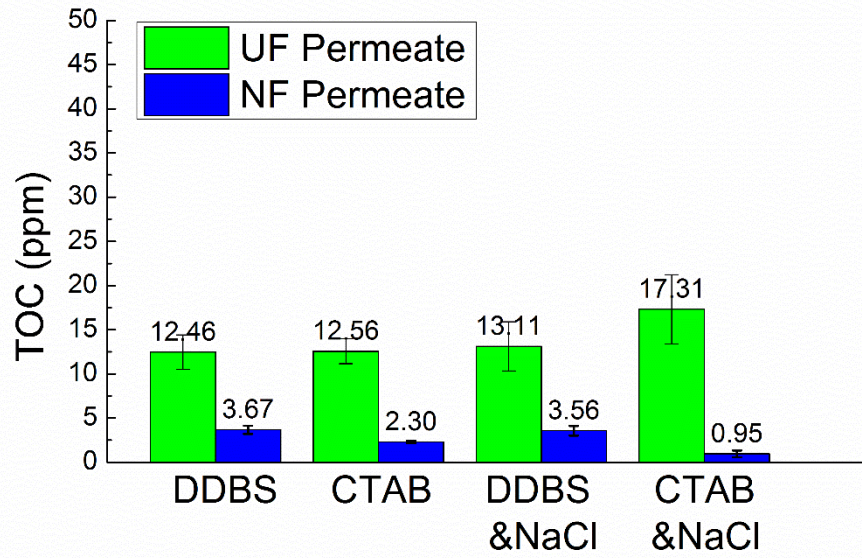


Figure 2.S5: TOC analysis of membrane permeate when treating surfactant solutions.

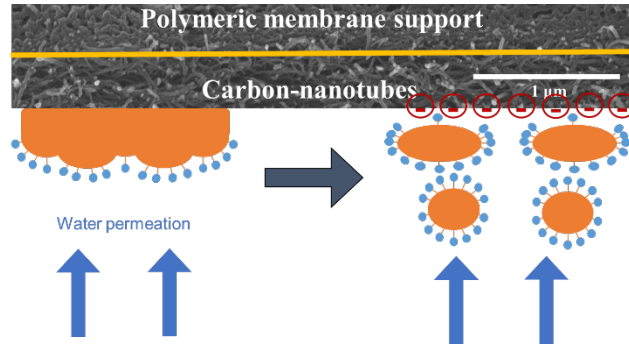
Chapter 3. **Field-Induced Redistribution of Surfactants at the Oil/Water Interface Reduces Membrane Fouling on Electrically Conducting Carbon Nanotube UF Membranes**

Adapted with permission from Ref. 23 Copyright 2018 American Chemical Society

Abstract

Membrane-based treatment of oily wastewater remains a significant challenge, particularly under high salinity conditions. The main difficulty associated with this separation process is membrane fouling, mostly caused by wetting and coalescence of emulsified oil droplets on the membrane surface. In this study, electrically conducting carbon nanotube-based ultrafiltration membranes were used to treat an emulsified oil suspension at ionic strengths as high as 100 mM. By tuning the electrical potential applied to the membrane surface, we demonstrate how fouling can be dramatically reduced, even under high salinity conditions. Permeate water quality is shown to improve upon application of a negative potential. Using optical microscopy, we observed dramatic changes in the shape of oil droplets at the membrane/water interface in response to the applied electric potential; this change is associated with a re-distribution of charged surfactant molecules at the oil/water interface in response to the external electric field. Specifically, using the membrane as a cathode repels surfactant molecules away from the oil/membrane interface, while anodic conditions lead to increased surfactant concentrations. We speculate that this change in surfactant molecule distribution is responsible for changes in the surface tension of oil droplets at the membrane/water interface, which results in a decrease in oil coalescence and subsequent fouling. The membranes used in this study offer an attractive treatment option when separating emulsified oil from water under high salinity conditions.

TOC Art



3.1 Introduction

Oily wastewater is generated from a wide range of industrial activities.^{129, 132, 195, 196} For example, hydraulic fracturing of geologic formations in the pursuit of oil and gas generates large volumes of produced water which can contain large amounts of emulsified oil.^{153, 156, 197} In the United States, there are approximately 60 million barrels of produced water generated daily.¹⁴ The disposal of this water often requires transportation to remote deep-well injection sites, dramatically increasing the cost of produced water treatment.^{198, 199} Another example is the treatment of oil-contaminated bilge water.¹³¹ Traditional gravity-based separation methods are effective at removing large and unstable oil droplets ($>10\ \mu\text{m}$).²⁰⁰ However, emulsified oil drops with sizes $<10\ \mu\text{m}$ are not easily removed by gravity.¹³² Thus, the treatment of contaminated bilge water has been particularly challenging for ship operators. The effective separation of emulsified oil from water would be a step towards the discharge of this contaminated water directly to receiving water bodies.²⁰¹

Membrane separation has been demonstrated to be an effective method for emulsified oil/water separation, with a variety of membrane processes explored for this purpose. Hydrophilic polysulfone ultrafiltration (UF) membranes can reject over 90% of well

stabilized droplets;¹³⁰ hydrophobic polyvinylidene difluoride membranes allow the hydrophobic oil phase rather than the water to pass through, increasing energy efficiency due to the smaller fraction of oil than water in an emulsion;²⁰² forward osmosis membranes demonstrated high water flux and oil rejection;^{145,203} thermally driven membrane distillation processes were shown to be capable of purifying produced water with high salinity and oil content;²⁰⁵⁻²⁰⁸ inorganic membranes, such as glass fiber and copper meshes, decorated with hydrophilic substances to become superhydrophilic or superoleophobic, achieved high rejection rates across a broad pH range (1-13).^{208,209} Due to the relatively large size of emulsified oil drops in water (typically $>1 \mu\text{m}$), low pressure membrane processes (such as UF) are highly effective at removing these oil drops from water;¹⁵ the low energy consumption associated with these membranes make them particularly attractive for the treatment of oily wastewater.¹⁴⁹

While membrane-based separation processes are highly effective for oil/water separations, membranes suffer from fouling, which reduces their performance and requires periodic cleaning.^{144, 163,210} During the treatment of oil emulsion in water, the emulsified oil droplets accumulate on the membrane surface, where they are subject to various forces. While some forces limit membrane fouling (electrostatic repulsive forces between neighboring emulsified oil drops, and between drops and the membrane surface, and lifting forces caused by the tangential flow of water across the membrane surface), other forces promote membrane fouling (drag forces generated by water flowing through the accumulated oil drop layer, and Van der Waals forces). In addition to these forces, the dielectrophoretic force has been used for particle separation due to a net repulsive force

resulting from a non-uniform electric field.^{211,212} When the fouling forces dominate, membrane fouling can result from oil drop coalescence and/or from membrane wetting (i.e., when the oil is absorbed by the membrane).^{15,16,213}

Droplet interfacial properties play an important role in droplet coalescence and membrane surface wetting. In general, an oil-in-water emulsion is stabilized by a layer of surfactant molecules that break strong hydrogen bonds between water molecules along the oil/water interface. This lowers the interfacial tension between oil and water, and also forms a charged droplet surface that can repel one droplet from another, preventing neighboring oil drops from coalescing.²¹⁴

The interfacial tension at the oil/water interface is dependent on the solution ionic strength, with higher salt concentrations leading to lower interfacial tensions;^{216,217} at elevated ionic strengths, screening of the charged surfactant head, as well as possibly a “salting-out” effect allows for higher surfactant packing density at the oil/water interface, leading to enhanced steric hindrance that prevents droplet coalescence.²¹⁶

Carbon nanotube (CNT)-based electrically conducting membranes have shown great promise in preventing numerous types of membrane fouling, such as organic fouling,^{91,115} biofilm formation,^{67,104} and inorganic salt scaling.^{85,92} The goal of study paper is to investigate the fouling behavior of electrically charged membranes during the treatment of well-stabilized oil emulsions under high salinity conditions. Different electrical potentials, as both AC and DC, were applied on CNT membranes at various fluxes and ionic strengths. Membrane properties, droplet characteristics and permeate chemistry were investigated accordingly.

3.2 Materials and Methods

3.2.1 Membranes and chemicals

Commercially available Polyethersulfone (PES) UF membranes with a molecular weight cut off of 20 kDa (Synder Filtration, CA) were used as the conducting membrane substrate in all filtration experiments. Hexadecane (99.8%, Fisher Scientific), sodium chloride (NaCl, 99.5%, Sigma Aldrich), dodecylbenzenesulfonate sodium salt (DDBS, technical grade, Sigma Aldrich) and carboxylic groups functionalized multi-walled CNTs (99wt%, Cheap Tubes, outer diameter of 13-18 nm, tube length of 3-30 μm , and COOH content of 7.0%) were used as received.

3.2.2 Membrane fabrication and characterization

Electrically conducting membranes were fabricated based on a previously published method.⁸⁵ In short, a solution containing 0.1 g/L CNTs and 1 g/L DDBS was sonicated for 30 min using a horn sonicator (450 Digital Sonifier, Branson), followed by centrifugation at 11000 rcf (Avanti J-E Centrifuge, Beckman Coulter) to remove undispersed particulates. After this, 75 ml of the CNT suspension were pressure-deposited on the PES membrane support using a dead-end filtration cell at 60 psi. A uniform CNT layer with a thickness of approximately 2 μm was formed. Membrane surface morphology, expressed as the root mean square of roughness, was characterized by atomic force microscopy (AFM) in tapping mode (scan rate: 0.2 Hz), based on a grid size of 10 μm x 10 μm (MFP-3D Classic, Asylum). A 4-point conductivity probe was used to characterize the membrane sheet resistance (MCP-T610, Mitsubishi). Membrane surface potentials vs. a Ag/AgCl reference

were measured using a 3-electrode configuration (with a Pt-coated Ti plate as a counter electrode) connected to a potentiostat (Figure 3.S1, 600E Potentialstat, CH Instruments).

3.2.3 Emulsion preparation and characterization

Oil emulsions were prepared by homogenizing 5 g/L hexadecane, 100 ppm DDBS, and 0, 10, or 100 mM NaCl in 1.5 L deionized (DI) water at 4000 rpm for 2 min (IKA T50 homogenizer, Cole-Parmer). Size and charge of the oil droplets were characterized by an optical microscope (Axioskop 2 plus, Zeiss) and a zeta potential analyzer (ZetaPALS, Brookhaven Instruments Corporation), respectively. Droplet size distributions were calculated based on the diameters of more than 100 drops, using image analysis software (ImageJ).

3.2.4 Contact angle and interfacial tension measurement

Hexadecane was injected into 100 ppm DDBS solution with 0 and 100 mM NaCl electrolyte. The underwater contact angle and interfacial tension (of the oil/water interface) were measured using a contact angle goniometer equipped with proprietary image analysis software (Model 250, Rame-hart).

3.2.5 Membrane filtration process

For the filtration experiments, electrically conducting membranes were placed into a custom-built cross-flow filtration cell (active membrane area of 10 cm x 4 cm, with a channel height of 3.8 mm) designed to accommodate electrically conducting membranes.⁹¹ A Pt-coated Ti plate, with dimensions identical to active membrane surface area, was placed 3.8 mm above the membrane surface and used as a counter-electrode. Water was circulated through the flow cell using a diaphragm pump (Hydra-Cell, MN), at a flow rate

of 1 L/min, which translates into a cross-flow velocity of 11 cm/s. Prior to studying membrane surface fouling, CNT membranes were prewetted with methanol, then compressed at 100 psi until water flux stabilized at between 60-90 L·m⁻²·h⁻¹ (LMH). Membrane fouling was investigated using a customized filtration system operating in constant flux mode, with the flux maintained at 10, 20 and 30 LMH.^{16,172} For each experimental condition, the filtration process was operated for 2 h in 3 cycles, with a 5-minute backwashing step and a 5-minute cross-flushing step (together termed “hydraulic cleaning”) using the feed solution at 0 psi between each cycle. Membrane fouling was expressed as an increase in the required pressure needed to maintain the constant flux. Electrical potentials of 0 V, 2.5 V_{dc}, 5 V_{dc}, and 2.5 V_{ac} @ 1 Hz were applied to the membrane/counter electrode during the entire filtration process using an arbitrary waveform generator (DG1022, Rigol), with the membrane always functioning as the cathode (i.e., the membrane was negatively charged) when DC potentials were applied; for the 2.5 V_{ac} conditions, a Sine waveform was used (i.e., ±2.5 V). Two ionic strength conditions, 0 and 100 mM NaCl, were tested. All experiments were done in triplicate.

3.2.6 Permeate water quality analysis

Permeate water quality was evaluated by measuring the total organic carbon (TOC) using a TOC analyzer (TOC, 1030W, O.I. Analytical). The surfactant concentration was measured using the formation of the ionic pair between methylene blue and the anionic surfactant.²¹⁷

3.3 Results and Discussions

3.3.1 Contact angle and interfacial tension

Contact angle and interfacial tension measurements are summarized in Figure 3.1e-f. PES-CNT membranes are readily wetted by DDBS stabilized oil emulsion in DI water, with a contact angle of 35.1 ± 3.5 degree (Figure 3.1e). The contact angle dramatically increased to 163.2 ± 1.7 degree when the solution was changed to 100 mM NaCl (Figure 3.1f). This dramatic shift is likely a result of the increased surfactant concentration at the oil/water interface, which forms a more robust layer between the membrane and oil and reduces the likelihood of the oil coming into direct contact with the membrane surface itself. This conclusion is further supported by interfacial tension measurements in the presence and absence of the electrolyte. The interfacial tensions of droplets in 0 mM NaCl and 100 mM NaCl solution were measured using the pendant drop method. In DI water, the oil/water interfacial tension was determined to be 22.8 ± 3.5 mN/m (Figure 3.1g); however, in the presence of 100 mM NaCl, the interfacial tension dropped by a factor of 10 to 2.0 ± 0.6 mN/m (Figure 3.1h). This drop in interfacial tension is associated with the higher packing of surfactant molecules at the oil/water interface enabled by the reduced electrostatic repulsion between the charged groups of the hydrophilic surfactant heads.

3.3.2 Membrane and emulsion characterization

Membrane surface contours, as measured by AFM in tapping mode, were used to evaluate surface roughness (Figure 3.1a, 1b). The pristine PES membranes have a very smooth surface with a roughness of 1.1 ± 0.8 nm (Figure 3.1a). The deposition of the CNT layer increased surface roughness to 47 ± 37 nm (Figure 3.1b). The sheet resistance of CNT

membranes was measured to be $176.1 \pm 9.3 \text{ } \Omega/\square$, which translates into a conductivity of $2839.3 \pm 149.9 \text{ S/m}$. The electrical resistance of the dry membrane inside the flow cell was $289.6 \pm 20.1 \text{ } \Omega$ (measured across a 10 cm flow channel); once water was introduced into the cell, the resistance increased to $412.1 \pm 20.4 \text{ } \Omega$, and stayed constant throughout the experiment. The increase in resistance is likely caused by slight swelling of the CNT layer, which would increase the contact resistance between neighboring CNTs. Furthermore, the fact that the electrical resistance did not change over the course of the experiments indicates that the CNTs formed a stable layer that did not lose CNTs. Our previous study indicated that the pore-size of these membranes was approximately 125 nm, which agrees with findings that state that the pore sizes of a fiber network range between 6 and 8X the fiber diameter.⁸⁹

The pH of the emulsion was determined to be 6.01 ± 0.50 and 5.72 ± 0.30 in the 0 and 100 mM NaCl solutions, respectively. Zeta potentials of oil droplets in DI water and in 100 mM NaCl solution are reported in Figure 3.1c. As can be seen, the zeta potential increased from -63.9 ± 3.5 to $-81.4 \pm 3.2 \text{ mV}$ with the addition of NaCl. Using the Gibbs adsorption isotherm (Section SI 3), we calculated that the surfactant concentration at the oil/water interface increased from $6.268 \times 10^{-7} \text{ mol/m}^2$ in 0 mM NaCl to $3.092 \times 10^{-6} \text{ mol/m}^2$ in 100 mM NaCl (Table S2, Figure 3.S2). This increase is a result of enhanced charge screening of the charged sulfonate groups of the surfactant molecules at higher electrolyte concentrations.^{218,219} This increase in charge density can lead to the observed enhanced zeta potential at higher ionic strengths (Figure 3.1c). While an increase in solution temperature leads to increased measured mobility, we determined that no significant

temperature differences occurred under the 0 mM and 100 mM conditions (due to resistive heating in the solution), and thus, the zeta potential measurements were reflective of enhanced surface charge density at higher ionic strengths. The increased adsorption of surfactant molecules at the oil/water interface is a result of decreased electrostatic repulsion between neighboring adsorbed surfactant molecules, which allows for higher surfactant concentrations at the oil/water interface. Interestingly, there was a dramatic reduction in droplet size after the membrane filtration process (in the retentate), with the size of emulsified oil drops decreasing from 14.9 ± 11.0 before the experiment to 2.4 ± 1.5 μm after the experiment in DI water, and from 7.5 ± 4.5 to 2.2 ± 0.9 μm in 100 Mm NaCl (Table S1, Figure 3.1d). This was likely caused by shear forces in the fluid channel and pump head, which sheared larger drops into progressively smaller droplets.²²⁰ Oil droplets in both DI water and NaCl solutions have similar sizes after filtration, which suggests that droplet size is controlled by the shear rate in the membrane filtration system. Figure 3.1d demonstrates the wide size distribution of freshly made emulsions, ranging from 0 to 40 μm , and the far narrower distribution following the filtration experiments. We believe that the relevant emulsion sizes during these experiments are 2.4 ± 1.5 μm in DI water, and 2.2 ± 0.9 μm in 100 mM NaCl.

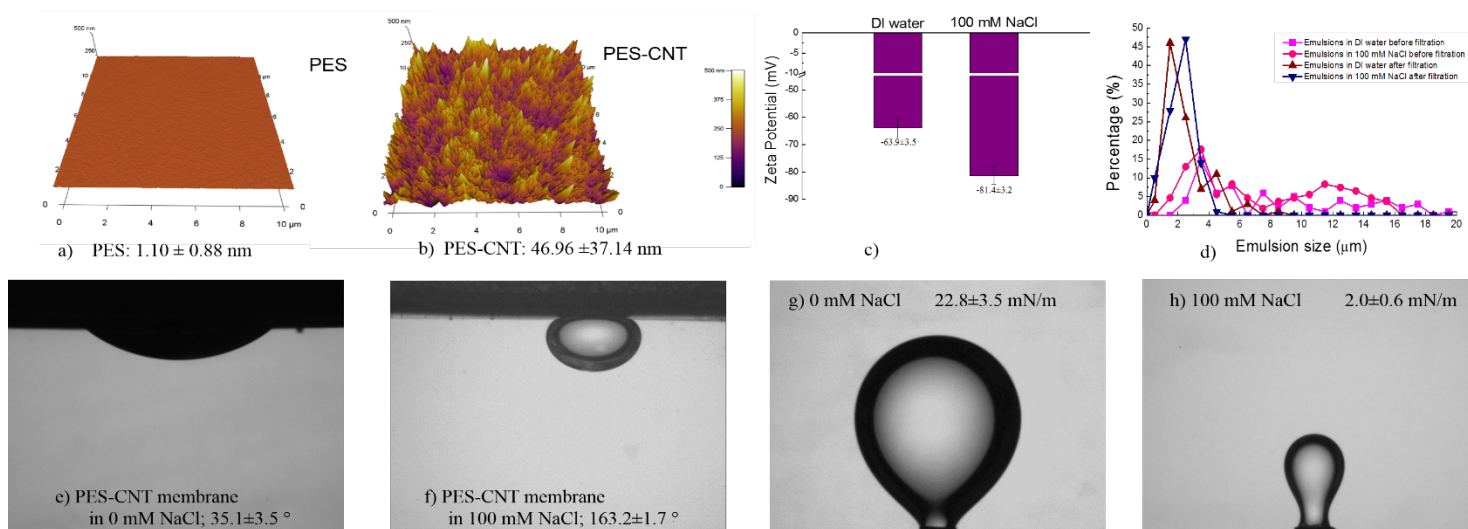


Figure 3.1: Membrane and droplet characterization: Membrane surface morphology and surface roughness of (a) PES membrane and (b) PES-CNT membrane; (c) droplet zeta potentials under different ionic strength conditions; (d) droplet size distribution in DI water and 100 mM NaCl solutions; contact angle of DDBS-stabilized oil droplets on CNT membranes in (e) DI water, and (f) 100 mM NaCl solution; interfacial tension of DDBS stabilized oil droplet in (g) DI water, and (h) 100 mM NaCl solution.

3.3.3 Membrane filtration results

Oil emulsions in DI water or in 100 mM NaCl were filtrated using PES-CNT membranes at 10, 20 and 30 LMH, under different applied electrical potentials (Figure 3.2); Membrane surface potentials versus a Ag/AgCl reference at 2.5 V_{dc} and 5 V_{dc} cell potentials were determined using the open circuit potential method,²¹¹ with potentials of -1,000 mV and -2,300 mV in DI water, and -1300 mV and -3400 mV in 100 mM NaCl, under 2.5 V_{dc} and 5 V_{dc} conditions, respectively (Figure 3.S1). While we did not observe any bubble formation (caused by water electrolysis on the membrane), we cannot completely rule out their formation and/or participation in the observed fouling phenomena. When filtering

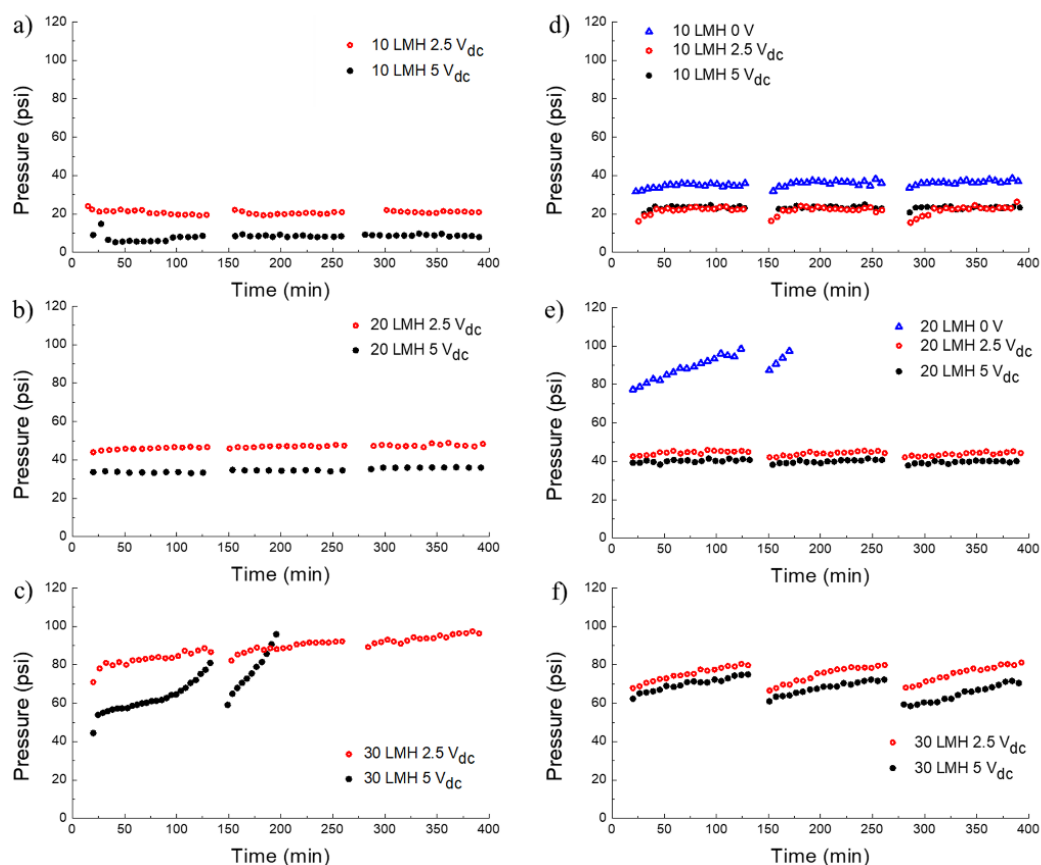


Figure 3.2: Membrane filtration process under different ionic strengths. Membranes were back-flushed every 2 h, as indicated by the break between symbols. Membranes were charged with 0, 2.5 V_{dc} , 5 V_{dc} , or 2.5 V_{ac} and system was operated at fluxes (a) 10, (b) 20 and (c) 30 LMH in 0 mM NaCl. (d), (e), and (f) represent the system being operated with under the same conditions except the solution was changed to 100 Mm NaCl.

emulsions in DI water, PES-CNT membranes experienced instant fouling at 0 V (data not shown). This indicates that intrinsic membrane properties such as surface hydrophobicity leads to rapid membrane wetting, which obstructs the flow of water. The application of 2.5 V_{dc} and 5 V_{dc} reduced membrane fouling, allowing the filtration process to run continuously, with no fouling observed, at 10 LMH (Figure 3.2a). A similar trend was observed in a study by Zhang & Vecitis, where they conclude that a potential-induced change in the concentration polarization layer is responsible for the observed anti-fouling

phenomena.¹¹⁶

Interestingly, the pressure required to maintain a flux of 10 LMH was dependent on the applied potential. When $2.5 V_{dc}$ were applied, the required pressure was 18 ± 3 psi, while when $5 V_{dc}$ were applied, the required pressure was 10 ± 2 psi. The lower initial pressure requirements at higher potentials ($5 V_{dc}$ vs. $2.5 V_{dc}$) may be caused by capacitance-induced hydrophilicity, which results in lower hydraulic resistance. These results indicate that under low ionic strength conditions, the induced electrostatic repulsive forces between the membrane and the emulsified oil drops (both negatively charged) are capable of repelling the oil drops from the membrane surface, which prevented membrane fouling.

When the flux was increased to 20 LMH, membrane fouling was very mild under both applied potentials (Figure 3.2b). Under these conditions, hydraulic pressure gradually increased from 44 to 48 psi, and from 33 to 36 psi after running three cycles under $2.5 V_{dc}$ and $5 V_{dc}$, respectively. Importantly, the fouling, while mild, was not reversible, with the hydraulic cleaning steps (backwashing and cross-flow washing) not capable of restoring flux. Once again, the higher applied potential resulted in lower pressures needed to maintain the flux. When flux increased to 30 LMH, pressure requirements rose sharply (from 80 to 95 psi, and from 55 to 100 psi under $2.5 V_{dc}$ and $5 V_{dc}$, respectively), indicating that severe fouling occurred (Figure 3.2c). Again, hydraulic cleaning was not capable of recovering the membrane's flux.

When treating emulsions in 100 mM NaCl solution, both AC potentials and DC potentials were investigated; here, AC conditions were tested with the goal of inducing dielectrophoresis, which may prevent oil drops from accumulating on the membrane

surface. DC potentials where the membrane serves as an anode were not studied because of the probable occurrence of CNT electro-oxidation.⁸⁹ As shown in Figure 3.2d and Figure 3.S4a, applying 2.5 V_{ac} potentials at 1 Hz and 10 Hz accelerated membrane fouling at 10 LMH, while DC potentials at 0 V, 2.5 V_{dc} and 5 V_{dc} did not foul membranes, with the required pressure remaining constant throughout the experiment. These results indicate that dielectrophoresis does not contribute to fouling prevention, but negative potentials were able to prevent fouling. When oil drops stabilized with the positively charged CTAB surfactant were treated at 10 LMH at 2.5 V_{dc}, the membranes experienced a rapid increase in pressure (Figure 3.S4b). This result shows that electrostatic attractive forces between the negatively charged membrane and the positively charged emulsified oil drops contribute to rapid membrane fouling. Furthermore, as in the DI water conditions, the application of a negative potential to the membrane surface resulted in lower pressures needed to maintain flux. When the flux was increased to 20 LMH, membranes were irreversibly fouled by oil droplets under 0 V, with pressure increasing rapidly from 65 psi to 100 psi (Figure 3.2e). However, the system pressure remained steady (i.e., no fouling was observed) when 2.5 V_{dc} and 5 V_{dc} were applied to the membrane surface, with pressures being slightly lower under the 5 V_{dc} conditions (Figure 3.2e). At 30 LMH, membrane fouling became more significant, resulting in a pressure increase from 68 to 80 psi (2.5 V_{dc}) and 60 to 75 psi (5 V_{dc}) within each cycle (Figure 3.2f). Interestingly, membrane fouling was reversible at this high ionic strength, and the flux could be restored using hydraulic cleaning.

The additional energy associated with the application of electrical potentials to the membrane surface is explored in the SI (SI 12). The energy was estimated to be 0.08

kWh/m³ and 0.42 kWh/m³ at 2.5 V and 5 V, respectively, in 100 mM NaCl, and 0.008 kWh/m³ and 0.10 kWh/m³ for 2.5 V and 5 V, respectively, in 0 M NaCl; these calculations assume a flux of 30 LMH.

3.3.4 Membrane permeate quality

TOC concentrations (a measure of water quality and oil rejection) were measured in the membrane permeate as a function of the applied electrical conditions and ionic strength (Figure 3.S3). In DI water under 0 V, the membrane fouled instantly and no permeate could be collected. When 2.5 V_{dc} and 5 V_{dc} were applied to the membrane surface, TOC values of 32 ± 13 and 21 ± 4 ppm were measured (99.3% and 99.5% removal), respectively. TOC concentrations in permeate generated from emulsions in 100 mM NaCl, were higher: 73 ± 12 and 30 ± 5 ppm under 2.5 V_{dc} and 5 V_{dc} (98.3% and 99.3% removal), respectively. Under 0 V and 2.5 V_{ac} conditions, the permeate showed higher TOC values of 170 ± 30, and 115 ± 45 ppm (96.1% and 97.3% removal), respectively. Not surprisingly, the applied negative electrical potentials behaved as a barrier that repelled both droplets and surfactants, reducing TOC values in the permeate.²²¹ Using the formation of the ionic pair between methylene blue and the anionic surfactant,²¹⁷ the concentrations of surfactant in the permeate were determined to be fairly independent of the ionic strength and electrical conditions, ranging between 10-18 ppm (Figure 3.S3). Thus, majority of the TOC measured in the permeate was likely contributed by oil penetrating through the membrane. Based on our calculations, an average-sized oil droplet in our system (2.2 μm in diameter) would require a minimum pressure of 554 psi to deform and penetrate through the membrane's pores, which is dramatically greater than the operating pressures in our system

(Section SI 10).¹⁶ However, the critical pressure needed to deform oil drops declines with their size. Thus, it is likely that smaller droplets could deform and penetrate the membrane. In addition, it is likely that the application of an electrical potential increases the rejection of these small oil droplets, which results in the overall lower TOC levels measured in the permeate upon the application of cathodic potentials (Figure 3.S3).

3.3.5 Force analysis for droplets near membrane surface

To understand the mechanism behind the observed anti-fouling phenomena, we conducted an overall force analysis on emulsified oil drops along the membrane surface. In our filtration system, the membranes were facing down, which caused the buoyancy force to push the oil drops against the membrane surface, as illustrated in Figure 3.3. The total attractive force between the membrane and the oil droplet is a sum of the permeate drag force (F_d), the buoyance force (F_b), and the short-range Van der Waal force (F_{vdw}). The repulsive force (keeping the oil away from the membrane) is the sum of the cross-flow lifting force (F_l) and the electrostatic repulsive force (F_{es}). The detailed equations used to calculate these specific forces are listed in the Supporting Information (SI 6). Based on our calculation, F_b gives a net attractive force of 10^{-5} nN; the repulsive lift force, F_l , has a value of 10^{-5} nN. These forces are independent of the distance from the membrane surface. At close ranges to the membrane surface (less than 100 nm), the magnitude of these forces was significantly smaller than the other forces in the system (F_d is larger than 10^{-3} nN at 100 nm and larger than 10^{-2} nN at 50 nm). The magnitude of the drag forces experienced by an oil drop are impacted by water flux (10, 20 or 30 LMH). However, these differences are not dramatic, with F_d values of 3×10^{-2} , 5×10^{-2} , and 8×10^{-2} nN for a flux of 10, 20, and

30 LMH at a distance of 5 nm, respectively (Figure 3.S4). The overall force curves at all fluxes are presented in Figure 3.S5. In these curves, positive values represent repulsive forces between the oil droplet and the membrane surface, while negative values represent attractive forces. We assumed a membrane surface potential of -100 mV when no electrical potential was applied, with the negative potential attributed to surface hydroxyl and carboxylic groups on the CNTs.^{115,222} Our modeling results indicate that using the membrane as a cathode can significantly enhance the maximum repulsive force in DI water; for example, at 20 LMH the maximum force increased from 2 nN at -100 mV to 21 nN at -1,000 mV (Figure 3.S5b). Increasing the applied potentials (to -2,300 mV) did not dramatically increase the repulsing force (maximum of 21 nN), although the distance from the surface where the maximum repulsive force occurs extended further away from the membrane (from 5.3 nm at -1,000 mV to 6.7 nm at -2,300 mV). This is not surprising, as the maximum repulsive force is a function of the maximum ionic concentration in the electrical double layer (EDL), with the concentrations reaching saturation at these high potentials.¹¹⁵ Therefore, increasing the potential from $2.5 V_{dc}$ to $5 V_{dc}$ simply increases the thickness of this saturated layer, pushing the point of maximum repulsive force away from the surface. When the ionic strength was increased to 100 mM, our calculations showed that the maximum repulsive force declined relative to the DI water case (Figure 3.S5d-f). Here, the maximum repulsive force was calculated to be 9 nN, 10 nN, and 10 nN for surface potentials of -100 mV, -1,300 mV, and -3,400 mV, respectively (at 20 LMH, Figure 3.S5e). This is caused by the increased ionic strength of the bulk solution, which results in a smaller difference between the concentration in the bulk and the EDL, and consequently to a

smaller difference in osmotic pressure between the bulk solution and the space between the membrane and oil drop. At 20 LMH, the distance where the maximum repulsion occurred increased from 3.6 nm (at -100 mV) to 5.2 nm (at -1,300 mV), to 6.3 nm (at -3,400 mV). Our model also indicates the presence of a very shallow secondary repulsive peak at approximately 17 nm, although it is unclear whether this shallow peak has any real significance. While the force models are quite similar across all fluxes, our experiments show rapid fouling at 30 LMH under all conditions (Figure 3.2c, 2f). Thus, we speculate that an additional mechanism/s are responsible for the observed fouling (i.e., other droplet/membrane and droplet/droplet processes are taking place, which are not accounted for by the force balance described above).

3.6 Proposed mechanisms of reduced membrane fouling

The impact of the applied electrical potential on the shape, contact angle, and interfacial tension of emulsified oil droplets at the membrane/water interface can be seen in Figure 3.3. The shape of the drop changed dramatically as a function of the applied potential. When the membrane was used as a cathode, the oil drop assumed a more oblong shape, compared to the 0 V case (Figure 3.3d and 3e). However, when the membrane was used as an anode, the oil drop became more circular (Figure 3.3f). The shape of an oil drop can be used to calculate the interfacial tension of the drop.²²³ Based on drop-shape image analysis, we determined that the interfacial tension was 1.55 ± 0.30 mN/m at 0 V, decreasing to 0.80

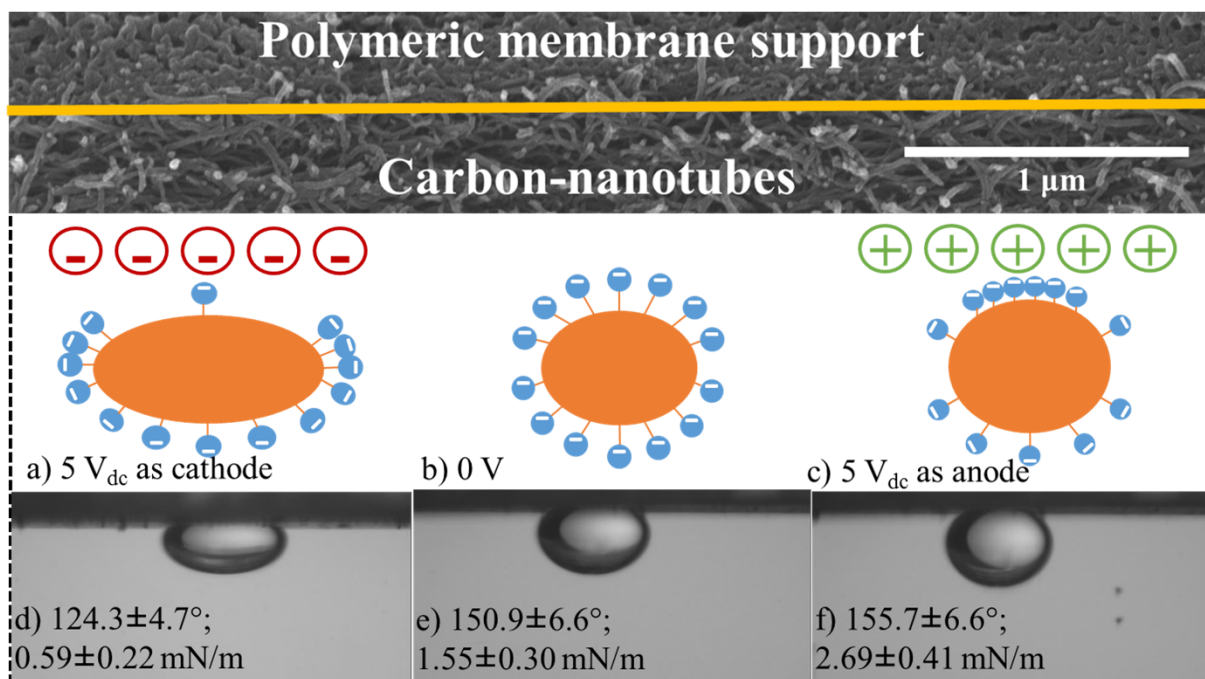


Figure 3.3: Proposed surfactant redistribution at (a) 5 V_{dc} with membrane as cathode, (b) 0 V, and (c) 5 V_{dc} with membrane as anode; Droplet contact angle and interfacial tension in 100 mM NaCl in response to the applied electrical potential (d-f).

± 0.11 and 0.59 ± 0.22 mN/m under cathodic 2.5 V and 5 V conditions, and increasing to 2.69 ± 0.41 mN/m under anodic conditions (Figures 3d-f). The applied potential also resulted in a change in the contact angle of the oil drop, with a contact angle of 150.9 ± 6.6° at 0 V, decreasing to 135.0 ± 4.0 and 124.3 ± 4.7° with a cathodic membrane (2.5 and 5 V_{dc}), and increasing to 155.7 ± 6.7° with an anodic membrane (Figures 3d-f). We propose that these changes are caused as a result of a change in the surfactant distribution at the oil/water interface in response to the applied potential. We confirmed this interfacial tension (oil-membrane interface) change using our experimental contact angle data in SI section 1.5 (used to model surface wetting). DDBS (used to stabilize the oil) is an anionic surfactant with a negatively charged sulfonated functional group. When the membrane was used as a cathode, the ionic heads of the surfactant were repelled from the membrane and

redistributed around the oil drop (Figure 3.3a). As a result, fewer surfactant molecules were left at the oil/membrane interface, while more surfactant molecules were located at the oil/water interface, which would explain the lowering of the membrane/oil contact angle, and the lower oil/water interfacial tension measurement. The opposite phenomenon occurred when the membrane was used as an anode, i.e., the negatively charged surfactant molecules were attracted to the membrane surface, which results in more surfactant at the membrane/oil interface (higher contact angle) and less surfactant at the oil/water interface (higher interfacial tension, and less electrostatic repulsion between neighboring droplets). Oil in water emulsions with a higher interfacial tension (at the oil/water interface) tend to coalesce more, which can lead to enhanced membrane fouling.²²⁴

In general, emulsions with lower contact angle will wet the membrane surface more easily, causing membrane fouling.²⁰⁵ However, in our system we observed an opposite phenomenon, namely, reduced fouling under cathodic conditions. Therefore, we propose that the dominant fouling mechanism under high ionic strength conditions is due to droplet coalescence, which results in larger oil droplets, making pore blocking and membrane wetting more likely.^{156,213} A schematic of our proposed fouling mechanism can be seen in Figure 3.4a. As can be seen, cathodic or anodic potentials lead to different surfactant distributions around oil drops along the membrane surface, which impacts their propensity to coalesce and wet the membrane. To determine the likelihood of oil drops at the membrane surface to experience coalescence under our experimental conditions, we used the film drainage model (SI 8, Table S4).²¹ In this model, the coalescence frequency, λ , is defined by the drainage time, $t_{drainage}$, and contact time, $t_{contact}$ (see Equation 1). The

explicit expressions used to describe $t_{drainage}$ and $t_{contact}$ are listed in the SI (Section 1.6). Upon rearrangement, λ can be expressed as a function of the interfacial tension, γ , and a positive constant (C) (Equation 1). Based on our calculations, λ decreases from 0.19 ± 0.04 at 0 V to 0.04 ± 0.02 at 2.5 V_{dc}, and 0.02 ± 0.01 at 5 V_{dc} in 100 mM NaCl. Under anodic 5 V condition, λ increased to 0.38 ± 0.02 . Therefore, negative membrane potentials reduced the probability of droplet coalescence.

$$\lambda = \exp\left(-\frac{t_{drainage}}{t_{contact}}\right) \sim \exp(-C\gamma^{-1}) \quad (1)$$

To estimate the relationship between the increased droplet size (from coalescence) and membrane wetting, we made some highly simplifying assumptions. Specifically, we assumed that when oil drops accumulate in the cake layer, they do not deform, instead acting as solid spheres that are in direct contact with each other. In fact, for droplet coalescence to occur, oil drops must first come in direct contact with each other (i.e., film drainage must occur). Thus, we believe these assumptions are supported by our experimental findings. We use these assumptions to calculate specific values for the different forces occurring at the membrane/oil interface; importantly, while these assumptions ignore certain droplet properties, we believe our results are relevant in terms of trends, if not necessarily in terms of absolute values.

The accumulation of oil drops at the membrane surface forms a cake-layer, which results in a pressure drop across the layer; this pressure-drop was determined from the increase in pressure during the first cycle (Figures 2d-f) and used to calculate the compressive force ($F_{\Delta p}$) acting on an oil drop at the membrane/water interface (SI 9; Table S5).^{16,6} We defined ΔF as the difference between $F_{\Delta p}$ and the surface force resisting

membrane oil wetting (F_{wr} ; Equations S25-S27). The magnitude of ΔF is highly dependent on the droplet size, with larger drops leading to more wetting (Equation S28). A positive ΔF value indicates membrane wetting will occur. ΔF values were plotted as a function of the droplet size (Figure 3.4b-d). At 10 LMH, ΔF is negative for droplet sizes smaller than the average droplet size (a radius of 1.1 μm in 100 mM NaCl), regardless of applied electrical potentials (Figure 3.4b). However, under the 2.5 Vac condition, droplets have a higher probability of coalescence ($\lambda = 0.38 \pm 0.02$). We speculate that under these conditions, droplets will coalesce, with their radius increasing beyond the size where ΔF becomes positive when (radius > 1.6 μm), resulting in membrane wetting (Figure 3.2d, Figure 3.4b). When flux was increased to 20 LMH, no significant fouling was observed under the 2.5 V_{dc} and 5 V_{dc} conditions, but the membrane rapidly fouled at 0 V (Figure 3.2e). In the case of 0 V, the model predicts wetting when droplets are larger than 0.2 μm (Figure 3.4c). In contrast, the model predicted positive ΔF values for droplets > 0.6 μm under the 2.5 V_{dc} and 5 V_{dc} conditions (Figure 3.4c). Under the 0 V conditions, some coalescence is likely taking place ($\lambda = 0.19 \pm 0.04$), which would grow the droplet drops, and facilitate wetting. Under 2.5 V_{dc} and 5 V_{dc} λ decreases to 0.04 ± 0.02 and 0.02 ± 0.01 , respectively, which would limit coalescence. It is known that small particles (droplets) are preferentially deposited on rough surfaces, such as our membrane.^{225,226} Thus, considering the droplet size distribution, and the very low coalescence probability, it is possible that the fouling layer is composed of non-coalescing drops with sizes < 0.6 μm , which do not wet the membrane, and do not lead to irreversible fouling. When the flux increased to 30 LMH, no irreversible fouling was observed under 2.5 V_{dc} and 5 V_{dc} conditions (Figure

3.2f), indicating that no membrane wetting occurred. Again, we reason that this is caused by the dominance of small oil drops in the cake layer ($<0.25 \mu\text{m}$) and the lack of coalescence events (Figure 3.4d). Interestingly, the model predicts larger ΔF values under $5 V_{dc}$ conditions, compared to $2.5 V_{dc}$ when the droplet size exceeds the critical threshold (Figure 3.4b-d). This is likely caused by the higher interfacial tension (oil-membrane interface) and lower contact angles at the higher potential induced by the enhanced redistribution of surfactants (section 1.5 in SI).

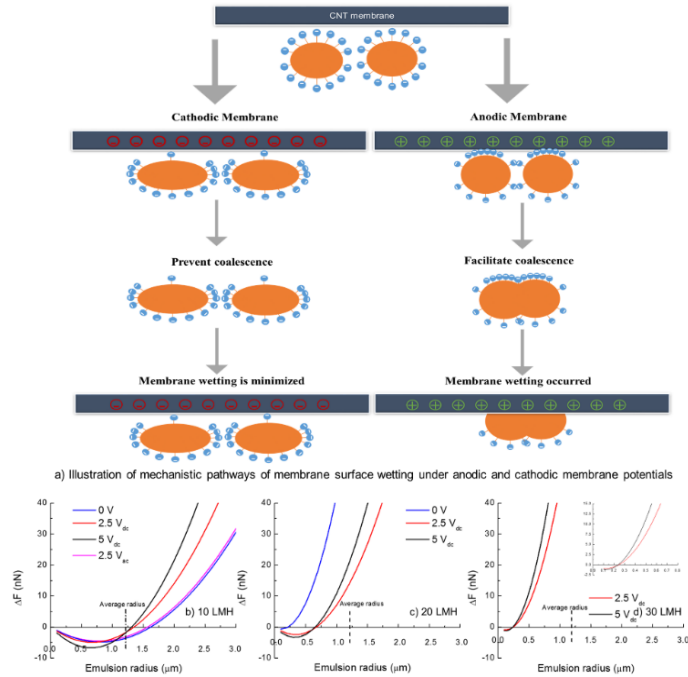


Figure 3.4: (a) Illustration of mechanistic pathways of membrane surface wetting under anodic and cathodic membrane potentials. Impact of droplet size on membrane surface wetting under (b) 10 LMH, (c) 20 LMH and (d) 30 LMH;

3.4 Additional Information

Detailed information on emulsion size distribution (Table S1); membrane surface open potential (Figure 3.S1); surfactant surface density (Table S2); the correlation between the interfacial tension and surfactant concentration (Figure 3.S2); membrane permeate quality (Figure 3.S3); additional membrane filtration results for 2.5Vac at 1 and 10 Hz, and cationic surfactant stabilized droplets (Figure 3.S4); force calculation and combined force curves (Table S3, Figure 3.S5); emulsion interfacial tension calculation (oil-membrane interface) (Figure 3.S6); coalescence probability calculation (Table S4); membrane surface wetting (Table S5); a summary of previous studies using membrane treating oily wastewater (Table S6); energy and cost analysis (SI 12).

3.5 Acknowledgements

This work was generously supported by the Office of Naval Research under award number N00014-14-1-0809, and the National Science Foundation under award number 1553756.

3.6 Supporting information

SI 1. Membrane surface potential

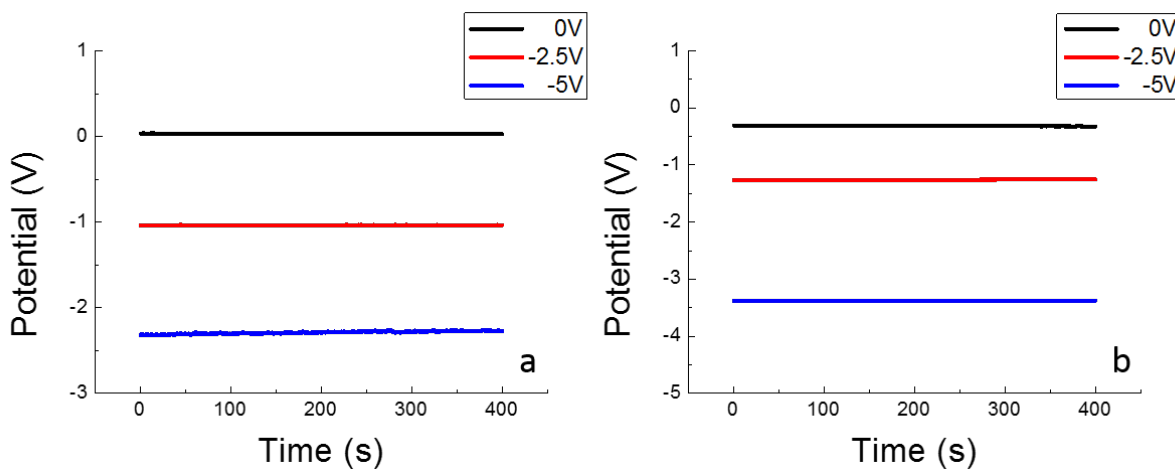


Figure 3.S1: Membrane surface open potentials versus Ag/AgCl in (a) DI water and (b) 100 mM NaCl.

In DI water, membrane surface potentials were -1000 mV and -2300 mV when external electrical potentials -2.5 V and -5 V were applied (Figure S1a). In 100 mM NaCl solution, the corresponding electrical potentials vs. Ag/AgCl were -1300 mV and -3400 mV when external -2.5 V and -5 V were added (Figure S1b).

SI 2. Emulsion size distribution

Table S1: Oil emulsion average size in the feed solution.

Feed solution	Freshly Made (μm)	After filtration (μm)
DI water	14.9 ± 11.0	2.4 ± 1.5
100 mM NaCl	7.5 ± 4.5	2.2 ± 0.9

SI 3. Surfactant surface density at oil-water interface

Gibbs isotherm was used to determine the surface excess concentration of surfactant at oil water interface (Γ_s , Equation S1),²¹⁸ where m is the factor determined by electrolyte ($m=1$ for the system with extra electrolytes, $m=2$ for the system without extra electrolytes). R , T , γ and C represent gas constant ($8.314 \text{ J K}^{-1} \text{ mol}^{-1}$), temperature (293 K), interfacial tension and the surfactant concentration in the bulk. Γ_s values were reported in Table S2 based on the slopes of lines from Figure S2.

$$\Gamma_s = -\frac{1}{mRT} \left(\frac{\partial \gamma}{\partial \ln C} \right) \quad (1)$$

Table S2: Surfactant excess concentration at emulsion interface based on Gibbs isotherm.

Ionic strength	Slope (N/m)	Γ_s (mol/m ²)
0 mM NaCl	-3.054×10^{-3}	6.268×10^{-7}
100 mM NaCl	-7.531×10^{-3}	3.092×10^{-6}

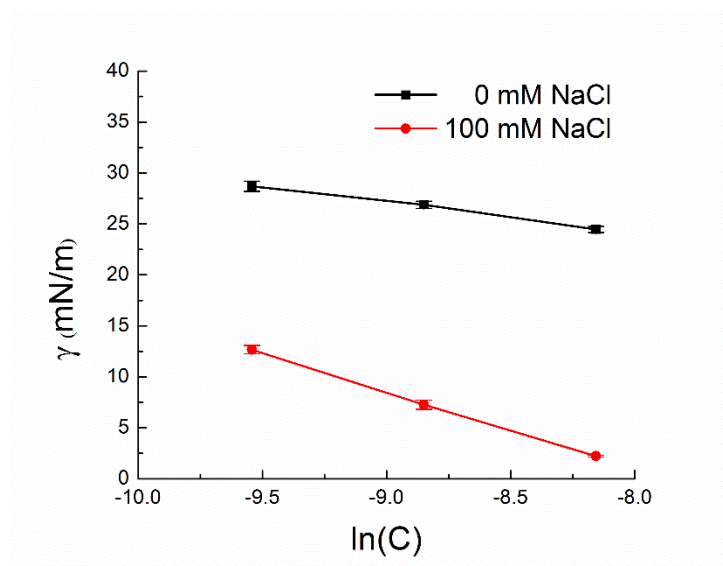


Figure 3.S2. The correlation between the interfacial tension of hexadecane/water and the DDBS surfactant concentration in the bulk.

SI 4 Membrane permeate quality

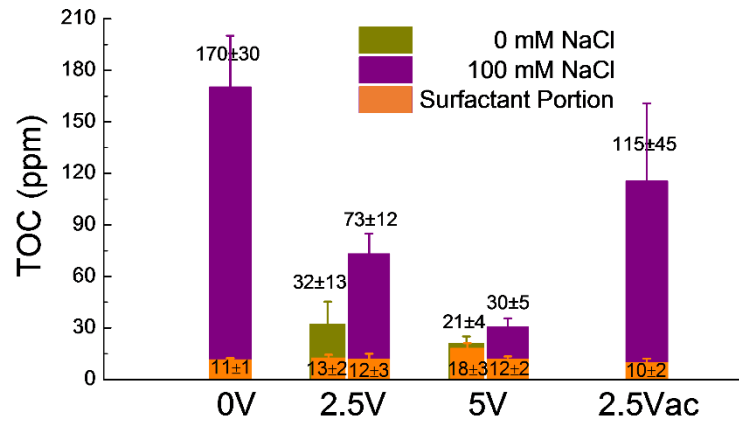


Figure 3.S3. Membrane permeate quality in terms of TOC. Purple bars are representing TOC values of surfactants

SI 5 Addition membrane filtration results

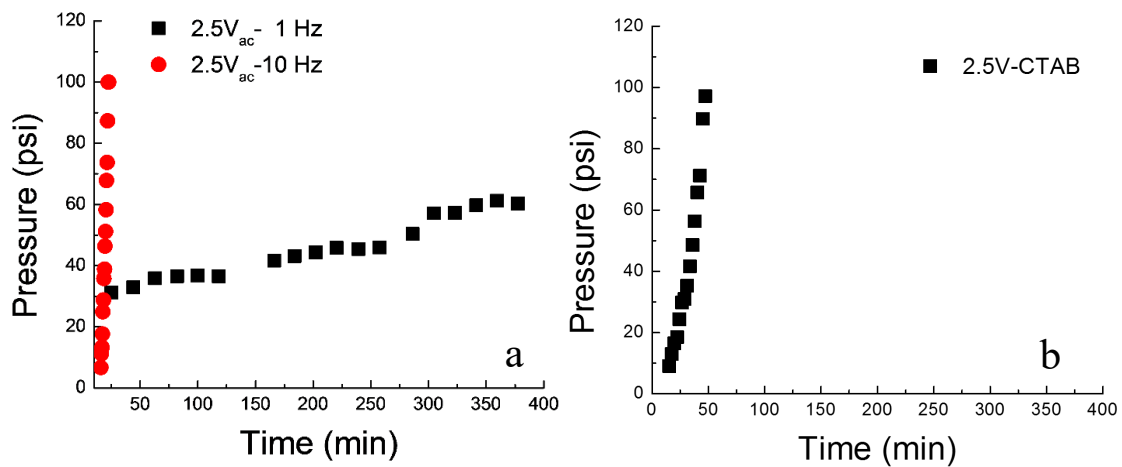


Figure 3.S4. Filtration results of 2.5V_{ac} with a frequency of 1 and 10 Hz (a), and cathodic 2.5 Vdc treating cationic surfactant CTAB stabilized droplets (b) at 10 LMH in 100 mM NaCl.

SI 6 Force analysis

Buoyancy force has a value between 10^{-6} to 10^{-5} nN which is less important because it is constant for the same oil emulsion and significantly smaller than the other forces (Equation S2), where ρ_w and ρ_{oil} are water and oil densities, g is standard gravity, and d is droplet diameter.¹⁵

$$F_b = (\rho_w - \rho_{oil})g \frac{\pi d^3}{6} \quad (2)$$

Continuous cross flow on membrane surface generates lifting force on oil emulsion that can sweep it from the membrane surface, calculated with a value of 10^{-5} nN (negligible), as described by F_l :^{222,227}

$$F_l = 81.2(\rho_w \mu_w \dot{\gamma}^3)^{0.5} \left(\frac{d}{2}\right)^3 \quad (3)$$

where $\dot{\gamma}$ represents the shear rate, and equation S4 is applied for laminar flow with a flowrate of Q_f in a rectangular channel with width W and height H (In our experiment the flow is laminar, $Re=761$):

$$\dot{\gamma} = \frac{3Q_f}{2WH^2} \quad (4)$$

Modified Stokes's law is used to calculate F_d , which serves as a constant attractive force at different distances and will act to help to bring emulsions close enough to break the energy barrier and simultaneously wet the membrane surface. In Equation S5, \emptyset is the wall correction factor, μ_w is dynamic water viscosity, and j is the permeate flux:

$$F_d = \emptyset 3\mu_w \pi d j \quad (5)$$

To calculate ϕ , film resistance R_m is required and obtained from Equation (S7), where TMP is transmembrane pressure:^{15,228,229}

$$\phi = \sqrt{\frac{R_m d}{3} + 1.072^2} \quad (6) \quad R_m = \frac{TMP}{\mu_w j} \quad (7)$$

The value of F_d can be complicated to calculate because the two events occurred in the system. Firstly, once some emulsions start to block or spread on membrane pores, R_m will increase and lead to a higher value of ϕ . In the meanwhile, emulsion coalescence would also lead to an increase of droplet size that also increases the driving force for emulsion to wet the membrane surface. Additionally, tabulated results from Goren were also effective for directly calculating ϕ based on the ratio between particle radius and the distance from planar surface to particle surface (used for this study).^{228,230}

F_{es} and F_{vdw} between emulsion and charged CNT layer can be calculated based on the previous study to determine the repulsive and attractive regions in nanometer size:¹¹⁵

Where F_{es} was calculated from the derivative of the free energy function at a separation distance. As described by:

$$F_{es} = 2\pi \int_0^r \left[-\frac{\delta F}{\delta x} \left(x + a - a \sqrt{1 - \left(\frac{r}{a}\right)^2} \right) + \frac{\delta F}{\delta x} \left(x + a + a \sqrt{1 - \left(\frac{r}{a}\right)^2} \right) \right] r dr \quad (8)$$

Whereas F free energy was calculated based on ion concentrations within the separation distance:

$$F(c) = \int_0^r -kTN_a \int_0^L \left(\frac{\sum c_i(x)}{c^\infty} - 1 \right) dx dc \quad (9)$$

$$F = F(c) - F(c_\infty) \quad (10)$$

A Modified Poisson-Boltzmann equation was used to calculate the ion concentration distributions away from the charged surface:

$$\frac{d^2\psi}{dx^2} = -\frac{1}{\epsilon} \frac{eN_a \sum_i z_i c_i^\infty \exp\left(-\frac{ze\psi(x)}{k_b T}\right)}{1 + \sum_i i \frac{c_i^\infty}{c_i^{max}} \left[\exp\left(-\frac{ze\psi(x)}{k_b T}\right) - 1\right]} \quad (11)$$

$$c_i(x) = \frac{c_i^\infty \exp\left(-\frac{ze\psi(x)}{k_b T}\right)}{1 + \sum_i i \frac{c_i^\infty}{c_i^{max}} \left[\exp\left(-\frac{ze\psi(x)}{k_b T}\right) - 1\right]} \quad (12)$$

F_{vdw} is expressed as a function of Hamaker constant A , and the ratio z between separation distance and particle diameter. A value used here is from the reference.²³¹

$$F_{vdw} = -\frac{A}{6d} \left(\frac{2}{z} - \frac{1}{z^2} - \frac{2}{z+1} - \frac{1}{(z+1)^2} \right) \quad (13)$$

Electrophoretic force, F_{ep} , for a particle in an electrical field can be described by:

$$F_{ep} = 3\pi d \eta \lambda \mu E \quad (14)$$

Where d , η , λ , μ , and E are representing droplet diameter (2.2 μm), dynamic viscosity (10^{-3} Pa.S), concentration correction coefficient, electrophoretic mobility (zeta potential*80*8.85*10e-12 F/m/10⁻³ Pa.S), and electric field. The calculated F_{ep} is in an order of 10^{-3} - 10^{-2} nN, which is significantly smaller than the electrostatic force calculated by modified Poisson-Boltzmann equation.

Dielectrophoretic force, F_{dep} , for a particle in a non-uniform electrical field can be described by:

$$F_{dep} = 2\pi\epsilon_0\epsilon_r r^3 \text{Re}[K(\omega)] \nabla E^2 \quad (15)$$

Where ϵ_0 , ϵ_r , r , $Re[K(\omega)]$, and ∇E^2 are vacuum permittivity (8.85e-12 F/m), medium permittivity (80), particle radius (1.1 μm), the real part of Clausius-Mossotti factor (less than 1), and the gradient electric field strength squared (1.97e8 V^2/m^2). The calculated F_{dep} has a negligible value of less than 10^{-8} nN.

Other parameters that were not considered are the surfactant layer between membrane and oil emulsion which could behave as the steric hindrance barrier preventing membrane wetting.

Table S3: Ion parameters for electrostatic force calculation. Hydrated ion sizes are found in the references.^{232,233}

Conditions	Ion	Concentration/mM	Valence	Radii/nm
DI water	Na+	0.3	1	0.45
	SDB-	0.3	-1	1.2
100 mM NaCl	Na+	100.3	1	0.45
	SDB-	0.3	-1	6.7
	Cl-	100	-1	0.45

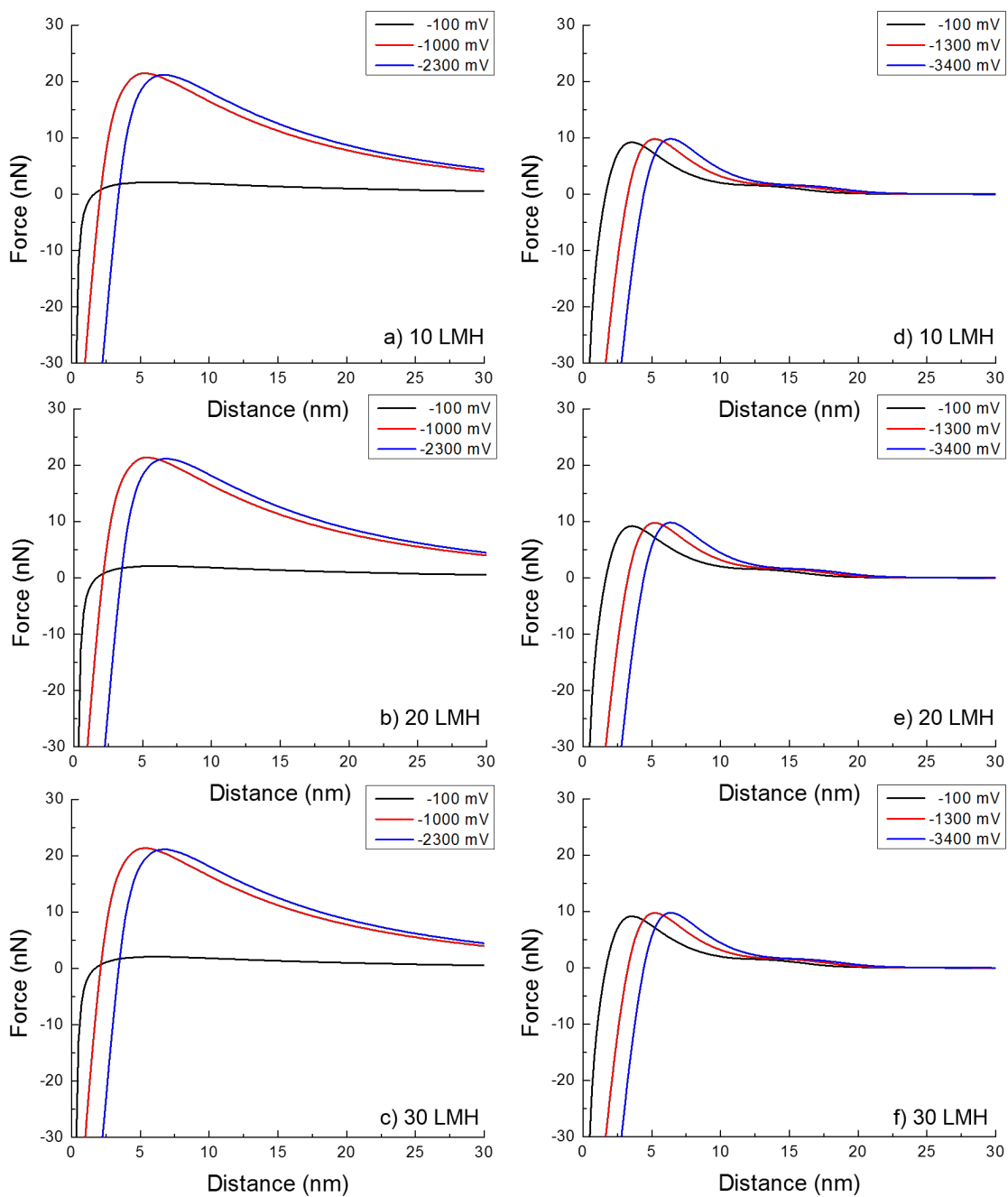


Figure 3.S5: Overall force curves between charged membrane surface and emulsions in DI water at (a) 10 LMH, (b) 20 LMH, and (c) 30 LMH; in 100 mM NaCl at (d) 10 LMH, (e) 20 LMH, and (f) 30 LMH. Potentials in legend are VS Ag/AgCl reference.

SI 7 Emulsion near membrane surface interfacial tension γ_{ow}

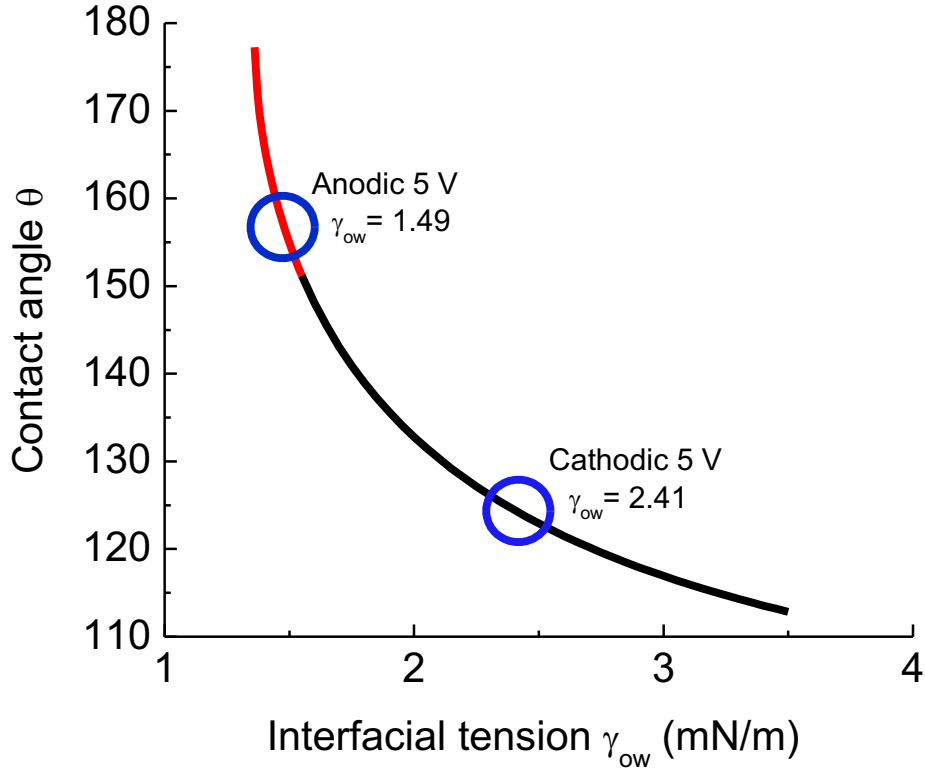


Figure 3.S6: Correlation between emulsion contact angle and interfacial tension near membrane surface using Equation S17.

Young's equation is widely-used to determine the contact angle of an oil drop on a surface (Equation S16);²³⁴ it has been modified to describe changes in the contact angle of emulsions under applied electrical potentials (Equation S17).^{235,236}

$$\cos \theta = \frac{\gamma_{sw} - \gamma_{so}}{\gamma_{ow}} \quad (16)$$

$$\cos \theta(V) = \left(\frac{\gamma_{sw} - \frac{\epsilon_0 \epsilon_r}{2e} V^2 - \gamma_{so}}{\gamma_{ow}} \right) \quad (17)$$

Here, θ is the oil-membrane contact angle; γ_{sw} , γ_{so} and γ_{ow} represent near-membrane interfacial tensions between solid-water, solid-oil and oil-water, respectively; ϵ_0 and ϵ_r denote vacuum permittivity (8.85×10^{-12} F/m) and relative permittivity of the film (80); e is the thickness of the charged material (2 μm in our membrane), and V is the applied electrical potential (5 V). In general, it is assumed that γ_{so} and γ_{ow} are constant under different electrical potentials. However, we observed a significant change in emulsion curvature when the membrane was polarized that resulted in different γ_{ow} values. More importantly, it is possible that γ_{ow} at the membrane/oil interface is quite different from γ_{ow} at the oil/water interface because of the change in surfactant distribution. To calculate γ_{ow} near the membrane surface, a correlation between θ and γ_{ow} is plotted in Figure S6 using Equation S17. Here, we assume that the overall concentration of surfactants at the interface is constant. Lower surfactant concentration corresponds to higher interfacial tension. As shown in Figure 3d and 3f, contact angles of emulsion on membrane under cathodic and anodic conditions are 124.3° and 155.7° degrees, respectively. By correlating these values to γ_{ow} , the near-membrane γ_{ow} was determined to be 2.41 and 1.49 mN/m under cathodic and anodic conditions, respectively (Figure S6).

SI 8 Emulsion coalescence event

$$\lambda = \exp\left(-\frac{t_{drainage}}{t_{contact}}\right) \quad (18)$$

$$t_{drainage} = \frac{\pi\mu f^2}{2\left(\frac{2\pi\gamma}{r}\right)^{\frac{3}{2}}}\left(\frac{1}{h_f} - \frac{1}{h_i}\right) \quad (19)$$

$$t_{contact} = \frac{\pi}{4}\left(\frac{\rho_c C_{VM} d^3}{3\gamma}\right)^{1/2} \quad (20)$$

$$\lambda \sim \exp(-C\gamma^{-1}) \quad (21)$$

Equation S18 is used to describe film drainage model, which correlates coalescence frequency to two time events $t_{drainage}$ and $t_{contact}$.²¹ $t_{drainage}$ is described by Equation S19 for drainage between two interfaces that are partially mobile and deformable.²²⁴ Where μ , f , γ , h_f and h_i represent dynamic viscosity of oil ($\mu = 3$ mPa.s),²³⁷ compressing force ($f = 10^{-11}$ nN, from permeate drag at 10 nm distance), interfacial tension (shown in Figure 5a-c), and final and initial film thickness ($h_f = 10^{-8}$ and $h_i = 10^{-4}$ m).²³⁸ $t_{contact}$ is determined by the density of continuous phase ρ_c (1 g/ml), the virtual mass coefficient C_{VM} (0.8),²³⁹ d (2.2 μ m) and γ .²⁴⁰ By combining equation S18, S19 and S20, equation S21 is obtained. It shows a positive correlation between γ and λ .

Table S4: Emulsion coalescence probability under different electrical potentials.

Potential	0	2.5 V _{dc}	5 V _{dc}	2.5 V _{ac}
λ	0.19 ± 0.04	0.04 ± 0.02	0.02 ± 0.01	0.38 ± 0.02

SI 9 Membrane surface wetting

To calculate the compressive force F for emulsions in contact with membranes, we simply used the pressure drop across the fouling layer on membrane surface:

$$F_{\Delta p} = \Delta p S \quad (22)$$

With Δp being the pressure increase in the linear region in Figure 2. S is the membrane and emulsion contact region, which can be expressed as:¹⁸⁹

$$S = \pi r_{dc}^2 \quad (23)$$

$$r_{dc} = \sin(\theta) \left(\frac{3V_d}{\pi((1 - \cos(\theta))^2(2 + \cos(\theta)))} \right)^{\frac{1}{3}} \quad (24)$$

With r_{dc} being the radius of the oil drop and membrane contact region. V_d is the volume of oil droplet.

The force F_{wr} required to wet the membrane can be determined using adhesion force

$$f_w: \quad F_{wr} = \frac{df_w(90^\circ)}{dr_{dc}} - \frac{df_w(\theta)}{dr_{dc}} \quad (25)$$

$$f_w = \pi r_{dc}^2 \gamma \left[\left(\frac{2A}{2 \sin(\theta)} \right)^{\frac{2}{3}} - A \right] \quad (26)$$

$$A = \frac{1}{1 + \cos(\theta)} - \cos(\theta) \quad (27)$$

To determine if membrane is wetted or not, ΔF is expressed as:

$$\Delta F = F_{\Delta p} - F_{wr} \quad (28)$$

Table S5: Compressive force caused by cake layer formation in 100 mM NaCl under different conditions. Values were calculated based on the averaged pressure increase in first 2 hr. Emulsion average size was used for calculation.

Flux (LMH)	Δp (psi)			
	0 V	2.5 V _{dc}	5 V _{dc}	2.5 V _{ac}
10	3	2	1	3
20	22	4	2	-
30	-	11	11	-

SI 10 Critical pressure for droplets entering membrane pores

$$P_{critical} = 2\gamma \frac{\cos(180 - \theta)}{r_{pore}} \times \left\{ 1 - \left[\frac{2 + 3 \cos(180 - \theta) - \cos^3(180 - \theta)}{4 \left(\frac{r_{drop}}{r_{pore}}\right)^3 \cos^3(180 - \theta) - (2 - 3 \sin(180 - \theta) + \sin^3(180 - \theta))} \right]^{1/3} \right\} \quad (29)$$

For emulsions in 100 mM NaCl, the required pressure for droplets penetrate through this membrane is around 554 psi, which is significantly higher than our operating range.¹⁶

SI 11 Previous studies of using membranes treating oily wastewater

Table S6: Previous studies of using membranes treating oily wastewater

Membrane type	Oily wastewater source	Oil Concentration (ppm)	Operating flux (LMH)	Rejection %	Reference
Polysulfone	Industrial oily wastewater	78	50-100	61.3-61.8	Salahi et al. ⁸
Polyacrylonitrile	Industrial oily wastewater	78	100-250	59.7-70.6	Salahi et al. ⁸
Cellulose	Synthetic produced water	5000	100-5000	94.0-97.5	Wandera et al. ²⁴¹
Polysulfone	Plam oil mill effluent	70900	4-10	46.9	Wu et al. ²⁴²
Modified polysulfone	Crude oil	100-1000	200-500	92-100	Gohari et al. ²⁴⁴
Modified polyethersulfone	Industrial oily wastewater	81	30-200	99.7	Salahi et al. ²⁴⁴
Polyethersulfone	Synthetic oily wastewater	5000	10-30	96.1-99.5	This work

SI 12 Energy and cost analysis

The additional energy requirement imposed by the application of an external electrical potential to the membrane surface was determined by measuring the electrical current as a function of the applied potential, and using this information together with the measured flux (30 LMH) to calculate the extra energy needed to generate a m^3 of treated water. The additional energy consumption for 2.5 V and 5 V at 100 mM NaCl was 0.08 and 0.42 kWh/ m^3 , respectively; in 0 mM NaCl, the energy consumption was 0.008 and 0.10 kWh/ m^3 for 2.5 V and 5 V, respectively. This additional energy translates to an additional cost of \$0.01/ m^3 and \$0.06/ m^3 at 2.5V and 5V in 100 mM NaCl, respectively, and \$0.001/ m^3 and \$0.02/ m^3 at 2.5V and 5V in 0 mM NaCl, respectively. This calculation assumed an energy cost of \$0.15/kWh (Los Angeles 2018). Operating the membrane at higher flux reduces the energy consumption per m^3 .

The extra capital expenses associated with electrically conducting membranes come (at least partially) from the additional cost of CNTs. Based on a CNT cost of \$10.00/g, the additional cost of the CNTs was determined to be \$9.38/ m^2 .

Chapter 4. **Tuning Salt Selectivity of Nanofiltration Membranes**
Using Carbon Nanotubes Embedded Polyamide
Membranes

Abstract

This research focused on the fabrication and characterization of electrically conductive polyamide (PA) based nanofiltration membranes embedded with the networks constructed by multi-walled carbon nanotubes (MWCNT) or single/double-walled carbon nanotubes (S/DWCNT). The membrane's characteristics including electrical conductivity, capacitance, chemical composition and surface morphology were examined. In addition, membrane's performance when treating single salt solution of NaCl, MgCl₂, Na₂SO₄, and MgSO₄, as well as mixed solution of NaCl and MgSO₄ were carefully monitored. Dynamic changes of ion selectivity and water flux for both membranes were observed under different electrical potentials. The application of high negative charges reduced water permeance for both membranes. However, membrane's ion selectivity was tuned in a dramatic different way. MWCNT-PA membrane showed enhanced selectivity towards Na⁺ and Cl⁻, reduced rejection for Mg²⁺ and no change for SO₄²⁻. In contrast, S/DWCNT-PA membrane exhibited decreased rejection for Na⁺, Cl⁻, and Mg²⁺, but slightly increased rejection for SO₄²⁻. Microscopic analysis revealed distinctive differences of PA and CNT films between two membranes. MWCNT-PA showed a clear and thick PA film that was formed on top of the MWCNT film. A less crosslinked PA film in S/DWCNT-PA membrane was embedded into the S/DWCNT network. The distinctive structure difference between two CNT-PA films were thought as the main cause of resulted difference.

4.1 Introduction

Nanofiltration (NF) utilizes semipermeable membranes to offer versatile treatments including water softening, heavy metal removal, and natural organic matter removal (or valuable organic compounds concentration).^{7,246–248} Thus it has been widely used for water reuse, food processing, and organic solvent separation applications.^{40,41,43} NF membranes are advantageous in providing more diverse selectivity toward salt ions and small organic compounds (dyes, sugars, proteins) compared to reverse osmosis (RO) and ultrafiltration (UF) membranes.⁶⁵ As their pore diameters were reported in the range of 0.8 to 2.0 nm,^{44–48} or the molecular weight cutoff (MWCO) were reported from 150 to 2000 Da,⁴² which is in between RO and UF membranes. For example, commercially available NF membranes exhibit a wide range of rejections toward salt species: The divalent salt MgSO_4 is generally well rejected (>90%), while the rejection of NaCl varies from 10% to 95%.⁴² Therefore, NF brings a better solution for a more comprehensive and selective separation of substances within the size of nanometer range.

The selective ion transport through NF membranes is governed by a combination of different transport mechanisms. The dominant transport mechanisms are size and charge based separations.⁵⁰ Namely, nanometer range pores create steric hindrance for rejecting large substances, and the electrical charges along the membrane surface and the pore walls allow a better separation due to the electrostatic interactions and charge neutrality conditions (Donnan Exclusion). In addition to these mechanisms, dielectric exclusion is proposed to account for the interaction between the ion and its induced charges on the surface of the transport channels.⁵¹ A more detailed mechanism is applied to account for

ion dehydration phenomena that resulted in different selectivity of monovalent ions which share similar charges and hydrated sizes in the transport process.^{54,249} However, large knowledge gaps of ion transport in nanopores still need to be filled.⁶⁴ Luo et al. summarized the pH effects on salt rejections: polyamide (PA) NF membranes demonstrate V-shape rejection curves for symmetric electrolytes (NaCl, KCl) and S-shape rejection curves for asymmetric salts (Na₂SO₄, MgCl₂) under different pHs, which correlate well with the Donnan exclusion.^{52,53} To understand different rejections of PA-NF membranes toward monovalent anions, Richards et al. used solute flux at different temperatures to quantify energy barriers of ion transport through NF membranes (Arrhenius equation), and linked energy barriers to ion hydration/dehydration phenomena.⁵⁴ Epsztein et al. further examined the ionic charge densities of these anions, and concluded that ions with higher ionic charge densities (higher hydration strength) are more affected by the Donnan exclusion mechanism.⁵⁵ All these fundamental studies provide guidelines for designing and fabricating novel NF membranes with higher charge densities.

Incorporating engineered nanomaterials into thin film nanocomposite (TFN) membranes are effective at modifying the active layer structure and the surface chemistry, thus improving membrane performance including permeability, selectivity, and antifouling properties. For example, Lee et al. immobilized silver nanoparticles on PA films to prevent the biofouling.⁷⁵ Rajaeian et al. fabricated TiO₂ based TFN membranes to alter the permeate flux and rejection.⁷⁶ Apart from these metal nanoparticles, carbon-based nanomaterials such as graphene oxide (GO) and carbon nanotubes (CNT) are drawing great attentions due to their great mechanical stability, antifouling property, and specific

molecular structure, which in turn contribute to superior permeability and selectivity.⁷⁷⁻⁷⁹ CNT intercalated GO membranes were shown to be effective at separating salt ions under low ionic strengths.⁸⁰ In particular, the excellent electrical conductivity of carbon materials made them possible for electrically adjusting the membrane surface charges. Hu et al. synthesized electrically conductive reduced GO-CNT membranes and tested their desalination performance at 50 mM feed concentration. The application of both ± 1 V cell potentials dramatically improved rejection of NaCl (25% to 65%), Na₂SO₄ (30% to 65%), and CaCl₂ (55% to 70%), comparing to no addition of electrical potentials. However, the membranes were limited to low permeate fluxes (0.2-0.3 Lm⁻²h⁻¹bar⁻¹, LMH/bar).⁸¹ Zhang et al. constructed conductive polyaniline-polystyrenesulfonate CNT membranes, which achieved high permeate fluxes of ~ 15 LMH/bar when treating 5 mM NaCl and Na₂SO₄ solutions. Rejections were also enhanced at negative 2.5V cell potentials (82% to 93% for Na₂SO₄; 54% to 82% for NaCl). Therefore, electrically conductive NF membranes are of great potentials, because their tunable surface charges provide smart control of salt rejections.

This study aims at fabricating and testing CNT-PA membranes for selective separation of different ion species under electrical potentials. In particular, single/double-walled CNT PA (S/DWCNT-PA) and multi-walled CNT (MWCNT-PA) membranes were fabricated and characterized. Their rejection performances of single salt solutions including NaCl, Na₂SO₄, MgCl₂, and MgSO₄, as well as the mixed salt solution of NaCl and MgSO₄ were evaluated under different electrical potentials.

4.2 Materials and Methods

4.2.1 Chemicals

MWCNT (99wt%, outer diameter of 13-18 nm, tube length of 3-30 μm , COOH content of 7.0%), and S/DWCNT (99wt%, SW/DW is around 50/50, outer diameter of 1-4 nm, tube length of 3-30 μm) were purchased from Cheaptubes and used as received. Surfactants including dodecylbenzenesulfonate sodium salt (DDBS, technical grade, Sigma Aldrich) and sodium dodecyl sulfate (SDS, Acros Organics, 99+%) were purchased and used as received. Salts including NaCl (99%, Certified ACS), $\text{MgCl}_2 \cdot 6\text{H}_2\text{O}$ (99%, Certified ACS), Na_2SO_4 (99%, Certified ACS), and $\text{MgSO}_4 \cdot 7\text{H}_2\text{O}$ (98%, Certified ACS, Fisher Scientific) were purchased and used as received. Chemicals for forming the PA film including piperazine anhydrous (PIP, 99%, Alfa Aesar) and 1,3,5-benzenetricarbonyl chloride (TMC, 98%, Alfa Aesar) were used as received.

4.2.2 Membrane fabrication

Two types of CNT suspensions were prepared and used to make CNT membranes. MWCNTs (1g/l) were dispersed in DI water using DDBS (10 g/l), and S/DWCNTs (0.1 g/l) were dispersed in DI water using SDS (10 g/l). Both solutions were sonicated using a horn sonicator (450 Digital Sonifier, Branson) for 30 minutes followed by centrifugation to remove impurities (Avanti J-E Centrifuge, Beckman Coulter, MWCNTs at 11000 rcf, SWCNTs/DWCNTs at 13000 rcf).

To fabricate CNT-PA membranes, CNT films with ideal thicknesses were formed on PS-35 ultrafiltration membrane support (Solecta Inc., Oceanside, CA) by pressure depositing a proper amount of CNT suspensions. The formed CNT films were further washed with DI

water to remove the excess surfactants. To form the PA film, CNT coated membranes were soaked in 2% PIP for 2 minutes, followed by using a plastic roller to remove excess amount of PIP solution. Then membranes were immersed in hexane with 0.15% TMC for 1 minute and cured in an oven at 80 degrees for 5 minutes. At last, cured membranes were soaked in DI water and stored at 4 degrees prior to using.^{85,91}

4.2.3 Membrane filtration process

Membranes were tested in a previously reported filtration system.^{16, 23,171,172} In brief, membranes were placed in a custom-built membrane module that has a fluid channel of 10 cm x 4 cm x 3.8 mm (length x width x height). Electrical potentials (cell potential) were applied to the membrane surface and the Titanium (Ti) counter electrode with a separation distance of 3.8 mm using an arbitrary waveform generator (DG1022, Rigol). Membranes were used as the cathode to prevent electro-oxidation. Feed solutions were circulated at a speed of 1.6 L/min using a diaphragm pump (Hydra-Cell, MN), which translates into a crossflow velocity of 18 cm/s. Prior to testing, membranes were compressed at 150 psi for at least 12 h with DI water. Then the system was operated in the constant pressure mode at 150 psi. Five feed solutions including NaCl, MgCl₂, Na₂SO₄, MgSO₄, and mixture of NaCl and MgSO₄ were tested at the same ionic strength of 34.2 mM (equivalent to 2000 ppm NaCl, for mixed salt, both NaCl and MgSO₄ were at the same ionic strength of 17.1 mM). Electrical potentials (cell potential) were applied in a sequence of 0V, 2V, 1.5V, 1V, 0.5V, 0V, 2V, and 0V. Feed and permeate samples were collected in every 30 minutes with respect to electrical potentials. The properties of the feed and permeate solutions were tested using pH and conductivity probes (Orion, Thermo Scientific). For single salt

solutions, membrane rejections were calculated based on the electrical conductivity of the feed and permeate solutions (Equation 1,2). In particular, to differentiate the rejection change caused by the increase of pH in the permeate, cation rejection (R_c) was reported to represent the observed rejection and was directly calculated based on the ratio of the electrical conductivity of the feed (C_f) and permeate (C_p) solutions (Equation 1). Anion rejection (R_a) was calculated based on the corrected electrical conductivity of the permeate, which was subtracted by the electrical conductivity of NaOH or Mg(OH)₂ solutions at the same pH (C_{MOH}), as shown in Equation 2. R_c and R_a were different only when the pH of the permeate was high. For the mixed salt solution, anion concentrations were analyzed by ion chromatography (IC, Dionex, Thermo Scientific) and the corresponding cation concentrations were characterized by inductively coupled plasma optical emission spectrometry (ICP-OES, ICPE-9000, Shimadzu).

$$R_c = 100\% \times \left(1 - \frac{C_p}{C_f}\right) \quad (1)$$

$$R_a = 100\% \times \left(1 - \frac{C_p - C_{MOH}}{C_f}\right) \quad (2)$$

4.2.4 Membrane characterization

Membrane's electrical conductivity was characterized by a 4-point conductivity probe (MCP-T610, Mitsubishi). Its corresponding capacitance was evaluated using cyclic voltammetry curves (CV, CH Instruments, Austin, TX), where Titanium (Ti) plate and Ag/AgCl electrode were used as counter and reference electrode. The CV curve was obtained in 34.2 mM NaCl solution with a scan rate (S) of 0.05 V/s, and the capacitance (C) is calculated based on Equation 3, where I_a and I_c represent anodic and cathodic currents at the open circuit potential.

$$C = \frac{I_a - I_c}{2S} \quad (3)$$

Membrane's real surface potentials versus reference electrode Ag/AgCl under applied DC potentials were investigated using the open circuit potentials.¹²⁴ In brief, CNT membranes, Ti counter plate, and Ag/AgCl electrode were immersed in 34.2 mM NaCl solution and connected as working, counter, and reference electrode to the electrochemical analyzer, and DC potentials were directly applied to the membrane surface and Ti plate using the arbitrary waveform generator. Membrane surface potentials were measured over time using the open circuit potential technique.

The chemical compositions of the membrane's surface were characterized using X-ray photoelectron spectroscopy (XPS, Kratos Axis Ultra DLD spectrometer equipped with a monochromatic Al K α X-ray source). Membrane's surface functional groups were analyzed using Fourier transform infrared spectroscopy in attenuated total reflectance mode (ATR-FTIR, Thermo Scientific, FTIR iS10 Smart iTR Basic). In these measurements, at least 3 pieces of samples were analyzed to confirm the results.

Membrane surface morphology was characterized using atomic force microscopy (AFM, Bruker Fastscan, CA) and scanning electron microscopy (SEM, Zeiss Supra 40VP, Germany). Additional cross-sectional SEM images were taken to further characterize the film structure.

4.3 Results and Discussions

4.3.1 Membrane characterization

4.3.1.1 Characterization of membrane's electrical properties

The electrical properties of both MWCNT and S/DWCNT membranes were evaluated and reported in Table 4.1. Membranes with different thicknesses were fabricated based on the volume of CNT suspension used. For MWCNT membranes, as the membrane thickness increased from 1 to 2 and 4 μm , membrane sheet resistance reduced from 164 ± 13 to 95 ± 8 and $39 \pm 4 \Omega/\text{sq}$ for 10 MWCNT, 20 MWCNT, and 40 MWCNT, respectively. A similar trend was also observed for more conductive S/DWCNT membranes, an increased thickness from 0.25 to 0.5 and 1 μm resulted in a decreased sheet resistance from 21 ± 1 to 12 ± 1 and $6 \pm 1 \Omega/\text{sq}$, respectively. The electrical conductivity of CNT films is reported to scale linearly with the density of tube to tube junctions in the network. Such a correlation can be mathematically explained by the Equation (4), where the electrical conductivity (σ_{DC}) is equal to the inverse of the product of sheet resistance (R_s) and film thickness (h), and proportional to a K factor that is dependent on the tube length, the mean junction resistance (R_j), film fill factor (V_f), and the mean diameter (D).^{249,250} A higher density of network junctions in S/DWCNT films indicate a much higher conductivity (lower R_s). In addition to the junction density, the R_j between CNTs in S/WCNT films are expected to be much lower than in MWCNT films due to the smaller tube diameters.²⁴⁹ Therefore, S/WCNT membranes are superior in terms of electrical conductivities.

$$\sigma_{DC} = \frac{1}{R_s * h} = \frac{K V_f^2}{R_j D^3} \quad (4)$$

Membrane's capacity of storing ions was investigated using cyclic voltammetry curves. A linear increase of capacitance versus membrane thickness was observed. The capacitance of MWCNT membranes at different thicknesses was substantially enhanced from $637 \pm 159 \mu\text{F}$ (for $1 \mu\text{m}$) to $1361 \pm 155 \mu\text{F}$ (for $2 \mu\text{m}$), and $2800 \pm 590 \mu\text{F}$ (for $4 \mu\text{m}$). At the same thickness, S/DWCNT membranes had much higher capacitance compared to MWCNT membranes. A $0.25 \mu\text{m}$ thick membrane contributed to a capacitance of $712 \pm 51 \mu\text{F}$, and 0.5 and $1 \mu\text{m}$ thick membranes could further increase capacitance to 934 ± 74 and $2277 \pm 203 \mu\text{F}$. The higher electrical conductivity and surface area enable S/DWCNT membranes a better ion storage capacity than MWCNT membranes.²⁵¹

Membrane's surface charge is of great importance for ion separations, which in turn can be determined from the membrane capacitance under electrical potentials. To explore the impact of CNT films on ion separations, 10 MWCNT and 20 S/WCNT membranes were selected and used as substrates for PA film formation. The fabricated NF membranes were further tested in the filtration process due to their similar capacitances (637 ± 159 and $712 \pm 51 \mu\text{F}$, respectively).

Table 4.1: CNT membrane electrical properties

Membrane types	10 MWCNT	20 MWCNT	40 MWCNT	20 S/DWCNT	35 S/DWCNT	75 S/DWCNT
Thickness (μm)	1	2	4	0.25	0.5	1
Sheet resistance (Ω/sq)	164 ± 13	95 ± 8	39 ± 4	21 ± 1	12 ± 1	6 ± 1
Capacitance (μF)	637 ± 159	1361 ± 155	2800 ± 590	712 ± 51	934 ± 74	2277 ± 203

4.3.1.2 Characterization of membrane's surface properties

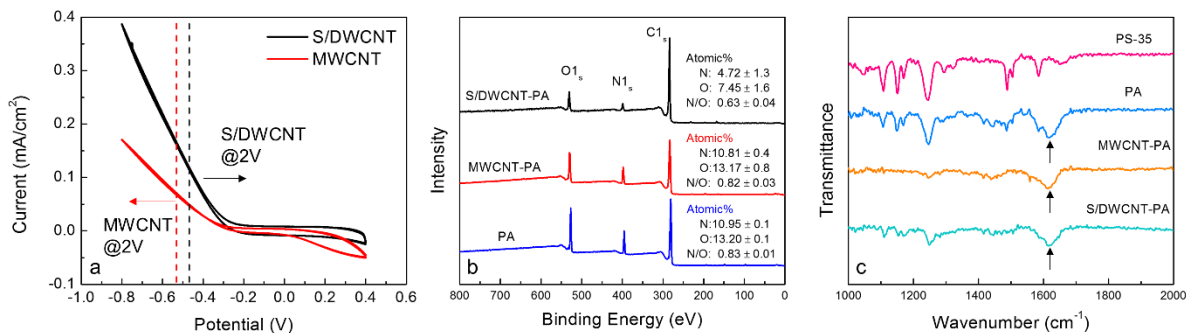


Figure 4.1: Membrane surface properties study using a) CV scans to determine possible chemical reactions; b) XPS analysis to quantify the surface chemical compositions; c) ATR-FTIR analysis to distinguish surface functional groups.

CV curves were used to determine the possible electrochemical reactions happening under applied negative potentials (Figure 4.1a). A dramatic increase of current density was observed when electrical potentials were increased from -0.3V to -0.8V, which indicated the occurrence of water splitting reaction. Open circuit potential measurements showed that surface potentials (versus Ag/AgCl electrode) of MWCNT membranes were at 0.53 ± 0.03 V and -0.26 ± 0.01 V, corresponding to 2V and 1.5V DC potentials. In contrast, S/DWCNT membranes showed surface potentials of -0.48 ± 0.02 V and -0.25 ± 0.01 V respectively. It is therefore confirmed that the application of 2V was able to drive water splitting reaction for both membranes due to increased current density (Figure 4.1a), while unnoticeable current density at 1.5V implied negligible water splitting reactions.

Membrane's surface chemistry was analyzed using XPS, and the atomic percentages of nitrogen, oxygen, and the nitrogen over oxygen ratios (N/O) were reported in Figure 4.1b. Plain PA and MWCNT-PA membranes exhibited similar nitrogen and oxygen percentages of around 11% and 13%, which translates into the N/O of 0.8. However, S/DWCNT-PA

membranes had less nitrogen and oxygen percentage of 5% and 7%, and its N/O ratio is only around 0.6. This observation implies less crosslinking degree of PA film in S/DWCNT-PA membranes than MWCNT-PA and plain PA membranes, thus leaving more free pendant carboxylic acid groups in the PA film.²⁵² In addition to XPS, FTIR was used to investigate more detailed surface functional groups on the membrane surface (Figure 4.1c). The same peak was observed at 1630 cm^{-1} for PA, MWCNT-PA, and S/DWCNT-PA membranes. This peak was assigned to the amide I band in a secondary amide group that includes the C=O stretching, C-N stretching, and C-C-N deformation vibration.²⁵³ Other different peaks shown in these PA membranes from 1000 to 1250 cm^{-1} and at 1587 cm^{-1} were associated with functional groups from PS-35 UF support. No significant difference of surface functional groups was found using FTIR analysis.

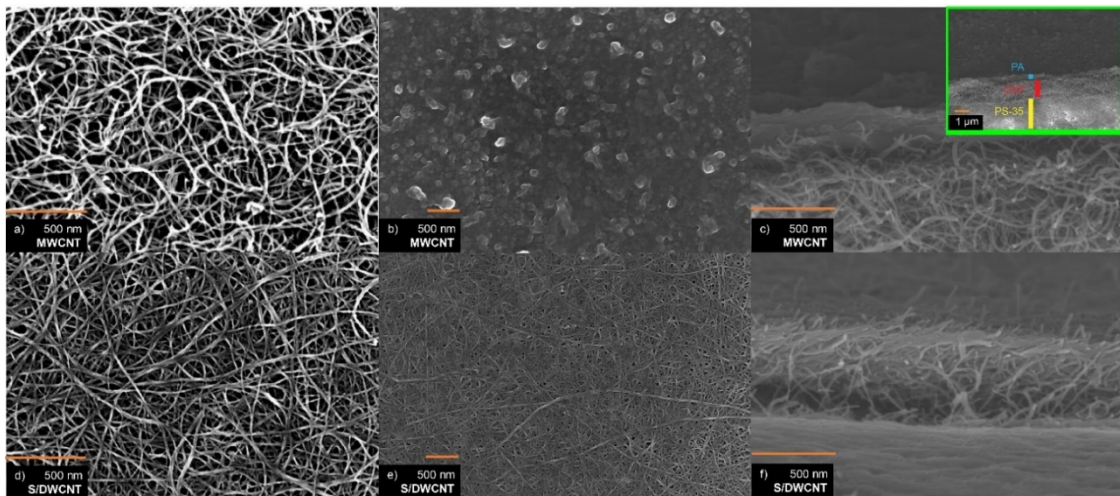


Figure 4.2: The comparison of membrane surface morphologies between MWCNT and S/DWCNT based membranes. a) and d) are the top view of pristine MWCNT and S/DWCNT membranes; b) and e) are the top view of MWCNT-PA and S/DWCNT PA membranes; c) and f) are the cross-sectional view of MWCNT-PA and S/DWCNT PA membranes.

4.3.2 Membrane morphology

Membrane's morphology was characterized using top view and cross-sectional view SEM images and illustrated in Figure 4.2. Figure 4.2a, 4.2d represent the surface of MWCNT and S/DWCNT membranes before interfacial polymerization. A denser film of S/DWCNT was formed compared to MWCNT film. The image analysis (ImageJ) of the membrane surface porosity showed that MWCNT film had a surface porosity of around 59% and an average pore diameter of 90 nm, while S/DWCNT membrane surface only has 35% porosity and its pore diameter is only about 47 nm. The smaller diameters of S/DWCNTs contributed to a more densely packed CNTs in the film and thus resulting in a smaller porosity compared to the MWCNT film. After the interfacial polymerization of PIP and TMC, the top view of MWCNT-PA and S/DWCNT-PA membranes were taken and shown in Figure 4.2b, 4.2e. MWCNT-PA membrane exhibited a rough surface which was commonly seen as the PIP based PA surface.²⁵⁴ S/DWCNT-PA membrane was porous and

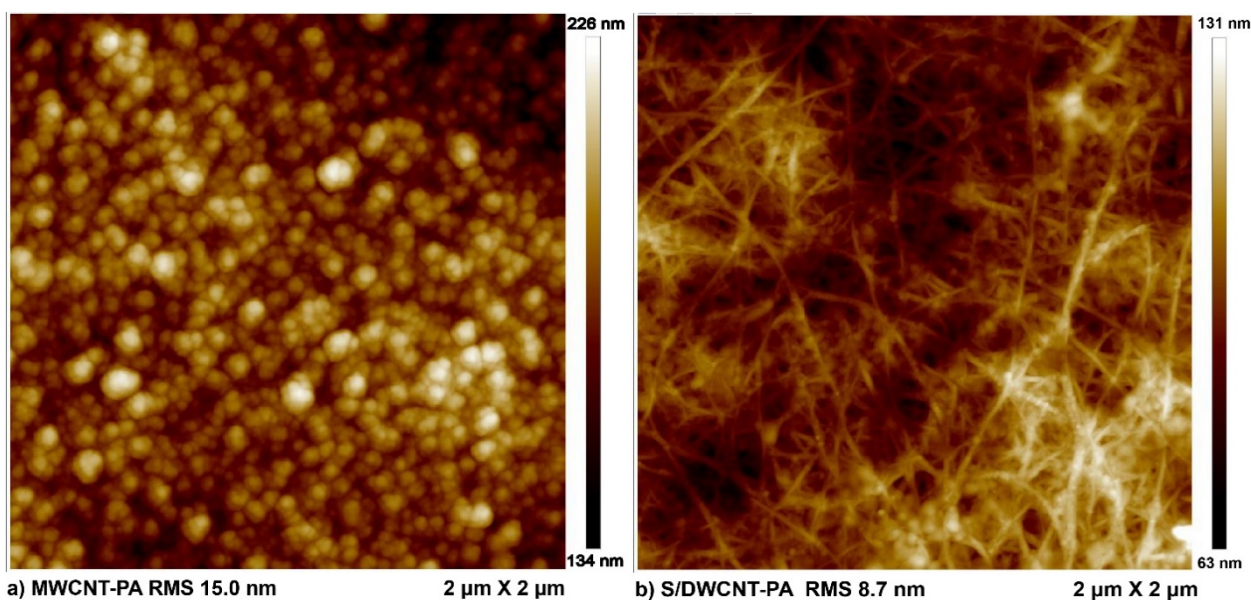


Figure 4.3: AFM topography images of a) MWCNT-PA membrane and b) S/DWCNT-PA membrane at a scan size of $2 \mu\text{m} \times 2 \mu\text{m}$.

similar to plain S/DWCNT membrane. However, its good salt rejection performance may indicate a PA film was formed within the membrane (shown in the next section). A more detailed analysis to identify different layers was studied using cross-sectional images. Figure 4.2c represented the cross-section of the MWCNT-PA membrane, where roughly a thickness of 200 nm PA layer was formed on top of the 1000 nm MWCNT layer. In contrast to MWCNT-PA membrane, no clear PA layer was observed in the S/DWCNT-PA membrane (Figure 4.2f), and the thickness of S/DWCNT film was approximately 200 nm. The height information of the membrane surface and the surface roughness calculated as root mean squared (RMS) were investigated and reported in Figure 4.3. The MWCNT-PA membrane showed a surface pattern that contains circular bumpers (Figure 4.3a), which is corresponding well with the SEM images in Figure 4.2b, and these circular bumpers result in an RMS value of 15.0 nm. S/DWCNT-PA showed a clear CNT network with some circular bumpers, and smaller surface roughness of 8.7 nm was observed. Such circular bumpers revealed the probable formation of PA within the CNT film pores.

4.3.3 Selective ion separation under electrical potentials

4.3.3.1 Single salt rejection

The ion separation performance of MWCNT-PA and S/DWCNT-PA membrane under electrical potentials and its corresponding pH were summarized in Figure 4.4 and Figure S1. Four types of single salt including NaCl, MgCl₂, Na₂SO₄ and MgSO₄ were used as the feed solution to evaluate membrane's rejection and flux. In all cases, no clear changes of membrane flux and rejection were made under electrical potentials at 0V, 0.5V and 1V. Moreover, high potentials have a similar impact on membrane permeate flux, as negative

1.5V and 2V potentials reduced all permeate fluxes comparing to their fluxes under no electrical potentials. However, these high potentials tuned salt rejections of MWCNT-PA and S/DWCNT-PA membranes in a dramatically different way. When NaCl solution was tested, MWCNT-PA membrane exhibited an initial rejection of around 32%. The application of electrical potentials dramatically enhanced its rejection to 43% at 1.5V, and 54% at 2V (Figure 4.4a). An opposite trend of rejection change was observed for S/DWCNT-PA membranes. As a significant drop of NaCl rejection from 47% (at 0V) to 31% and 21% was made under 2V and 1.5V (Figure 4.4d). When membranes were tested with MgCl₂ solution, the rejections of both membranes were reduced at high electrical potentials. With increased electrical potentials from 0V to 1.5V and 2V, the rejection of MWCNT-PA membrane decreased from 89% to 73% and 57% (Figure 4.4b). Similarly, S/DWCNT-PA membrane had a reduced rejection from 92% to 80% and 36% (Figure 4.4f). For Na₂SO₄ solution, the rejection of MWCNT-PA membrane remained constant around 92% under these potentials, expect a small drop of rejection to 88% at 2V, which was due to the water electrolysis that resulted in the higher concentration of hydroxide ions in the permeate. This hypothesis is proved by the high pH of the permeate under 2V (Figure S1). In addition, membrane's anion rejection (SO₄²⁻) at negative 2V potential remained same (92%) compared to its cation rejections at other electrical potentials. Therefore, we concluded that unnoticeable change of rejection was made at these potentials. S/DWCNT-PA membrane had a much lower initial rejection of around 55%, which was enhanced to 91% and 93% at 1.5V and 2V. The pH corrected anion rejection even reached 98%. In the case of MgSO₄ solution, MWCNT-PA membrane showed a similar trend of rejection

change compared to Na_2SO_4 solution, where the rejections of both cation and anion were around 91%, only except the cation rejection at 2V dropped to 85% due to the increase of hydroxide ion concentration. On the other hand, the electrical potentials increased the rejection of S/DWCNT-PA membrane from 91% (0V) to 96% (1.5V) and 93% (2V), and the calculated anion rejection went further up to 97% at 2V.

4.3.3.2 Mixed salt rejection

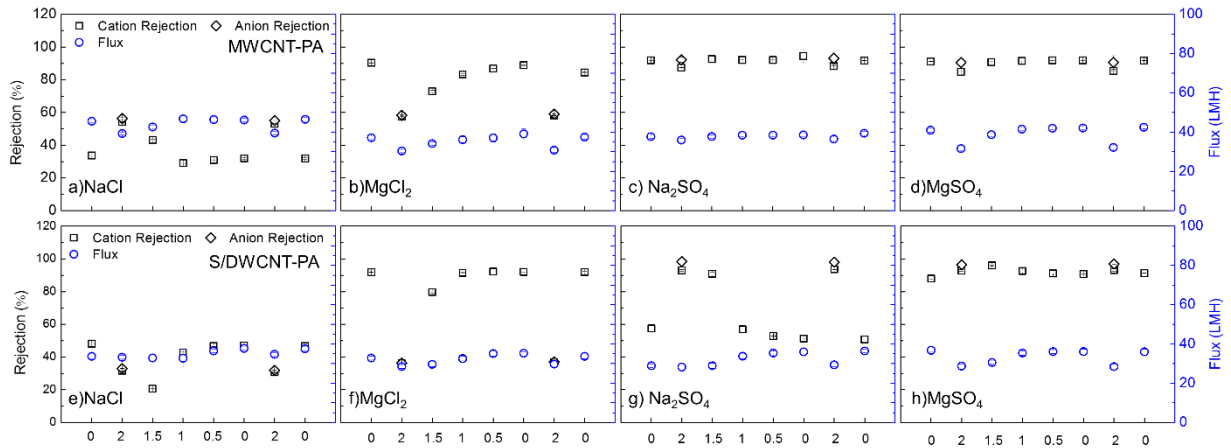


Figure 4.4: Membrane flux and rejection evaluation under electrical potentials. The rejection (black square for cation, and black diamond for anion, left y axis) and flux (blue circle, right y axis) of MWCNT-PA (a-d) and S/WNT-PA (e-h) when treating NaCl, MgCl_2 , Na_2SO_4 and MgSO_4 solutions at different electrical potentials. Cell potentials ranging from 0-2V were applied repeatedly to the membrane surface and the counter electrode and reported in x axis. Membranes are used as cathode. Anion rejection was only reported at 2V due to its high pHs.

Mixed salt of NaCl and MgSO_4 solution was prepared and used to evaluate membrane's performance (Figure 4.5, Table 2). Figure 4.5a, 4.5b represented the ion rejections under different electrical potentials when using MWCNT-PA membrane and S/DWCNT-PA membrane, respectively, and detailed rejection was summarized in Table 4.2. Interestingly, the rejection of Na^+ increased from 28% to 45 % under 2V, and then gradually decreased to 32% when potentials dropped to 0.5V for MWCNT-PA membrane. However, S/DWCNT-PA membrane exhibited a higher initial rejection of 43% (at 0V). high

potentials of 2V and 1.5V both substantially dropped its rejection to around 33%, and lower potentials of 1V and 0.5V recovered the rejection back to 44%-46%. Similarly, the rejection of Cl^- was increased from 35% (0V) to 45% (2V) and dropped to 36%-40% at 1.5V, 1V, and 0.5V for MWCNT-PA membrane. While S/DWCNT-PA membrane had a dramatic drop of Cl^- rejection from 49% (0V) to 20% (2V), and gradually recovered back to 27% (1.5V) and 48% (1V and 0.5V). For divalent Mg^{2+} ions, both membranes experienced a similar rejection decline under 2V and 1.5V. The rejections dropped from initial rejection of 91% to 81% and 83% for MWCNT-PA membrane, and 93% to 65% and 84%, respectively. The increased surface potentials contributed a much less impact on the rejection of SO_4^{2-} , as MWCNT-PA membrane showed consistent rejections around 91-92%, and S/DWCNT-PA membrane showed a slightly higher rejection from 83% (0V, 0.5V, 1V) to 95-96% (1.5V and 2V).

The addition of high electrical potentials on the membrane surface created extra surface charges on the membrane surface, thus enhanced the charge-based separation. However, the dramatic difference of rejections towards Na^+ and Cl^- for MWCNT-PA and S/DWCNT-PA membranes are quite surprising. MWCNT-PA membrane behaved just like a regular PA membrane, where higher surface charges enhanced its rejection for NaCl (through pH adjustment). While S/DWCNT-PA membrane was abnormal, the enhancement of surface charges, in turn, caused a less effective separation of NaCl, but an increased rejection for SO_4^{2-} . The transport mechanism is still unclear to us, we speculate that this is determined

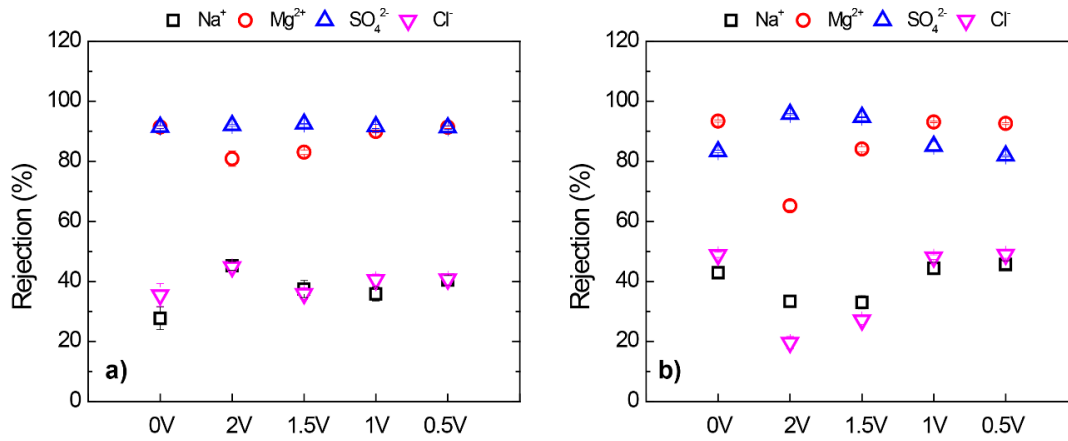


Figure 4.5: Mixed salt rejection towards specific ions including Na⁺ (black square), Mg²⁺ (red circle), SO₄²⁻ (blue triangle), Cl⁻ (inverted triangle) of a) MWCNT-PA and b) S/DWCNT-PA membranes. The feed solution was tested at pH 5.8.

by the intrinsic properties of the membrane film structure. Porous CNT network in SWCNT-PA membrane provides ionic channels with tunable surface charges. Thus, facilitates NaCl passage through the film. However, molecular simulations of ion transport in S/DWCNT networks may be required to have a better understanding of observed phenomena.

Table 4.2: Ion separation performance of mixed salt at different electrical potentials

Membrane	Potential	Na ⁺	Cl ⁻	Mg ²⁺	SO ₄ ²⁻
MWCNT-PA	0V	28 ± 4	35 ± 4	91 ± 0	91 ± 1
	2V	45 ± 1	45 ± 1	81 ± 3	92 ± 0
	1.5V	37 ± 3	36 ± 2	83 ± 1	92 ± 0
S/DWCNT-PA	0V	43 ± 2	49 ± 1	93 ± 0	83 ± 0
	2V	33 ± 2	20 ± 2	65 ± 1	96 ± 0
	1.5V	33 ± 2	27 ± 1	84 ± 1	95 ± 0

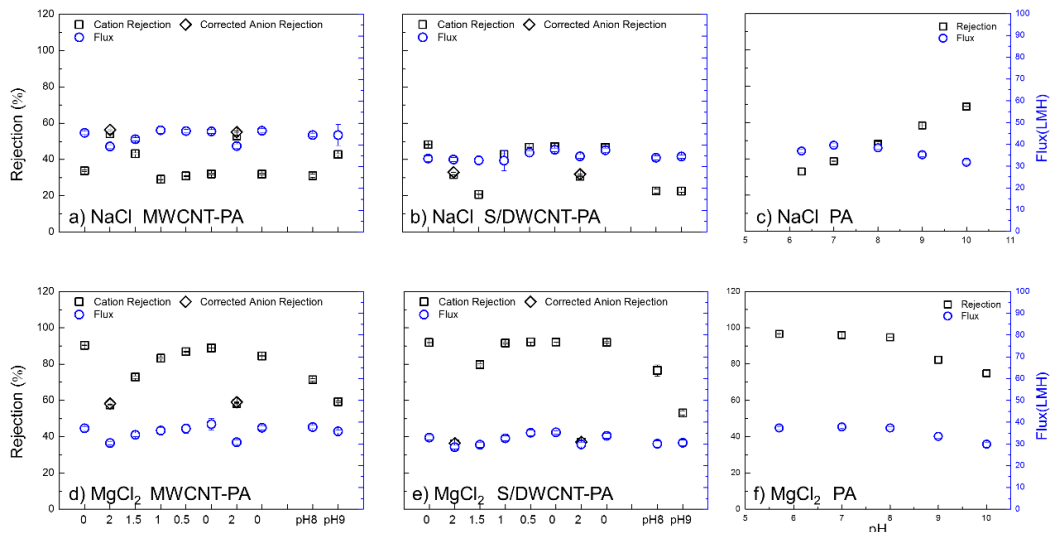


Figure 4.6: Membrane flux and rejection evaluation under different pHs. The rejection and flux (black square and blue circle) of MWCNT-PA and S/DWCNT membranes when treating NaCl and MgCl₂ solutions at elevated pHs (a, b, d, e). Their rejection and flux at electrical potentials from 0-2V were presented as references. Plain PA membrane's rejection and flux for NaCl and MgCl₂ solutions (c, f) at pHs from 5-10.

4.3.3.3 The evaluation of pH impact on single salt rejection

The ion separation is mainly governed by a combined membrane pore size and surface charges. The increase of surface potentials through direct charging and local pH enhancement at the membrane water interface allowed higher electrostatic interactions between the membrane surface and ion species. To better understand the observed phenomena, MWCNT-PA and S/DWCNT-PA membranes were tested under different pHs, as well as plain PA membranes that were fabricated with the same approach (Figure 4.6). As expected, in regard to NaCl solution, MWCNT-PA membranes had increased ion rejection (Figure 4.6a), while S/DWCNT-PA membranes showed lower rejection when the pH increased to 9 (Figure 4.6b). Furthermore, the rejections of MgCl₂ solution were reduced for both membranes as the pH went up to 9 (Figure 4.6d, 4.6e). Plain PA membranes were tested as the reference that the increase of pH (from 6 to 10) resulted in an enhanced rejection of NaCl and a drop of MgCl₂ rejection, which exhibited a similar trend to MWCNT-PA membranes. The distinctive rejection of SWCNT-PA membranes toward NaCl solution under different pH and electrical potentials was probably due to the intrinsic properties of its film structure.

4.4 Conclusions

This work has presented the successful fabrication of electrically conductive NF membranes by incorporating MWCNT and S/DWCNT into PA film. The ion selectivity of both membranes was evaluated using single and mixed salt solutions. Two types of CNT networks tuned membrane's ion selectivity in dramatic different ways under electrical potentials. The two distinctive PA-CNT film structure is probably the main cause of the

resulted difference. However, it is still not clear how does the film structure change membrane's ion selection under different charges.

The use of this novel NF membranes allows a more powerful and dynamic control of ion selectivity. In addition, it addresses the low ionic strength limitation and still performs well at a relatively high ionic strength. Therefore, these membranes can be potentially used for advanced NF treatment processes when the dynamic gating is needed, not only for ion separations, but also potentially for small organic compound separations, such as purifying multicomponent proteins and dyes systems.

4.5 Acknowledgements

This work was generously supported by the Office of Naval Research under award number N00014-14-1-0809, and the National Science Foundation under award number 1553756.

4.6 Supporting information

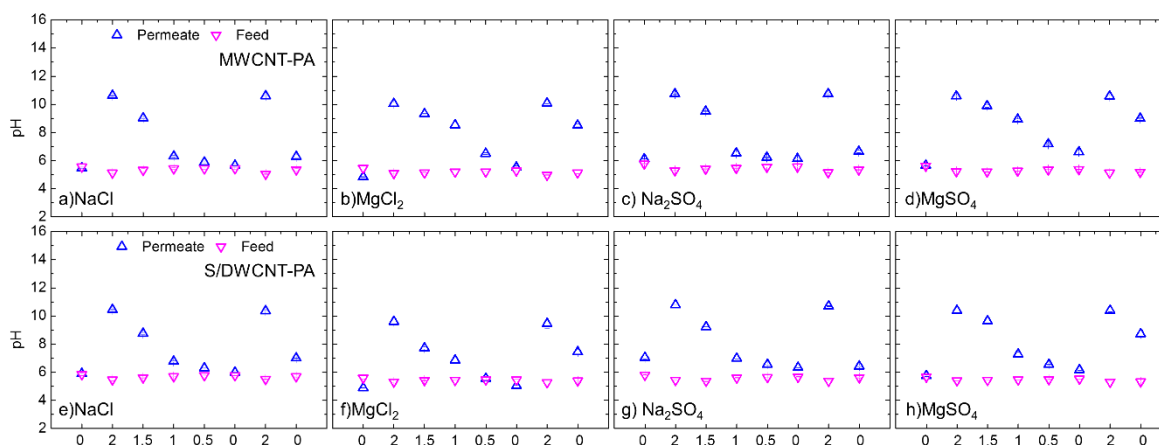


Figure 4.S1: The pH of the feed (pink inverted triangle) and the permeate solutions (blue triangle) of MWCNT-PA (a-d) and S/WNT-PA (e-h) when treating NaCl, MgCl₂, Na₂SO₄ and MgSO₄ solutions at different electrical potentials. Cell potentials ranging from 0-2V were applied repeatedly to the membrane surface and the counter electrode. Membranes are used as cathode to avoid electrooxidation.

Chapter 5. Conclusion

The dissertation presented potential applications of electrically conductive membranes fabricated with CNTs. In particular, by tuning the membrane's surface charges via external potentials, electroactive membranes were excellent at preventing oil fouling and adjusting its' selectivity towards salt ions.

In **Chapter 1**, we briefly stated that membrane technology was effective at addressing water scarcity issue, then further discussed its fundamentals including membrane classification, transport mechanism, and concentration polarization. We presented the overview of membranes for oil/water separation. Soon after we discussed their fouling mechanisms and recent achievements. Additionally, we emphasized the background of nanofiltration membranes, summarized their separation mechanisms and several new developments. Finally, we reviewed applications of electroactive membranes for water reuse and desalination. An economic analysis was provided to evaluate the potentials of utilizing electroactive membranes for real applications.

Chapter 2 discussed the surfactants' effect on membrane oil fouling in UF and NF processes. Specifically, the membrane surface fouling by different types of surfactant-stabilized oil emulsions in UF and NF processes were studied. Two commercially available UF and NF membranes were tested. Three different surfactants including DDBS, CTAB, and TX-100, which have a negative, positive and neutral hydrophilic head were used to stabilize oil droplets. Those stabilized emulsions were systematically characterized in terms of their charge, size and surface tensions. Membrane process was operated in

constant flux mode and tested in the electrolyte of DI water and 10 mM NaCl solutions. The membrane fouling event was evaluated based on the operating pressures, and the membrane's effective separation of oil/water was examined by conducting the TOC analysis of the permeate. The hydraulic cleaning was also used to test the effectiveness of restoring membrane flux.

It was observed that electrostatic interactions between the membrane surface and emulsion droplets were important for membrane fouling and rejection. Positively charged CTAB stabilized emulsion droplets were preferentially attracted and fouled membranes rapidly, as well as easily penetrating through the UF membranes. However, no significant difference was observed between CTAB and DDDBS stabilized emulsions at the elevated ionic strength of 10 mM NaCl. This result corresponded well with the reduced surface charges for both membranes and emulsion droplets due to electrical double layer compression. The increase of ionic strength reduced surface tensions of oil droplets, which lead to easier penetration of oil droplets through UF membranes. In addition, once membranes were wetted by emulsion droplets, hydraulic cleaning was not effective at recovering membrane flux.

Two model approaches were used to illustrate the penetration of oil droplets through UF membranes and the membrane surface wetting event by emulsion droplets. Emulsion's properties including droplet size, contact angle, and interfacial tension were determining factors in these models. We also proposed that cake layer formation was responsible for the linear pressure increase in both UF and NF processes. However, once the pressure drop

across the cake layer exceeded a critical point, droplets wetted the membrane, which resulted in irreversible fouling.

This study conveyed a message that droplets' surface charges were fundamentally important for membrane surface fouling, which also provided insights that the electrostatic force between emulsion droplets and membrane surface was crucial for membrane fouling, which lead to a continued study in Chapter 3. The results may be helpful for industrial companies to use proper detergents when creating oily wastewater.

Chapter 3 presented the oil fouling reduction on membrane surface using CNT based electrically conductive membranes. Oil droplets were prepared by stabilizing hexadecane using DDBS in the electrolyte of DI water and 100 mM NaCl solution. Prepared emulsion droplets were characterized with respect to their zeta potential, droplet size, and interfacial tension. Commercial UF membranes were coated with a conductive CNT film and tested in a constant flux mode. A dramatic reduction of membrane fouling was achieved with the assistance of electrical potentials. A systematic analysis of force acting on droplets near membrane surface was done to understand the fouling phenomena. The model indicated that using the membrane as a cathode can significantly enhance the maximum repulsive force in DI water. Increasing the negative potentials of membrane surface didn't increase the force, it only extended the distance between the droplet and membrane surface further away where the maximum force occurred.

We investigated the impact of applied electrical potentials on emulsion droplets using a contact angle goniometer. Emulsion droplets experienced a reversible shape change when

membrane surface was charged under different electrical potentials. A cathodic potential turned droplet into a more oblong shape, and an anodic potential restored droplet to a more circular shape. We hypothesized this phenomenon was due to an uneven distribution of surfactants on the emulsion droplets. A droplet with oblong shape indicated a denser packing of surfactants away from the membrane surface that prevented emulsion coalescence. While a droplet with circular shape revealed a completely opposite packing of surfactants and favored emulsion coalescence. We used film drainage model to quantify the emulsion coalescence efficiency, and further linked it the subsequent membrane wetting event.

This study provided a fundamental study of the potential impact on oil emulsion droplets in a UF filtration process. It proved that membranes were able to reduce emulsion droplets fouling through increasing their surface charges, even at high ionic strengths of 100 mM NaCl. Electroactive membranes were one promising tool to deal with oily wastewater, which contained high salinity, such as bilge water and produced water. However, these electroactive membranes were not stable under anodic potentials, which may lead to electro-oxidation of carbon materials in water. Besides, the proper selection of membrane supports was important, because membranes with large pores may lead to the breakout of emulsion droplets. In particular, oil droplets had extremely low interfacial tensions at high ionic strengths, which can easily penetrate through highly porous membranes.

Chapter 4 reported the application of two electrically conducting NF membranes for selective separation of salt ions. PA film was acted as the active layer, MWCNT and S/DWCNT formed conductive skeletons and used to provide extra surface charges. The

characterization of membrane's electrical conductivity revealed that S/DWCNT membrane was much more conductive and had higher capacity for ion storage. Filtration results of treating single salt, and mixed salt solution demonstrated that MWCNT-PA membrane behaved similar to plain PA membrane, where extra negative surface charges contributed to higher rejections for Na^+ and Cl^- , and lower rejection for Mg^{2+} . In contrast, S/DWCNT-PA membrane was better for releasing Na^+ , Mg^{2+} , Cl^- ions and rejecting SO_4^{2-} with increased negative surface charges. The XPS analysis confirmed that MWCNT-PA had similar crosslinking degree of PA film compared to plain PA membrane, while S/DWCNT-PA membrane was less crosslinked, which left more free carboxylic groups. AFM and SEM confirmed that a complete PA film of 200 nm was formed on top of the MWCNT network, while no clear and complete PA film was found on top of the S/DWCNT film, but several bumps were found within CNT film. We speculate that PA film was rather embedded into the S/DWCNT membranes. This surface morphology may result in a completely different behavior of ion selectivity under different electrical potentials. However, it still requires additional theoretical study which is completely different than traditional NF transport mechanisms.

Electroactive NF membranes demonstrated new promises to dynamically adjust ion's selectivity via applying electrical potentials. It may be helpful for industrial separation processes which need different selectivity at different stages, or require more precise separation of nanometer ranged substances. For example, these membranes would be beneficial for treating textile wastewater and recovering valuable components. In addition, adjusting surface potentials could theoretically use for separating biomolecules with

different molecular weights. However, it is still necessary to further conduct the research to study the impact of electrical potentials on the rejection of small organic compounds using electroactive membranes.

References

- (1) Gleick, P. H. *Encyclopedia of Climate and Weather (2 Ed.)*; 2011.
- (2) Mekonnen, M. M.; Hoekstra, Y. A. Four Billion People Experience Water Scarcity. *Sci. Adv.* **2016**, *2*, 1–7.
- (3) Shannon, M. A.; Bohn, P. W.; Elimelech, M.; Georgiadis, J. G.; Mariñas, B. J.; Mayes, A. M. Science and Technology for Water Purification in the Coming Decades. *Nature* **2008**, *452*, 301–310.
- (4) Berkoff, J. China: The South-North Water Transfer Project - Is It Justified? *Water Policy* **2003**, *5*, 1–28.
- (5) Elimelech, M.; Phillip, W. a. The Future of Seawater Desalination: Energy, Technology, and the Environment. *Science* **2011**, *333*, 712–717.
- (6) Pellegrin, M.-L.; Aguinaldo, J.; Arabi, S.; Sadler, M. E.; Min, K.; Liu, M.; Salamon, C.; Greiner, A. D.; Diamond, J.; McCandless, R.; Owerdieck, C.; Wert, J.; Padhye, L. P. Membrane Processes. *Water Environ. Res.* **2013**, *85*, 1092–1175.
- (7) Jacangelo, J. G.; Trussell, R. R.; Watson, M. Role of Membrane Technology in Drinking Water Treatment in the United States. *Desalination* **1997**, *113*, 119–127.
- (8) Salahi, A.; Gheshlaghi, A.; Mohammadi, T.; Madaeni, S. S. Experimental Performance Evaluation of Polymeric Membranes for Treatment of an Industrial Oily Wastewater. *Desalination* **2010**, *262*, 235–242.
- (9) Fujioka, T.; Nghiem, L. D.; Khan, S. J.; McDonald, J. A.; Poussade, Y.; Drewes, J. E. Effects of Feed Solution Characteristics on the Rejection of N-Nitrosamines by Reverse Osmosis Membranes. *J. Memb. Sci.* **2012**, *409–410*, 66–74.
- (10) Greenlee, L. F.; Lawler, D. F.; Freeman, B. D.; Marrot, B.; Moulin, P. Reverse Osmosis Desalination: Water Sources, Technology, and Today's Challenges. *Water Res.* **2009**, *43*, 2317–2348.
- (11) Baker, R. W. *Membrane Technology and Applications*; John Wiley & Sons, Ltd: Chichester, UK, 2004.
- (12) Wijmans, J. G.; Baker, R. W. The Solution-Diffusion Model: A Review. *J. Memb. Sci.* **1995**, *107*, 1–21.
- (13) Choo, K. H.; Lee, C. H. Membrane Fouling Mechanisms in the Membrane-Coupled Anaerobic Bioreactor. *Water Res.* **1996**, *30*, 1771–1780.

- (14) Kemp, J. Waste Water: America's Hidden 60 Million Barrel A Day Industry https://www.huffingtonpost.com/2012/01/16/waste-water-barrel_n_1208587.html.
- (15) Tummons, E. N.; Tarabara, V. V.; Chew, J. W.; Fane, A. G. Behavior of Oil Droplets at the Membrane Surface during Crossflow Microfiltration of Oil-Water Emulsions. *J. Memb. Sci.* **2016**, *500*, 211–224.
- (16) Zhu, X.; Dudchenko, A.; Gu, X.; Jassby, D. Surfactant-Stabilized Oil Separation from Water Using Ultrafiltration and Nanofiltration. *J. Memb. Sci.* **2017**, *529*, 159–169.
- (17) Hermia, J. Constant Pressure Blocking Filtration Laws - Application Topower-Law Non-Newtonian Fluids. *Trans Inst Chem Eng* **1982**, *V 60*, 183–187.
- (18) Duclos-Orsello, C.; Li, W.; Ho, C. C. A Three Mechanism Model to Describe Fouling of Microfiltration Membranes. *J. Memb. Sci.* **2006**, *280*, 856–866.
- (19) Lu, D.; Zhang, T.; Ma, J. Ceramic Membrane Fouling during Ultrafiltration of Oil/Water Emulsions: Roles Played by Stabilization Surfactants of Oil Droplets. *Environ. Sci. Technol.* **2015**, *49*, 4235–4244.
- (20) Wang, F.; Tarabara, V. V. Pore Blocking Mechanisms during Early Stages of Membrane Fouling by Colloids. *J. Colloid Interface Sci.* **2008**, *328*, 464–469.
- (21) Liao, Y.; Lucas, D. A Literature Review on Mechanisms and Models for the Coalescence Process of Fluid Particles. *Chem. Eng. Sci.* **2010**, *65*, 2851–2864.
- (22) Shinnar, R.; Church, J. M. Statistical Theories of Turbulence In... Predicting Particle Size in Agitated Dispersions. *Ind. Eng. Chem.* **1960**, *52*, 253–256.
- (23) Zhu, X.; Dudchenko, A. V.; Khor, C. M.; He, X.; Ramon, G.; Jassby, D. Field-Induced Redistribution of Surfactants at the Oil/Water Interface Reduces Membrane Fouling on Electrically Conducting Carbon Nanotube UF Membranes. *Environ. Sci. Technol.* **2018**, *52*, 11591–11600.
- (24) Sovová, H. Breakage and Coalescence of Drops in a Batch Stirred Vessel-II Comparison of Model and Experiments. *Chem. Eng. Sci.* **1981**.
- (25) Rekvig, L.; Hafskjold, B.; Smit, B. Molecular Simulations of Surface Forces and Film Rupture in Oil/Water/Surfactant Systems. *Langmuir* **2004**, *20*, 11583–11593.
- (26) Wang, Z.; Elimelech, M.; Lin, S. Environmental Applications of Interfacial Materials with Special Wettability. *Environ. Sci. Technol.* **2016**, *50*, 2132–2150.
- (27) Otitoju, T. A.; Ahmad, A. L.; Ooi, B. S. Polyvinylidene Fluoride (PVDF) Membrane for Oil Rejection from Oily Wastewater: A Performance Review. *J. Water Process*

Eng. **2016**, *14*, 41–59.

- (28) Ochoa, N. A.; Masuelli, M.; Marchese, J. Effect of Hydrophilicity on Fouling of an Emulsified Oil Wastewater with PVDF/PMMA Membranes. *J. Memb. Sci.* **2003**, *226*, 203–211.
- (29) Ong, C. S.; Lau, W. J.; Goh, P. S.; Ng, B. C.; Matsuura, T.; Ismail, A. F. Effect of PVP Molecular Weights on the Properties of PVDF-TiO₂ Composite Membrane for Oily Wastewater Treatment Process. *Sep. Sci. Technol.* **2014**, *49*, 2303–2314.
- (30) Bowen, W. R.; Cheng, S. Y.; Doneva, T. A.; Oatley, D. L. Manufacture and Characterisation of Polyetherimide/Sulfonated Poly(Ether Ether Ketone) Blend Membranes. *J. Memb. Sci.* **2005**, *250*, 1–10.
- (31) Masuelli, M.; Marchese, J.; Ochoa, N. A. SPC/PVDF Membranes for Emulsified Oily Wastewater Treatment. *J. Memb. Sci.* **2009**, *326*, 688–693.
- (32) Chen, W.; Su, Y.; Peng, J.; Dong, Y.; Zhao, X.; Jiang, Z. Engineering a Robust, Versatile Amphiphilic Membrane Surface through Forced Surface Segregation for Ultralow Flux-Decline. *Adv. Funct. Mater.* **2011**.
- (33) Revanur, R.; McCloskey, B.; Breitenkamp, K.; Freeman, B. D.; Emrick, T. Reactive Amphiphilic Graft Copolymer Coatings Applied to Poly(Vinylidene Fluoride) Ultrafiltration Membranes. *Macromolecules* **2007**.
- (34) Liu, F.; Du, C. H.; Zhu, B. K.; Xu, Y. Y. Surface Immobilization of Polymer Brushes onto Porous Poly(Vinylidene Fluoride) Membrane by Electron Beam to Improve the Hydrophilicity and Fouling Resistance. *Polymer (Guildf)*. **2007**, *48*, 2910–2918.
- (35) Yu, H.; Cao, Y.; Kang, G.; Liu, J.; Li, M.; Yuan, Q. Enhancing Antifouling Property of Polysulfone Ultrafiltration Membrane by Grafting Zwitterionic Copolymer via UV-Initiated Polymerization. *J. Memb. Sci.* **2009**, *342*, 6–13.
- (36) Wavhal, D. S.; Fisher, E. R. Hydrophilic Modification of Polyethersulfone Membranes by Low Temperature Plasma-Induced Graft Polymerization. *J. Memb. Sci.* **2002**, *209*, 255–269.
- (37) Zhu, L. P.; Dong, H. B.; Wei, X. Z.; Yi, Z.; Zhu, B. K.; Xu, Y. Y. Tethering Hydrophilic Polymer Brushes onto PPESK Membranes via Surface-Initiated Atom Transfer Radical Polymerization. *J. Memb. Sci.* **2008**, *320*, 407–415.
- (38) Wang, B.; Liang, W.; Guo, Z.; Liu, W. Biomimetic Super-Lyophobic and Super-Lyophilic Materials Applied for Oil/Water Separation: A New Strategy beyond Nature. *Chem. Soc. Rev.* **2015**, *44*, 336–361.

- (39) Bixler, G. D.; Bhushan, B. Review Article: Biofouling: Lessons from Nature. *Philos. Trans. R. Soc. A Math. Phys. Eng. Sci.* **2012**, *370*, 2381–2417.
- (40) Hilal, N.; Al-Zoubi, H.; Darwish, N. A.; Mohammad, A. W.; Abu Arabi, M. A Comprehensive Review of Nanofiltration Membranes: Treatment, Pretreatment, Modelling, and Atomic Force Microscopy. *Desalination* **2004**, *170*, 281–308.
- (41) Zhou, D.; Zhu, L.; Fu, Y.; Zhu, M.; Xue, L. Development of Lower Cost Seawater Desalination Processes Using Nanofiltration Technologies - A Review. *Desalination* **2015**, *376*, 109–116.
- (42) Mohammad, A. W.; Teow, Y. H.; Ang, W. L.; Chung, Y. T.; Oatley-Radcliffe, D. L.; Hilal, N. Nanofiltration Membranes Review: Recent Advances and Future Prospects. *Desalination* **2015**, *356*, 226–254.
- (43) Marchetti, P.; Jimenez Solomon, M. F.; Szekely, G.; Livingston, A. G. Molecular Separation with Organic Solvent Nanofiltration: A Critical Review. *Chem. Rev.* **2014**, *114*, 10735–10806.
- (44) Sharma, R. R.; Agrawal, R.; Chellam, S. Temperature Effects on Sieving Characteristics of Thin-Film Composite Nanofiltration Membranes: Pore Size Distributions and Transport Parameters. *J. Memb. Sci.* **2003**, *223*, 69–87.
- (45) Bowen, W. R.; Mohammad, A. W.; Hilal, N. Characterisation of Nanofiltration Membranes for Predictive Purposes - Use of Salts, Uncharged Solutes and Atomic Force Microscopy. *J. Memb. Sci.* **1997**, *126*, 91–105.
- (46) Wang, X. L.; Tsuru, T.; Masanori, M.; Togoh, T.; Nakao, S. I.; Kimura, S. Evaluation of Pore Structure and Electrical Properties of Nanofiltration Membranes. *Journal of Chemical Engineering of Japan*. 1995, pp 186–192.
- (47) VAN DER BRUGGEN, B.; SCHAEP, J.; WILMS, D.; VANDECASTEELE, C. A Comparison of Models to Describe the Maximal Retention of Organic Molecules in Nanofiltration. *Sep. Sci. Technol.* **2002**, *35*, 169–182.
- (48) Seidel, A.; Waypa, J. J.; Elimelech, M. Role of Charge (Donnan) Exclusion in Removal of Arsenic from Water by a Negatively Charged Porous Nanofiltration Membrane. *Environ. Eng. Sci.* **2001**, *18*, 105–113.
- (49) Galanakis, C. M.; Tornberg, E.; Gekas, V. Clarification of High-Added Value Products from Olive Mill Wastewater. *J. Food Eng.* **2010**, *99*, 190–197.
- (50) Yaroshchuk, A. E. Non-Steric Mechanism of Nanofiltration: Superposition of Donnan and Dielectric Exclusion. *Sep. Purif. Technol.* **2001**, *22–23*, 143–158.

- (51) Bowen, W. R.; Welfoot, J. S. Modelling the Performance of Membrane Nanofiltration-Critical Assessment and Model Development. *Chem. Eng. Sci.* **2002**, *57*, 1121–1137.
- (52) Wang, J.; Mo, Y.; Mahendra, S.; Hoek, E. M. V. Effects of Water Chemistry on Structure and Performance of Polyamide Composite Membranes. *J. Memb. Sci.* **2014**, *452*, 415–425.
- (53) Szoke, S.; Patzay, G.; Weiser, L. Characteristics of Thin-Film Nanofiltration Membranes at Various PH-Values. *Desalination* **2003**, *151*, 123–129.
- (54) Richards, L. A.; Schäfer, A. I.; Richards, B. S.; Corry, B. The Importance of Dehydration in Determining Ion Transport in Narrow Pores. *Small* **2012**, *8*, 1701–1709.
- (55) Epsztein, R.; Shaulsky, E.; Dizge, N.; Warsinger, D. M.; Elimelech, M. Role of Ionic Charge Density in Donnan Exclusion of Monovalent Anions by Nanofiltration. *Environ. Sci. Technol.* **2018**, *52*, 4108–4116.
- (56) Levi, M. D.; Sigalov, S.; Salitra, G.; Elazari, R.; Aurbach, D. Assessing the Solvation Numbers of Electrolytic Ions Confined in Carbon Nanopores under Dynamic Charging Conditions. *J. Phys. Chem. Lett.* **2011**, *2*, 120–124.
- (57) Yang, L.; Garde, S. Modeling the Selective Partitioning of Cations into Negatively Charged Nanopores in Water. *J. Chem. Phys.* **2007**, *126*, 1–22.
- (58) Bargeman, G.; Vollenbroek, J. M.; Straatsma, J.; Schroën, C. G. P. H.; Boom, R. M. Nanofiltration of Multi-Component Feeds. Interactions between Neutral and Charged Components and Their Effect on Retention. *J. Memb. Sci.* **2005**, *247*, 11–20.
- (59) Mänttari, M.; Pihlajamäki, A.; Nyström, M. Effect of PH on Hydrophilicity and Charge and Their Effect on the Filtration Efficiency of NF Membranes at Different PH. *J. Memb. Sci.* **2006**, *280*, 311–320.
- (60) Bouchoux, A.; Roux-De Balman, H.; Lutin, F. Nanofiltration of Glucose and Sodium Lactate Solutions: Variations of Retention between Single- and Mixed-Solute Solutions. *J. Memb. Sci.* **2005**, *258*, 123–132.
- (61) Escoda, A.; Fievet, P.; Lakard, S.; Szymczyk, A.; Déon, S. Influence of Salts on the Rejection of Polyethyleneglycol by an NF Organic Membrane: Pore Swelling and Salting-out Effects. *J. Memb. Sci.* **2010**, *347*, 174–182.
- (62) Luo, J.; Wan, Y. Effect of Highly Concentrated Salt on Retention of Organic Solutes by Nanofiltration Polymeric Membranes. *J. Memb. Sci.* **2011**, *372*, 145–153.

- (63) Wang, X.; Zhang, C.; Ouyang, P. The Possibility of Separating Saccharides from a NaCl Solution by Using Nanofiltration in Diafiltration Mode. *J. Memb. Sci.* **2002**, *204*, 271–281.
- (64) Faucher, S.; Aluru, N.; Bazant, M. Z.; Blankschtein, D.; Brozena, A. H.; Cumings, J.; Pedro de Souza, J.; Elimelech, M.; Epsztein, R.; Fourkas, J. T.; Rajan, A. G.; Kulik, H. J.; Levy, A.; Majumdar, A.; Martin, C.; McEldrew, M.; Misra, R. P.; Noy, A.; Pham, T. A.; et al. Critical Knowledge Gaps in Mass Transport through Single-Digit Nanopores: A Review and Perspective. *J. Phys. Chem. C* **2019**, *acs.jpcc.9b02178*.
- (65) Van der Bruggen, B.; Mänttari, M.; Nyström, M. Drawbacks of Applying Nanofiltration and How to Avoid Them: A Review. *Sep. Purif. Technol.* **2008**, *63*, 251–263.
- (66) Antony, A.; Low, J. H.; Gray, S.; Childress, A. E.; Le-Clech, P.; Leslie, G. Scale Formation and Control in High Pressure Membrane Water Treatment Systems: A Review. *J. Memb. Sci.* **2011**, *383*, 1–16.
- (67) De Lannoy, C. F.; Jassby, D.; Gloe, K.; Gordon, A. D.; Wiesner, M. R. Aquatic Biofouling Prevention by Electrically Charged Nanocomposite Polymer Thin Film Membranes. *Environ. Sci. Technol.* **2013**, *47*, 2760–2768.
- (68) Falk, K.; Sedlmeier, F.; Joly, L.; Netz, R. R.; Bocquet, L. Molecular Origin of Fast Water Transport in Carbon Nanotube Membranes: Superlubricity versus Curvature Dependent Friction. *Nano Lett.* **2010**, *10*, 4067–4073.
- (69) Agrawal, K. V.; Shimizu, S.; Draushuk, L. W.; Kilcoyne, D.; Strano, M. S. Observation of Extreme Phase Transition Temperatures of Water Confined inside Isolated Carbon Nanotubes. *Nat. Nanotechnol.* **2017**.
- (70) Gelb, L. D.; Gubbins, K. E.; Radhakrishnan, R.; Sliwinski-Bartkowiak, M. Phase Separation in Confined Systems. *Reports Prog. Phys.* **1999**.
- (71) Goldsmith, B. R.; Coroneus, J. G.; Khalap, V. R.; Kane, A. A.; Weiss, G. A.; Collins, P. G. Conductance-Controlled Point Functionalization of Single-Walled Carbon Nanotubes. *Science (80-)*. **2007**.
- (72) Luo, Z. X.; Xing, Y. Z.; Ling, Y. C.; Kleinhammes, A.; Wu, Y. Electroneutrality Breakdown and Specific Ion Effects in Nanoconfined Aqueous Electrolytes Observed by NMR. *Nat. Commun.* **2015**.
- (73) Luo, Z. X.; Xing, Y. Z.; Liu, S.; Ling, Y. C.; Kleinhammes, A.; Wu, Y. Dehydration of Ions in Voltage-Gated Carbon Nanopores Observed by in Situ NMR. *J. Phys. Chem. Lett.* **2015**.

- (74) Werber, J. R.; Osuji, C. O.; Elimelech, M. Materials for Next-Generation Desalination and Water Purification Membranes. *Nature Reviews Materials*. 2016.
- (75) Lee, S. Y.; Kim, H. J.; Patel, R.; Im, S. J.; Kim, J. H.; Min, B. R. Silver Nanoparticles Immobilized on Thin Film Composite Polyamide Membrane: Characterization, Nanofiltration, Antifouling Properties. *Polym. Adv. Technol.* **2007**, *18*, 562–568.
- (76) Rajaeian, B.; Rahimpour, A.; Tade, M. O.; Liu, S. Fabrication and Characterization of Polyamide Thin Film Nanocomposite (TFN) Nanofiltration Membrane Impregnated with TiO₂ Nanoparticles. *Desalination* **2013**, *313*, 176–188.
- (77) Goh, K.; Jiang, W.; Karahan, H. E.; Zhai, S.; Wei, L.; Yu, D.; Fane, A. G.; Wang, R.; Chen, Y. All-Carbon Nanoarchitectures as High-Performance Separation Membranes with Superior Stability. *Adv. Funct. Mater.* **2015**, *25*, 7348–7359.
- (78) Liu, G.; Jin, W.; Xu, N. Graphene-Based Membranes. *Chem. Soc. Rev.* **2015**, *44*, 5016–5030.
- (79) Hinds, B. J. Aligned Multiwalled Carbon Nanotube Membranes. *Science (80-)*. **2004**, *303*, 62–65.
- (80) Zhang, H.; Quan, X.; Chen, S.; Fan, X.; Wei, G.; Yu, H. Combined Effects of Surface Charge and Pore Size on Co-Enhanced Permeability and Ion Selectivity through RGO-OCNT Nanofiltration Membranes. *Environ. Sci. Technol.* **2018**, *52*, 4827–4834.
- (81) Hu, C.; Liu, Z.; Lu, X.; Sun, J.; Liu, H.; Qu, J. Enhancement of the Donnan Effect through Capacitive Ion Increase Using an Electroconductive RGO-CNT Nanofiltration Membrane. *J. Mater. Chem. A* **2018**, *6*, 4737–4745.
- (82) Zhu, X.; Jassby, D. Electroactive Membranes for Water Treatment: Enhanced Treatment Functionalities, Energy Considerations, and Future Challenges. *Acc. Chem. Res.* **2019**, *52*, 1177–1186.
- (83) Shaffer, D. L.; Arias Chavez, L. H.; Ben-Sasson, M.; Romero-Vargas Castrillón, S.; Yip, N. Y.; Elimelech, M. Desalination and Reuse of High-Salinity Shale Gas Produced Water: Drivers, Technologies, and Future Directions. *Environ. Sci. Technol.* **2013**, *47*, 9569–9583.
- (84) Jassby, D.; Cath, T. Y.; Buisson, H. The Role of Nanotechnology in Industrial Water Treatment. *Nat. Nanotechnol.* **2018**, *13*, 670–672.
- (85) Glater, J.; Hong, S. kwan; Elimelech, M. The Search for a Chlorine-Resistant Reverse Osmosis Membrane. *Desalination* **1994**, *95*, 325–345.

- (86) Duan, W.; Dudchenko, A.; Mende, E.; Flyer, C.; Zhu, X.; Jassby, D. Electrochemical Mineral Scale Prevention and Removal on Electrically Conducting Carbon Nanotube-Polyamide Reverse Osmosis Membranes. *Environ. Sci. Process. Impacts* **2014**, *16*, 1300–1308.
- (87) Dong, Y.; Ma, L.; Tang, C. Y.; Yang, F.; Quan, X.; Jassby, D.; Zaworotko, M. J.; Guiver, M. D. Stable Superhydrophobic Ceramic-Based Carbon Nanotube Composite Desalination Membranes. *Nano Lett.* **2018**, *18*, acs.nanolett.8b01907.
- (88) Dudchenko, A. V.; Chen, C.; Cardenas, A.; Rolf, J.; Jassby, D. Frequency-Dependent Stability of CNT Joule Heaters in Ionizable Media and Desalination Processes. *Nat. Nanotechnol.* **2017**, *12*, 557–563.
- (89) de Lannoy, C. F.; Jassby, D.; Davis, D. D.; Wiesner, M. R. A Highly Electrically Conductive Polymer-Multiwalled Carbon Nanotube Nanocomposite Membrane. *J. Memb. Sci.* **2012**, *415–416*, 718–724.
- (90) Duan, W.; Ronen, A.; Walker, S.; Jassby, D. Polyaniline-Coated Carbon Nanotube Ultrafiltration Membranes: Enhanced Anodic Stability for in Situ Cleaning and Electro-Oxidation Processes. *ACS Appl. Mater. Interfaces* **2016**, *8*, 22574–22584.
- (91) Zhou, Y.; Hu, L.; Grüner, G. A Method of Printing Carbon Nanotube Thin Films. *Appl. Phys. Lett.* **2006**, *88*, 1–4.
- (92) Duan, W.; Ronen, A.; de Leon, J. V.; Dudchenko, A.; Yao, S.; Corbala-Delgado, J.; Yan, A.; Matsumoto, M.; Jassby, D. Treating Anaerobic Sequencing Batch Reactor Effluent with Electrically Conducting Ultrafiltration and Nanofiltration Membranes for Fouling Control. *J. Memb. Sci.* **2016**, *504*, 104–112.
- (93) Tang, L.; Iddya, A.; Zhu, X.; Dudchenko, A. V.; Duan, W.; Turchi, C.; Vanneste, J.; Cath, T. Y.; Jassby, D. Enhanced Flux and Electrochemical Cleaning of Silicate Scaling on Carbon Nanotube-Coated Membrane Distillation Membranes Treating Geothermal Brines. *ACS Appl. Mater. Interfaces* **2017**, *9*, 38594–38605.
- (94) Ong, C. S.; Goh, P. S.; Lau, W. J.; Misdan, N.; Ismail, A. F. Nanomaterials for Biofouling and Scaling Mitigation of Thin Film Composite Membrane: A Review. *Desalination* **2016**, *393*, 2–15.
- (95) Umar, A. A.; Saaid, I. M. Effects of Temperature on Silicate Scale Inhibition During ASP Flooding. *J. Appl. Sci.* **2014**, No. 14, 1769–1774.
- (96) Tzotzi, C.; Pahiadaki, T.; Yiantisios, S. G.; Karabelas, A. J.; Andritsos, N. A Study of CaCO₃ scale Formation and Inhibition in RO and NF Membrane Processes. *J. Memb. Sci.* **2007**, *296*, 171–184.

- (97) Hasson, D.; Drak, A.; Semiat, R. Inception of CaSO₄ scaling on RO Membranes at Various Water Recovery Levels. *Desalination* **2001**, *139*, 73–81.
- (98) Greenlee, L. F.; Testa, F.; Lawler, D. F.; Freeman, B. D.; Moulin, P. The Effect of Antiscalant Addition on Calcium Carbonate Precipitation for a Simplified Synthetic Brackish Water Reverse Osmosis Concentrate. *Water Res.* **2010**, *44*, 2957–2969.
- (99) Tran, Q. K.; Schwabe, K. A.; Jassby, D. Wastewater Reuse for Agriculture: Development of a Regional Water Reuse Decision-Support Model (RWRM) for Cost-Effective Irrigation Sources. *Environ. Sci. Technol.* **2016**, *50*, 9390–9399.
- (100) Matin, A.; Khan, Z.; Zaidi, S. M. J.; Boyce, M. C. Biofouling in Reverse Osmosis Membranes for Seawater Desalination: Phenomena and Prevention. *Desalination* **2011**, *281*, 1–16.
- (101) Herzberg, M.; Elimelech, M. Biofouling of Reverse Osmosis Membranes: Role of Biofilm-Enhanced Osmotic Pressure. *J. Memb. Sci.* **2007**, *295*, 11–20.
- (102) Baker, J. S.; Dudley, L. Y. Biofouling in Membrane Systems — A Review. *Desalination* **1998**, *118*, 81–89.
- (103) Ang, W. S.; Yip, N. Y.; Tiraferri, A.; Elimelech, M. Chemical Cleaning of RO Membranes Fouled by Wastewater Effluent: Achieving Higher Efficiency with Dual-Step Cleaning. *J. Memb. Sci.* **2011**, *382*, 100–106.
- (104) Gao, G.; Vecitis, C. D. Doped Carbon Nanotube Networks for Electrochemical Filtration of Aqueous Phenol: Electrolyte Precipitation and Phenol Polymerization. *ACS Appl. Mater. Interfaces* **2012**, *4*, 1478–1489.
- (105) Ronen, A.; Duan, W.; Wheeldon, I.; Walker, S.; Jassby, D. Microbial Attachment Inhibition through Low-Voltage Electrochemical Reactions on Electrically Conducting Membranes. *Environ. Sci. Technol.* **2015**, *49*, 12741–12750.
- (106) Pandit, S.; Shanbhag, S.; Mauter, M.; Oren, Y.; Herzberg, M. Influence of Electric Fields on Biofouling of Carbonaceous Electrodes. *Environ. Sci. Technol.* **2017**, *51*, 10022–10030.
- (107) Vecitis, C. D.; Schnoor, M. H.; Rahaman, M. S.; Schiffman, J. D.; Elimelech, M. Electrochemical Multiwalled Carbon Nanotube Filter for Viral and Bacterial Removal and Inactivation. *Environ. Sci. Technol.* **2011**, *45*, 3672–3679.
- (108) Agarwal, A.; Jern Ng, W.; Liu, Y. Removal of Biofilms by Intermittent Low-Intensity Ultrasonication Triggered Bursting of Microbubbles. *Biofouling* **2014**, *30*, 359–365.

- (109) Deshmukh, A.; Boo, C.; Karanikola, V.; Lin, S.; Straub, A. P.; Tong, T.; Warsinger, D. M.; Elimelech, M. Membrane Distillation at the Water-Energy Nexus: Limits, Opportunities, and Challenges. *Energy Environ. Sci.* **2018**, *11*, 1177–1196.
- (110) Finnerty, C.; Zhang, L.; Sedlak, D. L.; Nelson, K. L.; Mi, B. Synthetic Graphene Oxide Leaf for Solar Desalination with Zero Liquid Discharge. *Environ. Sci. Technol.* **2017**, *51*, 11701–11709.
- (111) Dongare, P. D.; Alabastri, A.; Pedersen, S.; Zodrow, K. R.; Hogan, N. J.; Neumann, O.; Wu, J.; Wang, T.; Deshmukh, A.; Elimelech, M.; Li, Q.; Nordlander, P.; Halas, N. J. Nanophotonics-Enabled Solar Membrane Distillation for off-Grid Water Purification. *Proc. Natl. Acad. Sci.* **2017**, *114*, 6936–6941.
- (112) Van Der Bruggen, B.; Vandecasteele, C.; Van Gestel, T.; Doyen, W.; Leysen, R. A Review of Pressure-Driven Membrane Processes in Wastewater Treatment and Drinking Water Production. *Environ. Prog.* **2003**, *22*, 46–56.
- (113) Porcelli, N.; Judd, S. Chemical Cleaning of Potable Water Membranes: A Review. *Sep. Purif. Technol.* **2010**, *71*, 137–143.
- (114) Guo, L.; Jing, Y.; Chaplin, B. P. Development and Characterization of Ultrafiltration TiO₂Magnéli Phase Reactive Electrochemical Membranes. *Environ. Sci. Technol.* **2016**, *50*, 1428–1436.
- (115) Gayen, P.; Spataro, J.; Avasarala, S. M.; Ali, A. M. S.; Cerrato, J. M. J. M.; Chaplin, B. P. Electrocatalytic Reduction of Nitrate Using Magnéli Phase TiO₂Reactive Electrochemical Membranes Doped with Pd-Based Catalysts. *Environ. Sci. Technol.* **2018**, *52*, 9370–9379.
- (116) Dudchenko, A. V.; Rolf, J.; Russell, K.; Duan, W.; Jassby, D. Organic Fouling Inhibition on Electrically Conducting Carbon Nanotube – Polyvinyl Alcohol Composite Ultra Filtration Membranes. *J. Memb. Sci.* **2014**, *468*, 1–10.
- (117) Zhang, Q.; Vecitis, C. D. Conductive CNT-PVDF Membrane for Capacitive Organic Fouling Reduction. *J. Memb. Sci.* **2014**, *459*, 143–156.
- (118) Liu, L.; Zhao, F.; Liu, J.; Yang, F. Preparation of Highly Conductive Cathodic Membrane with Graphene (Oxide)/PPy and the Membrane Antifouling Property in Filtrating Yeast Suspensions in EMBR. *J. Memb. Sci.* **2013**, *437*, 99–107.
- (119) Lee, N.; Amy, G.; Croué, J. P.; Buisson, H. Identification and Understanding of Fouling in Low-Pressure Membrane (MF/UF) Filtration by Natural Organic Matter (NOM). *Water Res.* **2004**, *38*, 4511–4523.
- (120) Jing, Y.; Guo, L.; Chaplin, B. P. Electrochemical Impedance Spectroscopy Study of

Membrane Fouling and Electrochemical Regeneration at a Sub-Stoichiometric TiO₂ reactive Electrochemical Membrane. *J. Memb. Sci.* **2016**, *510*, 510–523.

- (121) Jing, Y.; Chaplin, B. P. Electrochemical Impedance Spectroscopy Study of Membrane Fouling Characterization at a Conductive Sub-Stoichiometric TiO₂ Reactive Electrochemical Membrane: Transmission Line Model Development. *J. Memb. Sci.* **2016**, *511*, 238–249.
- (122) Huang, J.; Wang, Z.; Zhang, J.; Zhang, X.; Ma, J.; Wu, Z. A Novel Composite Conductive Microfiltration Membrane and Its Anti-Fouling Performance with an External Electric Field in Membrane Bioreactors. *Sci. Rep.* **2015**, *5*, 1–8.
- (123) Yang, Y.; Qiao, S.; Jin, R.; Zhou, J.; Quan, X. A Novel Aerobic Electrochemical Membrane Bioreactor with CNTs Hollow Fiber Membrane by Electrochemical Oxidation to Improve Water Quality and Mitigate Membrane Fouling. *Water Res.* **2019**.
- (124) Gayen, P.; Chen, C.; Abiade, J. T.; Chaplin, B. P. Electrochemical Oxidation of Atrazine and Clothianidin on Bi-Doped SnO₂-TiO₂ⁿ⁻¹ Electrocatalytic Reactive Electrochemical Membranes. *Environ. Sci. Technol.* **2018**, *52*, 12675–12684.
- (125) Duan, W.; Chen, G.; Chen, C.; Sanghvi, R.; Iddya, A.; Walker, S.; Liu, H.; Ronen, A.; Jassby, D. Electrochemical Removal of Hexavalent Chromium Using Electrically Conducting Carbon Nanotube/Polymer Composite Ultrafiltration Membranes. *J. Memb. Sci.* **2017**, *531*, 160–171.
- (126) Zaky, A. M.; Chaplin, B. P. Porous Substoichiometric TiO₂ Anodes as Reactive Electrochemical Membranes for Water Treatment. *Environ. Sci. Technol.* **2013**, *47*, 6554–6563.
- (127) Vecitis, C. D.; Gao, G.; Liu, H. Electrochemical Carbon Nanotube Filter for Adsorption, Desorption, and Oxidation of Aqueous Dyes and Anions. *J. Phys. Chem. C* **2011**, *115*, 3621–3629.
- (128) Hou, D.; Iddya, A.; Chen, X.; Wang, M.; Zhang, W.; Ding, Y.; Jassby, D.; Ren, Z. J. Nickel Based Membrane Electrodes Enable High Rate Electrochemical Ammonia Recovery. *Environ. Sci. Technol.* **2018**, *52*, 8930–8938.
- (129) Hafez, A.; El-Manharawy, S. Economics of Seawater RO Desalination in the Red Sea Region, Egypt. Part 1. A Case Study. *Desalination* **2003**, *153*, 335–347.
- (130) Desalination Committe. *Seawater Desalination Power Consumption, White Paper*; Alexandria, VA, 2011.
- (131) Zhong, J.; Sun, X.; Wang, C. Treatment of Oily Wastewater Produced from Refinery

- Processes Using Flocculation and Ceramic Membrane Filtration. *Sep. Purif. Technol.* **2003**, *32*, 93–98.
- (132) Chakrabarty, B.; Ghoshal, A. K.; Purkait, M. K. Ultrafiltration of Stable Oil-in-Water Emulsion by Polysulfone Membrane. *J. Memb. Sci.* **2008**, *325*, 427–437.
- (133) Gryta, M.; Karakulski, K.; Morawski, A. W. Purification of Oily Wastewater by Hybrid UF/MD. *Water Res.* **2001**, *35*, 3665–3669.
- (134) Ghidossi, R.; Veyret, D.; Scotto, J. L.; Jalabert, T.; Moulin, P. Ferry Oily Wastewater Treatment. *Sep. Purif. Technol.* **2009**, *64*, 296–303.
- (135) Yan, L.; Hong, S.; Li, M. L.; Li, Y. S. Application of the Al₂O₃-PVDF Nanocomposite Tubular Ultrafiltration (UF) Membrane for Oily Wastewater Treatment and Its Antifouling Research. *Sep. Purif. Technol.* **2009**, *66*, 347–352.
- (136) Cheryan, M.; Rajagopalan, N. Membrane Processing of Oily Streams. Wastewater Treatment and Waste Reduction. *J. Memb. Sci.* **1998**, *151*, 13–28.
- (137) Al-Shamrani, A. A.; James, A.; Xiao, H. Destabilisation of Oil-Water Emulsions and Separation by Dissolved Air Flotation. *Water Res.* **2002**, *36*, 1503–1512.
- (138) Oller, I.; Malato, S.; Sánchez-Pérez, J. A. Combination of Advanced Oxidation Processes and Biological Treatments for Wastewater Decontamination—A Review. *Sci. Total Environ.* **2011**, *409*, 4141–4166.
- (139) Wang, X.; Wang, Q.; Wang, S.; Li, F.; Guo, G. Effect of Biostimulation on Community Level Physiological Profiles of Microorganisms in Field-Scale Biopiles Composed of Aged Oil Sludge. *Bioresour. Technol.* **2012**, *111*, 308–315.
- (140) Li, A.; Sun, H.-X.; Tan, D.-Z.; Fan, W.-J.; Wen, S.-H.; Qing, X.-J.; Li, G.-X.; Li, S.-Y.; Deng, W.-Q. Superhydrophobic Conjugated Microporous Polymers for Separation and Adsorption. *Energy Environ. Sci.* **2011**, *4*, 2062.
- (141) Adebajo, M. O.; Frost, R. L.; Kloprogge, J. T.; Carmody, O.; Kokot, S. Porous Materials for Oil Spill Cleanup : A Review of Synthesis. *J. Porous Mater.* **2003**, *10*, 159–170.
- (142) Chen, W.; Peng, J.; Su, Y.; Zheng, L.; Wang, L.; Jiang, Z. Separation of Oil/Water Emulsion Using Pluronic F127 Modified Polyethersulfone Ultrafiltration Membranes. *Sep. Purif. Technol.* **2009**, *66*, 591–597.
- (143) Li, Y. S.; Yan, L.; Xiang, C. B.; Hong, L. J. Treatment of Oily Wastewater by Organic-Inorganic Composite Tubular Ultrafiltration (UF) Membranes. *Desalination* **2006**, *196*, 76–83.

- (144) Zhu, Y.; Xie, W.; Li, J.; Xing, T.; Jin, J. PH-Induced Non-Fouling Membrane for Effective Separation of Oil-in-Water Emulsion. *J. Memb. Sci.* **2015**, *477*, 131–138.
- (145) Muppalla, R.; Jewrajka, S. K.; Reddy, A. V. R. Fouling Resistant Nanofiltration Membranes for the Separation of Oil-Water Emulsion and Micropollutants from Water. *Sep. Purif. Technol.* **2015**, *143*, 125–134.
- (146) Zhu, L.; Chen, M.; Dong, Y.; Tang, C. Y.; Huang, A.; Li, L. A Low-Cost Mullite-Titania Composite Ceramic Hollow Fiber Microfiltration Membrane for Highly Efficient Separation of Oil-in-Water Emulsion. *Water Res.* **2016**, *90*, 277–285.
- (147) Duong, P. H. H.; Chung, T. S. Application of Thin Film Composite Membranes with Forward Osmosis Technology for the Separation of Emulsified Oil-Water. *J. Memb. Sci.* **2014**, *452*, 117–126.
- (148) Hu, X.; Bekassy-Molnar, E.; Vatai, G. Study of Ultrafiltration Behaviour of Emulsified Metalworking Fluids. *Desalination* **2002**, *149*, 191–197.
- (149) Ntroduction, S. E. I. Oily Bilgewater Separators. *Environ. Prot.* **2011**, No. November.
- (150) George-Ares, A.; Clark, J. R. Aquatic Toxicity of Two Corexit® Dispersants. *Chemosphere* **2000**, *40*, 897–906.
- (151) Padaki, M.; Surya Murali, R.; Abdullah, M. S.; Misdan, N.; Moslehyani, A.; Kassim, M. A.; Hilal, N.; Ismail, A. F. Membrane Technology Enhancement in Oil-Water Separation. A Review. *Desalination* **2015**, *357*, 197–207.
- (152) Kasemset, S.; Lee, A.; Miller, D. J.; Freeman, B. D.; Sharma, M. M. Effect of Polydopamine Deposition Conditions on Fouling Resistance, Physical Properties, and Permeation Properties of Reverse Osmosis Membranes in Oil/Water Separation. *J. Memb. Sci.* **2013**, *425–426*, 208–216.
- (153) Srijaroonrat, P.; Julien, E.; Aurelle, Y. Unstable Secondary Oil/Water Emulsion Treatment Using Ultrafiltration: Fouling Control by Backflushing. *J. Memb. Sci.* **1999**, *159*, 11–20.
- (154) Nazzal, F. F.; Wiesner, M. R. Microfiltration of Oil-in-Water Emulsions. *Water Environ. Res.* **1996**, *68*, 1187–1192.
- (155) Mueller, J.; Cen, Y.; Davis, R. H. Crossflow Microfiltration of Oily Water. *J. Memb. Sci.* **1997**, *129*, 221–235.
- (156) Ozgun, H.; Ersahin, M. E.; Erdem, S.; Atay, B.; Kose, B.; Kaya, R.; Altinbas, M.; Sayili, S.; Hoshan, P.; Atay, D.; Eren, E.; Kinaci, C.; Koyuncu, I. Effects of the Pre-

- Treatment Alternatives on the Treatment of Oil-Gas Field Produced Water by Nanofiltration and Reverse Osmosis Membranes. *J. Chem. Technol. Biotechnol.* **2013**, *88*, 1576–1583.
- (157) Zhu, Y.; Wang, D.; Jiang, L.; Jin, J. Recent Progress in Developing Advanced Membranes for Emulsified Oil/Water Separation. *NPG Asia Mater.* **2014**, *6*, e101.
- (158) Dickhout, J. M.; Moreno, J.; Biesheuvel, P. M.; Boels, L.; Lammertink, R. G. H.; de Vos, W. M. Produced Water Treatment by Membranes: A Review from a Colloidal Perspective. *J. Colloid Interface Sci.* **2017**, *487*, 523–534.
- (159) Hong, A.; Fane, A. G.; Burford, R. Factors Affecting Membrane Coalescence of Stable Oil-in-Water Emulsions. *J. Memb. Sci.* **2003**, *222*, 19–39.
- (160) Lipp, P.; Lee, C. H.; Fane, A. G.; Fell, C. J. D. A Fundamental Study of the Ultrafiltration of Oil-Water Emulsions. *J. Memb. Sci.* **1988**, *36*, 161–177.
- (161) Falahati, H.; Tremblay, A. Y. Flux Dependent Oil Permeation in the Ultrafiltration of Highly Concentrated and Unstable Oil-in-Water Emulsions. *J. Memb. Sci.* **2011**, *371*, 239–247.
- (162) F.M. Tiller. The Role of Porosity in Filtration-Numerical Methods for Constant Rate and Constant Pressure Filtration Based on Kozeny Law. *Chem. Eng. Prog* **1953**, *49*, 467–469.
- (163) Kovalsky, P.; Bushell, G.; Waite, T. D. Prediction of Transmembrane Pressure Build-up in Constant Flux Microfiltration of Compressible Materials in the Absence and Presence of Shear. *J. Memb. Sci.* **2009**, *344*, 204–210.
- (164) Mohammadi, T.; Kazemimoghadam, M.; Saadabadi, M. Modeling of Membrane Fouling and Flux Decline in Reverse Osmosis during Separation of Oil in Water Emulsions. *Desalination* **2003**, *157*, 369–375.
- (165) Matsumoto, Y.; Kawakatsu, T.; Nakajima, M.; Kikuchi, Y. Visualization of Filtration Phenomena of a Suspended Solution Including O/W Emulsion or Solid Particle and Membrane Separation Properties of the Solution. *Water Res.* **1999**, *33*, 929–936.
- (166) Field, R. W.; Wu, D.; Howell, J. A.; Gupta, B. B. Critical Flux Concept for Microfiltration Fouling. *J. Memb. Sci.* **1995**, *100*, 259–272.
- (167) Lee, S.; Aurelle, Y.; Roques, H. Concentration Polarization, Membrane Fouling and Cleaning in Ultrafiltration of Soluble Oil. *J. Memb. Sci.* **1984**, *19*, 23–38.
- (168) Nandi, B. K.; Uppaluri, R.; Purkait, M. K. *Treatment of Oily Waste Water Using*

Low-Cost Ceramic Membrane: Flux Decline Mechanism and Economic Feasibility; Taylor & Francis Group, 2009; Vol. 44.

- (169) Kota, A. K.; Kwon, G.; Choi, W.; M.Mabry, J.; Tuteja, A. Hygro-Responsive Membranes for Effective Oil–Water Separation. *Nat. Commun.* **2012**, *1025*.
- (170) Lin, S.-Y.; McKeigue, K.; Maldarelli, C. Diffusion-Controlled Surfactant Adsorption Studied by Pendant Drop Digitization. *AIChE J.* **1990**, *36*, 1785–1795.
- (171) Nakao, S. Determination of Pore Size and Pore Size Distribution: 3. Filtration Membranes. *J. Memb. Sci.* **1994**, *96*, 131–165.
- (172) She, F. H.; Tung, K. L.; Kong, L. X. Calculation of Effective Pore Diameters in Porous Filtration Membranes with Image Analysis. *Robot. Comput. Integr. Manuf.* **2008**, *24*, 427–434.
- (173) Dudchenko, A. V; Rolf, J.; Shi, L.; Olivas, L.; Duan, W.; Jassby, D. Coupling Underwater Superoleophobic Membranes with Magnetic Pickering Emulsions for Fouling-Free Separation of Crude Oil/Water Mixtures: An Experimental and Theoretical Study. *ACS Nano* **2015**, *9*, 9930–9941.
- (174) Slade, A.; Jassby, D. Affordable, Flexible, and Modular: A Guide to Open-Source Membrane-Based Water Treatment Systems. *Environ. Sci. Water Res. Technol.* **2016**, *2*, 965–974.
- (175) Le Clech, P.; Jefferson, B.; Chang, I. S.; Judd, S. J.; Le, P.; Jefferson, B.; Soung, I.; Judd, S. J. Critical Flux Determination by the Flux-Step Method in a Submerged Membrane Bioreactor. *J. Memb. Sci.* **2003**, *227*, 81–93.
- (176) Marinova, K. G.; Alargova, R. G.; Denkov, N. D.; Velev, O. D.; Petsev, D. N.; Ivanov, I. B.; Borwankar, R. P. Charging of Oil–Water Interfaces Due to Spontaneous Adsorption of Hydroxyl Ions. *Langmuir* **1996**, *12*, 2045–2051.
- (177) Al-Shamrani, A. .; James, A.; Xiao, H. Separation of Oil from Water by Dissolved Air Flotation. *Colloids Surfaces A Physicochem. Eng. Asp.* **2002**, *209*, 15–26.
- (178) Keurentjes, J. T. F.; Stuart, M. A. C.; Brinkman, D.; Schroën, C. G. P. H.; van 't Riet, K. Surfactant-Induced Wetting Transitions: Role of Surface Hydrophobicity and Effect on Oil Permeability of Ultrafiltration Membranes. *Colloids and Surfaces* **1990**, *51*, 189–205.
- (179) Pashley, R. M. Hydration Forces between Mica Surfaces in Aqueous Electrolyte Solutions. *J. Colloid Interface Sci.* **1981**, *80*, 153–162.
- (180) Kim, K. S.; Lee, K. H.; Cho, K.; Park, C. E. Surface Modification of Polysulfone

- Ultrafiltration Membrane by Oxygen Plasma Treatment. *J. Memb. Sci.* **2002**, *199*, 135–145.
- (181) Adamczyk, Z.; Para, G.; Warszyński, P. Influence of Ionic Strength on Surface Tension of Cetyltrimethylammonium Bromide. *Langmuir* **1999**, *15*, 8383–8387.
- (182) Nabi, N.; Aimar, P.; Meireles, M. Ultrafiltration of an Olive Oil Emulsion Stabilized by an Anionic Surfactant. *J. Memb. Sci.* **2000**, *166*, 177–188.
- (183) Religa, P.; Kowalik-Klimczak, A. Effect of Interaction between Anionic Surfactants and Poly(Piperazine-Amide) Nanofiltration Membranes Used for Chromium(III) Recovery from Saline Solution. *Water Sci. Technol.* **2015**, *72*.
- (184) Lin, P.-J.; Yang, M.-C.; Li, Y.-L.; Chen, J.-H. Prevention of Surfactant Wetting with Agarose Hydrogel Layer for Direct Contact Membrane Distillation Used in Dyeing Wastewater Treatment. *J. Memb. Sci.* **2015**, *475*, 511–520.
- (185) Coday, B. D.; Luxbacher, T.; Childress, A. E.; Almaraz, N.; Xu, P.; Cath, T. Y. Indirect Determination of Zeta Potential at High Ionic Strength: Specific Application to Semipermeable Polymeric Membranes. *J. Memb. Sci.* **2015**, *478*, 58–64.
- (186) Braghetta, A.; DiGiano, F. A.; Ball, W. P. Nanofiltration of Natural Organic Matter: PH and Ionic Strength Effects. *J. Environ. Eng.* **1997**, *123*, 628–641.
- (187) Goyal, P. S.; Dasannacharya, B. A.; Kelkar, V. K.; Manohar, C.; Srinivasa Rao, K.; Valaulikar, B. S. Shapes and Sizes of Micelles in CTAB Solutions. *Phys. B Condens. Matter* **1991**, *174*, 196–199.
- (188) Wang, T.; Yang, Y.; Zheng, J.; Zhang, Q.; Zhang, S. A Novel Highly Permeable Positively Charged Nanofiltration Membrane Based on a Nanoporous Hyper-Crosslinked Polyamide Barrier Layer. *J. Memb. Sci.* **2013**, *448*, 180–189.
- (189) Zheng, Y.; Yao, G.; Cheng, Q.; Yu, S.; Liu, M.; Gao, C. Positively Charged Thin-Film Composite Hollow Fiber Nanofiltration Membrane for the Removal of Cationic Dyes through Submerged Filtration. *Desalination* **2013**, *328*, 42–50.
- (190) Raza, A.; Ding, B.; Zainab, G.; El-Newehy, M.; Al-Deyab, S. S.; Yu, J. In Situ Cross-Linked Superwetting Nanofibrous Membranes for Ultrafast Oil-Water Separation. *J. Mater. Chem. A* **2014**, *2*, 10137–10145.
- (191) Schrader, M. E. Young-Dupre Revisited. *Langmuir* **1995**, *11*, 3585–3589.
- (192) Tadros, T. F. F. Fundamental Principles of Emulsion Rheology and Their Applications. *Colloids Surfaces A Physicochem. Eng. Asp.* **1994**, *91*, 39–55.

- (193) Spielman, L. A.; Goren, S. Theory of Coalescence by Flow through Porous Media. *Ind. Eng. Chem. Fundam.* **1972**, *11*, 66–72.
- (194) Saiki, Y.; Prestidge, C. A.; Horn, R. G. Effects of Droplet Deformability on Emulsion Rheology. *Colloids Surfaces A Physicochem. Eng. Asp.* **2007**, *299*, 65–72.
- (195) Nasiru, T.; Avila, L.; Levine, M. " Determination of Critical Micelle Concentrations Using UV- Visible Spectroscopy "; *J. High Sch. Res* **2011**, *2*.
- (196) Bahri, M. A.; Hoebeke, M.; Grammenos, A.; Delanaye, L.; Vandewalle, N.; Seret, A. Investigation of SDS, DTAB and CTAB Micelle Microviscosities by Electron Spin Resonance. *Colloids Surf A Colloids Surf A Colloids Surf A* **2006**, *290290290*, 206–212.
- (197) Peng, H.; Tremblay, A. Y. Membrane Regeneration and Filtration Modeling in Treating Oily Wastewaters. *J. Memb. Sci.* **2008**, *324*, 59–66.
- (198) Tomaszewska, M.; Orecki, A.; Karakulski, K. Treatment of Bilge Water Using a Combination of Ultrafiltration and Reverse Osmosis. *Desalination* **2005**, *185*, 203–212.
- (199) Neff, J.; Lee, K.; Deblois, E. M. *Produced Water : Overview of Composition , Fates , and Effects*; Springer Science+Business Media, 2011.
- (200) Produced Water Beneficial Use Case Studies, http://aqwatec.mines.edu/produced_water/assessbu/case/.
- (201) C. Johnston. EPA Regulation of Discharges to Surface Waters; IPEC: Houston, 2007.
- (202) Fakhru'l-Razi, A.; Pendashteh, A.; Abdullah, L. C.; Biak, D. R. A.; Madaeni, S. S.; Abidin, Z. Z. Review of Technologies for Oil and Gas Produced Water Treatment. *J. Hazard. Mater.* **2009**, *170*, 530–551.
- (203) Seals, S. T. Phase I Final Rule and Technical Development Document of Uniform National Discharge Standards (UNDS) Stern Tube Seals and Underwater Bearing Lubrication : Nature of Discharge. **1999**, No. April.
- (204) Kong, J.; Li., K. Oil Removal from Oil-in-Water Emulsions Using PVDF Membranes. *Sep. Purif. Technol.* **1999**, *16*, 83–93.
- (205) Han, G.; de Wit, J. S.; Chung, T. S. Water Reclamation from Emulsified Oily Wastewater via Effective Forward Osmosis Hollow Fiber Membranes under the PRO Mode. *Water Res.* **2015**, *81*, 54–63.

- (206) Alkhudhiri, A.; Darwish, N.; Hilal, N. Produced Water Treatment: Application of Air Gap Membrane Distillation. *Desalination* **2013**, *309*, 46–51.
- (207) Wang, Z.; Lin, S. Membrane Fouling and Wetting in Membrane Distillation and Their Mitigation by Novel Membranes with Special Wettability. *Water Res.* **2017**, *112*, 38–47.
- (208) Huang, Y. X.; Wang, Z.; Jin, J.; Lin, S. Novel Janus Membrane for Membrane Distillation with Simultaneous Fouling and Wetting Resistance. *Environ. Sci. Technol.* **2017**, *51*, 13304–13310.
- (209) Hou, D.; Wang, Z.; Wang, K.; Wang, J.; Lin, S. Composite Membrane with Electrospun Multiscale-Textured Surface for Robust Oil-Fouling Resistance in Membrane Distillation. *J. Memb. Sci.* **2018**, *546*, 179–187.
- (210) Zhang, S.; Lu, F.; Tao, L.; Liu, N.; Gao, C.; Feng, L.; Wei, Y. Bio-Inspired Anti-Oil-Fouling Chitosan-Coated Mesh for Oil/Water Separation Suitable for Broad Ph Range and Hyper-Saline Environments. *ACS Appl. Mater. Interfaces* **2013**, *5*, 11971–11976.
- (211) Zhou, X.; He, C. Tailoring the Surface Chemistry and Morphology of Glass Fiber Membranes for Robust Oil/Water Separation Using Poly(Dimethylsiloxanes) as Hydrophobic Molecular Binders. *J. Mater. Chem. A* **2018**, *00*, 1–9.
- (212) Norouzbahari, S.; Roostaazad, R.; Hesampour, M. Crude Oil Desalter Effluent Treatment by a Hybrid UF/RO Membrane Separation Process. *Desalination* **2009**, *238*, 174–182.
- (213) Lee, H.; Yoon, S. W.; Kim, E. J.; Park, J. In-Situ Growth of Copper Sulfide Nanocrystals on Multiwalled Carbon Nanotubes and Their Application as Novel Solar Cell and Amperometric Glucose Sensor Materials. *Nano Lett.* **2007**, *7*, 778–784.
- (214) Zhang, Q.; Arribas, P.; Remillard, E. M.; García-Payo, M. C.; Khayet, M.; Vecitis, C. D. Interlaced CNT Electrodes for Bacterial Fouling Reduction of Microfiltration Membranes. *Environ. Sci. Technol.* **2017**, *51*, 9176–9183.
- (215) Fux, G.; Ramon, G. Z. Microscale Dynamics of Oil Droplets at a Membrane Surface: Deformation, Reversibility, and Implications for Fouling. *Environ. Sci. Technol.* **2017**, *51*, 13842–13849.
- (216) Gragson, D. E.; Richmond, G. L. Investigations of the Structure and Hydrogen Bonding of Water Molecules at Liquid Surfaces by Vibrational Sum Frequency Spectroscopy. *J. Phys. Chem. B* **1998**, *102*, 3847–3861.

- (217) Santos, F. K. G.; Neto, E. L. B.; Moura, M. C. P. A.; Dantas, T. N. C.; Neto, A. A. D. Molecular Behavior of Ionic and Nonionic Surfactants in Saline Medium. *Colloids Surfaces A Physicochem. Eng. Asp.* **2009**, *333*, 156–162.
- (218) Gurkov, T. D.; Dimitrova, D. T.; Marinova, K. G.; Bilke-Crause, C.; Gerber, C.; Ivanov, I. B. Ionic Surfactants on Fluid Interfaces: Determination of the Adsorption; Role of the Salt and the Type of the Hydrophobic Phase. *Colloids Surfaces A Physicochem. Eng. Asp.* **2005**, *261*, 29–38.
- (219) Jurado, E.; Fernández-Serrano, M.; Núñez-Olea, J.; Luzón, G.; Lechuga, M. Simplified Spectrophotometric Method Using Methylene Blue for Determining Anionic Surfactants: Applications to the Study of Primary Biodegradation in Aerobic Screening Tests. *Chemosphere* **2006**, *65*, 278–285.
- (220) Para, G.; Jarek, E.; Warszynski, P. The Surface Tension of Aqueous Solutions of Cetyltrimethylammonium Cationic Surfactants in Presence of Bromide and Chloride Counterions. *Colloids Surfaces A Physicochem. Eng. Asp.* **2005**, *261*, 65–73.
- (221) Ghosh, P.; Banik, M. Effects of Salts Containing Mono-, Di-, and Trivalent Ions on Electrical and Rheological Properties of Oil-Water Interface in Presence of Cationic Surfactant: Importance in the Stability of Oil-in-Water Emulsions. *J. Dispers. Sci. Technol.* **2014**, *35*, 471–481.
- (222) Mabile, C.; Schmitt, V.; Gorria, P.; Leal Calderon, F.; Faye, V.; Deminière, B.; Bibette, J. Rheological and Shearing Conditions for the Preparation of Monodisperse Emulsions. *Langmuir* **2000**, *16*, 422–429.
- (223) Yi, G.; Chen, S.; Quan, X.; Wei, G.; Fan, X.; Yu, H. Enhanced Separation Performance of Carbon Nanotube–Polyvinyl Alcohol Composite Membranes for Emulsified Oily Wastewater Treatment under Electrical Assistance. *Sep. Purif. Technol.* **2018**, *197*, 107–115.
- (224) Kang, S. T.; Subramani, A.; Hoek, E. M. V.; Deshusses, M. A.; Matsumoto, M. R. Direct Observation of Biofouling in Cross-Flow Microfiltration: Mechanisms of Deposition and Release. *J. Memb. Sci.* **2004**, *244*, 151–165.
- (225) Kingery, W. D.; Humenik, M. Surface Tension. At Elevated Temperatures. I. Furnace and Method for Use of the Sessile Drop Method; Surface Tension of Silicon, Iron and Nickel. *J. Phys. Chem.* **1953**, *57*, 359–363.
- (226) Chesters, a. K. The Modelling of Coalescence Process in Fluid-Liquid Dispersions: A Review of Current Understanding. *Chem. Eng. Res. Des.* **1991**, *69*, 259–270.
- (227) Li, X.; Zhang, P.; Lin, C. L.; Johnson, W. P. Role of Hydrodynamic Drag on

- Microsphere Deposition and Re-Entrainment in Porous Media under Unfavorable Conditions. *Environ. Sci. Technol.* **2005**, *39*, 4012–4020.
- (228) Wiesner, M. R.; Bottero, J.-Y. *Environmental Nanotechnology Applications and Impacts of Nanomaterials*; McGraw-Hill New York, NY, 2007.
- (229) Davis, R. Modeling of Fouling of Crossflow Microfiltration Membranes. *Sep. Purif. Rev.* **1992**, *21*, 75–126.
- (230) Goren, S. L. The Hydrodynamic Force Resisting the Approach of a Sphere to a Plane Permeable Wall. *J. Colloid Interface Sci.* **1979**, *69*, 78–85.
- (231) McCloskey, B. D.; Park, H. B.; Ju, H.; Rowe, B. W.; Miller, D. J.; Chun, B. J.; Kin, K.; Freeman, B. D. Influence of Polydopamine Deposition Conditions on Pure Water Flux and Foulant Adhesion Resistance of Reverse Osmosis, Ultrafiltration, and Microfiltration Membranes. *Polymer (Guildf)*. **2010**, *51*, 3472–3485.
- (232) Kim, S.; Marion, M.; Jeong, B. H.; Hoek, E. M. V. Crossflow Membrane Filtration of Interacting Nanoparticle Suspensions. *J. Memb. Sci.* **2006**, *284*, 361–372.
- (233) Stark, A. Y.; Badge, I.; Wucinich, N. A.; Sullivan, T. W.; Niewiarowski, P. H.; Dhinojwala, A. Surface Wettability Plays a Significant Role in Gecko Adhesion Underwater. *Proc. Natl. Acad. Sci.* **2013**, *110*, 6340–6345.
- (234) Šegota, S.; Heimer, S.; Težak, D. New Catanionic Mixtures of Dodecyldimethylammonium Bromide/Sodium Dodecylbenzenesulphonate/Water: I. Surface Properties of Dispersed Particles. *Colloids Surfaces A Physicochem. Eng. Asp.* **2006**, *274*, 91–99.
- (235) Ohtaki, H.; Radnai, T. Structure and Dynamics of Hydrated Ions. *Chem. Rev.* **1993**, *93*, 1157–1204.
- (236) White, L. R. On Deviations from Young's Equation. *J. Chem. Soc. Faraday Trans. 1 Phys. Chem. Condens. Phases* **1977**, *73*, 390–398.
- (237) Roques-Carmes, T.; Palmier, S.; Hayes, R. A.; Schlangen, L. J. M. The Effect of the Oil/Water Interfacial Tension on Electrowetting Driven Fluid Motion. *Colloids Surfaces A Physicochem. Eng. Asp.* **2005**, *267*, 56–63.
- (238) Vallet, M.; Berge, B.; Vovelle, L. Electrowetting of Water and Aqueous Solutions on Poly(Ethylene Terephthalate) Insulating Films. *Polymer (Guildf)*. **1996**, *37*, 2465–2470.
- (239) Hardy, R. C. Viscosity of N-Hexadecane. *J. Res. Natl. Bur. Stand. (1934)*. **1958**, *61*, 433–436.

- (240) Prince, M. J.; Blanch, H. W. Bubble Coalescence and Breakup in Air Sparged Bubble Columns. *AIChE J.* **1990**, *36*, 1485–1499.
- (241) Sulaymon, A. H.; Wilson, C. A. M. E.; Alwarded, A. I. Experimental Determination of the Virtual Mass Coefficient for Two Spheres Accelerating in a Power Law Fluid. *J. Fluids Eng.* **2010**, *132*, 121204.
- (242) Kamp, A. M.; Chesters, A. K.; Colin, C.; Fabre, J. *Bubble Coalescence in Turbulent Flows: A Mechanistic Model for Turbulence-Induced Coalescence Applied to Microgravity Bubbly Pipe Flow*; 2001; Vol. 27.
- (243) Wandera, D.; Wickramasinghe, S. R.; Husson, S. M. Modification and Characterization of Ultrafiltration Membranes for Treatment of Produced Water. *J. Memb. Sci.* **2011**, *373*, 178–188.
- (244) Wu, T. Y.; Mohammad, A. W.; Md. Jahim, J.; Anuar, N. Palm Oil Mill Effluent (POME) Treatment and Bioresources Recovery Using Ultrafiltration Membrane: Effect of Pressure on Membrane Fouling. *Biochem. Eng. J.* **2007**, *35*, 309–317.
- (245) Jamshidi Gohari, R.; Korminouri, F.; Lau, W. J.; Ismail, A. F.; Matsuura, T.; Chowdhury, M. N. K.; Halakoo, E.; Jamshidi Gohari, M. S. A Novel Super-Hydrophilic PSf/HAO Nanocomposite Ultrafiltration Membrane for Efficient Separation of Oil/Water Emulsion. *Sep. Purif. Technol.* **2015**, *150*, 13–20.
- (246) Salahi, A.; Mohammadi, T.; Mosayebi Behbahani, R.; Hemmati, M. Asymmetric Polyethersulfone Ultrafiltration Membranes for Oily Wastewater Treatment: Synthesis, Characterization, ANFIS Modeling, and Performance. *J. Environ. Chem. Eng.* **2015**, *3*, 170–178.
- (247) Lee, S.; Lee, C. H. Effect of Operating Conditions on CaSO₄ Scale Formation Mechanism in Nanofiltration for Water Softening. *Water Res.* **2000**, *34*, 3854–3866.
- (248) Al-Rashdi, B. A. M.; Johnson, D. J.; Hilal, N. Removal of Heavy Metal Ions by Nanofiltration. *Desalination* **2013**, *315*, 2–17.
- (249) Bidhendi, G. N.; Nasrabadi, T. Use of Nanofiltration for Concentration and Demineralization in the Dairy Industry. *Pakistan J. Biol. Sci.* **2006**, *9*, 991–994.
- (250) Tansel, B.; Sager, J.; Rector, T.; Garland, J.; Strayer, R. F.; Levine, L.; Roberts, M.; Hummerick, M.; Bauer, J. Significance of Hydrated Radius and Hydration Shells on Ionic Permeability during Nanofiltration in Dead End and Cross Flow Modes. *Sep. Purif. Technol.* **2006**, *51*, 40–47.
- (251) Nirmalraj, P. N.; Lyons, P. E.; De, S.; Coleman, J. N.; Boland, J. J. Electrical Connectivity in Single-Walled Carbon Nanotube Networks. *Nano Lett.* **2009**, *9*,

3890–3895.

- (252) Lyons, P. E.; De, S.; Blighe, F.; Nicolosi, V.; Pereira, L. F. C.; Ferreira, M. S.; Coleman, J. N. The Relationship between Network Morphology and Conductivity in Nanotube Films. *J. Appl. Phys.* **2008**, *104*.
- (253) González, A.; Goikolea, E.; Barrena, J. A.; Mysyk, R. Review on Supercapacitors: Technologies and Materials. *Renew. Sustain. Energy Rev.* **2016**, *58*, 1189–1206.
- (254) Kim, S. H.; Kwak, S. Y.; Suzuki, T. Positron Annihilation Spectroscopic Evidence to Demonstrate the Flux-Enhancement Mechanism in Morphology-Controlled Thin-Film-Composite (TFC) Membrane. *Environ. Sci. Technol.* **2005**, *39*, 1764–1770.
- (255) Tang, C. Y.; Kwon, Y. N.; Leckie, J. O. Effect of Membrane Chemistry and Coating Layer on Physiochemical Properties of Thin Film Composite Polyamide RO and NF Membranes. I. FTIR and XPS Characterization of Polyamide and Coating Layer Chemistry. *Desalination* **2009**, *242*, 149–167.
- (256) Tan, Z.; Chen, S.; Peng, X.; Zhang, L.; Gao, C. Polyamide Membranes with Nanoscale Turing Structures for Water Purification. *Science (80-.)*. **2018**, No. May, 1–14.